REPRINTS OF PUBLISHED PAPERS

Radiation Physics and Chemistry

Neutron capture cross section of 186W isotope in the energy range from 0.6-3.2 MeV with covariance analysis

--Manuscript Draft--

Manuscript Number:	
Article Type:	Review Article
Keywords:	Neutron capture cross section, Tungsten, 7Li(p,n)7Be reaction neutron source, off-line -ray spectrometry, Covariance analysis
Corresponding Author:	Mayur Harshadbhai Mehta Institute for Plasma Research Gandhinagar, Gujarat INDIA
First Author:	Mayur Harshadbhai Mehta
Order of Authors:	Mayur Harshadbhai Mehta
	N.L. Singh
	A. Gandhi
	P.V. Subhash
	Rebecca Pachuau
	RatanKumar Singh
	R. Makwana
	S.V. Suryanarayana
	B.K. Nayak
	H. Naik
	Karel Katovsky
Abstract:	The cross section of 186W(n,γ)187W reaction WAS measured at the neutron energies 0.61 ± 0.01 (0.046618 barns), 2.11 ± 0.02 (0.026396 barns) and 3.13 ± 0.02 (0.019474 barns) MeV using the activation method followed by off-line γ-ray spectroscopy. The 115In(n,n')115mIn monitor reaction was used to determine the neutron flux during the experiments. The neutron beams were produced from the 7Li(p,n)7Be reaction by using 2.6, 4 and 5 MeV proton beams at Folded Tandem Ion-beam Accelerator (FOTIA) facility, BARC-Mumbai. A detailed analysis of uncertainty propagation was performed with covariance analysis method. The γ-ray self-absorption, neutron flux attenuation and low energy corrections have been presented in the experiment. The measured cross sections values were compared with the published data in EXFOR database and with theoretically predicted data by TALYS-1.96 and EXPIRE-3.2 nuclear codes and also with the evaluated nuclear data from ENDF/B-VIII.0, JEFF-3.3 and JENDL-5. The measured cross section values at 0.61 ± 0.01 and 2.11 ± 0.02 MeV are in good agreement with the literature data while there is no data available at 3.13 ± 0.02 MeV, the measured values are consistent with the cross section values available at 3.11 MeV. The measured values are also in good agreement with the ENDF/B-VIII.0 data and predicted data by EMPIRE-3.2 code.
Suggested Reviewers:	G.D. Kim gdkim@rock25t.kigam.re.kr Reviewer has been working in cross section measurement work for years and have experience of working for tungsten cross section measurements.
	V. Semkova vsemkova@inrne.bas.bg
	Megha Bhike megha.bhike@gmail.com

Communicated

Neutron capture cross section of ^{186}W isotope in the energy range from 0.6-3.2 MeV with covariance analysis

Mayur Mehta[1,2,a], N. L. Singh[1,3], A. Gandhi[4,5], P.V. Subhash[6,7], Rebecca Pachuau[4], Ratankumar Singh[1], R. Makwana[1], S.V. Suryanarayana[8], B.K. Nayak[7,8], H. Naik[9] and K. Katovsky[10]

[1] Department of Physics, Faculty of Science, The M.S. University, Baroda-390002, India

[2] Institute for Plasma Research, Gandhinagar-382428, India

[3] Depart of Physics, Netaji Subhash University of Technology, Dwarka, Delhi-110078, India

[4] Department of Physics, Banaras Hindu University, Varanasi-221005, India

[5] Horia Hulubei National Institute of Physics and Nuclear Engineering-IFIN-HH, Bucharest, 077125, Romania

[6] ITER-India, Institute for Plasma Research, Gandhinagar-382428, India

[7] Homi Bhabha National Institute, Anushaktinagar, Mumbai-400094, India

[8] Nuclear Physics Division, Bhabha Atomic Research Centre, Trombay, Mumbai-400085, India

[9] Radiochemistry Division, Bhabha Atomic Research Centre, Trombay, Mumbai-400085, India

[10] Department of Electrical Power Engineering, Brno University of Technology, Brno-61600, Czech Republic

Abstract: The cross section of $^{186}W(n,\gamma)^{187}W$ reaction WAS measured at the neutron energies 0.61 ± 0.01 (0.046618 barns), 2.11 ± 0.02 (0.026396 barns) and 3.13 ± 0.02 (0.019474 barns) MeV using the activation method followed by off-line γ-ray spectroscopy. The $^{115}In(n,n')^{115m}In$ monitor reaction was used to determine the neutron flux during the experiments. The neutron beams were produced from the $^{7}Li(p,n)^{7}Be$ reaction by using 2.6, 4 and 5 MeV proton beams at Folded Tandem Ion-beam Accelerator (FOTIA) facility, BARC-Mumbai. A detailed analysis of uncertainty propagation was performed with covariance analysis method. The γ-ray self-absorption, neutron flux attenuation and low energy corrections have been presented in the experiment. The measured cross sections values were compared with the published data in EXFOR database and with theoretically predicted data by TALYS-1.96 and EXPIRE-3.2 nuclear codes and also with the evaluated nuclear data from ENDF/B-VIII.0, JEFF-3.3 and JENDL-5. The measured cross section values at 0.61 ± 0.01 and 2.11 ± 0.02 MeV are in good agreement with the literature data while there is no data available at 3.13 ± 0.02 MeV, the measured values are consistent with the cross section values available at 3.11 MeV. The measured values are also in good agreement with the ENDF/B-VIII.0 data and predicted data by EMPIRE-3.2 code.

[a] E-mail: mayur@ipr.res.in (corresponding author)

Keywords: Neutron capture cross section, Tungsten, $^{7}Li(p,n)^{7}Be$ reaction neutron source, off-line γ-ray spectrometry, Covariance analysis

1. Introduction

Tungsten (W) is a prime material used in First-wall and Plasma Facing Components (PFCs) in ITER (International Thermonuclear Experimental Reactor) like fusion reactors, target material for high-current accelerator-type systems (ADS), and for neutron dosimetry via $^{186}W(n,\gamma)$ reaction. For the transmutation and operational studies of fusion reactors, there is a need for accurate nuclear data of tungsten isotopes. The neutron capture cross-section of ^{186}W isotopes is also important in astrophysics applications [1-5]. The $^{186}W(n,\gamma)^{187}W$ reaction cross section data are reported at multiple energy points in the energy range of present work but no data found having details of uncertainty propagation and covariance analysis [6-18]. For the accurate knowledge of nuclear reaction database, the sufficient information regarding the uncertainties of the experiments are required [19]. Therefore, in present work the $^{186}W(n,\gamma)^{187}W$ reaction cross section is measured in the neutron energy range 0.6 to 3.2 MeV and the details of uncertainty propagation and covariance analysis is reported with fractional uncertainties of all attributed considered in the activation formula. The absolute neutron flux was determined using the $^{115}In(n,n')^{115m}In$ monitor reaction. The experimental $^{186}W(n,\gamma)^{187}W$ reaction cross-section was compared with the available literature data from EXFOR database [18] and the available data from Evaluated Nuclear Data File (ENDF/B-VIII.0), Joint Evaluated Nuclear Data Library(JEFF-3.3) and Japanese Evaluated Nuclear Data Library (JENDL-5) [20-22]. The $^{186}W(n,\gamma)^{187}W$ reaction cross-section was also compared with the theoretically predicted cross-section based on TALYS-1.96 [23] and EMPIRE-3.2 [24] codes. The cross-section of $^{186}W(n,\gamma)^{187}W$ reaction reported in the present work at different neutron energies will enhance the data in the nuclear data library.

2. Experimental Details

2.1 Neutron irradiation facility

In the present study, 6 MV Folded Tandem Ion Accelerator (FOTIA) Facility, Bhabha Atomic Research Centre (BARC)-Mumbai was used for irradiation experiments [25]. The proton beam of 2.6, 4 and 5 MeV energies were bombarded on natural lithium (^{nat}Li) foil of thickness 4.0 mg/cm^2

to produce neutrons through $^{7}Li(p,n)^{7}Be$ reaction (E_{th} = 1.881 MeV) [26, 27]. The energy spread of proton beam is ± 0.02 MeV whereas the beam current during irradiation was 100 nA.

2.2 Estimation of Average neutron energy

In this work, the neutron beam energy spectrum cannot measured using the Time of Flight technique due to continuous proton beam. Therefore EPEN- (Energy of Proton Energy of Neutron) code was used to calculate the neutron flux energy spectrum (Φ(E)) from the $^{7}Li(p,n)^{7}Be$ reaction. EPEN code was used for the incident proton energies from reaction threshold to 7.0 MeV [28, 29]. The proton beam energies in this case were above threshold energy of $^{7}Li(p,n)^{7}Be$ reaction, there will be the contribution of the second energy group of lower energy neutrons produced from the $^{7}Li(p,n_1)^{7}Be^*$ and $^{7}Li(p,n+^{3}He)^{4}He$ reactions in addition to the $^{7}Li(p,n_0)^{7}Be$ reaction. The neutron flux energy spectra $\Phi_0(E)$ of 2.6, 4 and 5 MeV proton beam energies calculated by the EPEN code, are shown in Figure 1. It can be seen that the neutron spectrum had a spread due to proton energy loss in the lithium target. The mean energy of the (p,n_0) neutron group was obtained by:

$$< E_n >= \frac{\int \Phi_0(E) E dE}{\int \Phi_0(E) dE} \quad (1)$$

Where, $\Phi_0(E)$ is the (p,n_0) neutron flux calculated from neutron flux energy spectra of Figure 1. The neutron energies for E_p = 2.6, E_p = 4 and E_p = 5 MeV are 0.61 ± 0.01, 2.11 ± 0.02 and 3.13 ± 0.02 MeV respectively.

2.3 Sample Preparations

Natural tungsten (W) metal foil of dimension 10×10× 0.1 mm and natural indium (In) metal foil of dimension 10×10×0.5 mm were used for irradiation experiments. They were separately wrapped with a 0.025 mm thick pure aluminium foil. The sample target with the monitor was stacked as "In-W" and mounted one stack at a time in forward direction of the incident beam at a distance of 12 mm from Li foil. The sample details are given in Table 1. The In-W stacks were irradiated with the neutron beam generated from the $^{7}Li(p,n)^{7}Be$ reaction with proton beam energies of 2.6, 4 and 5 MeV, respectively.

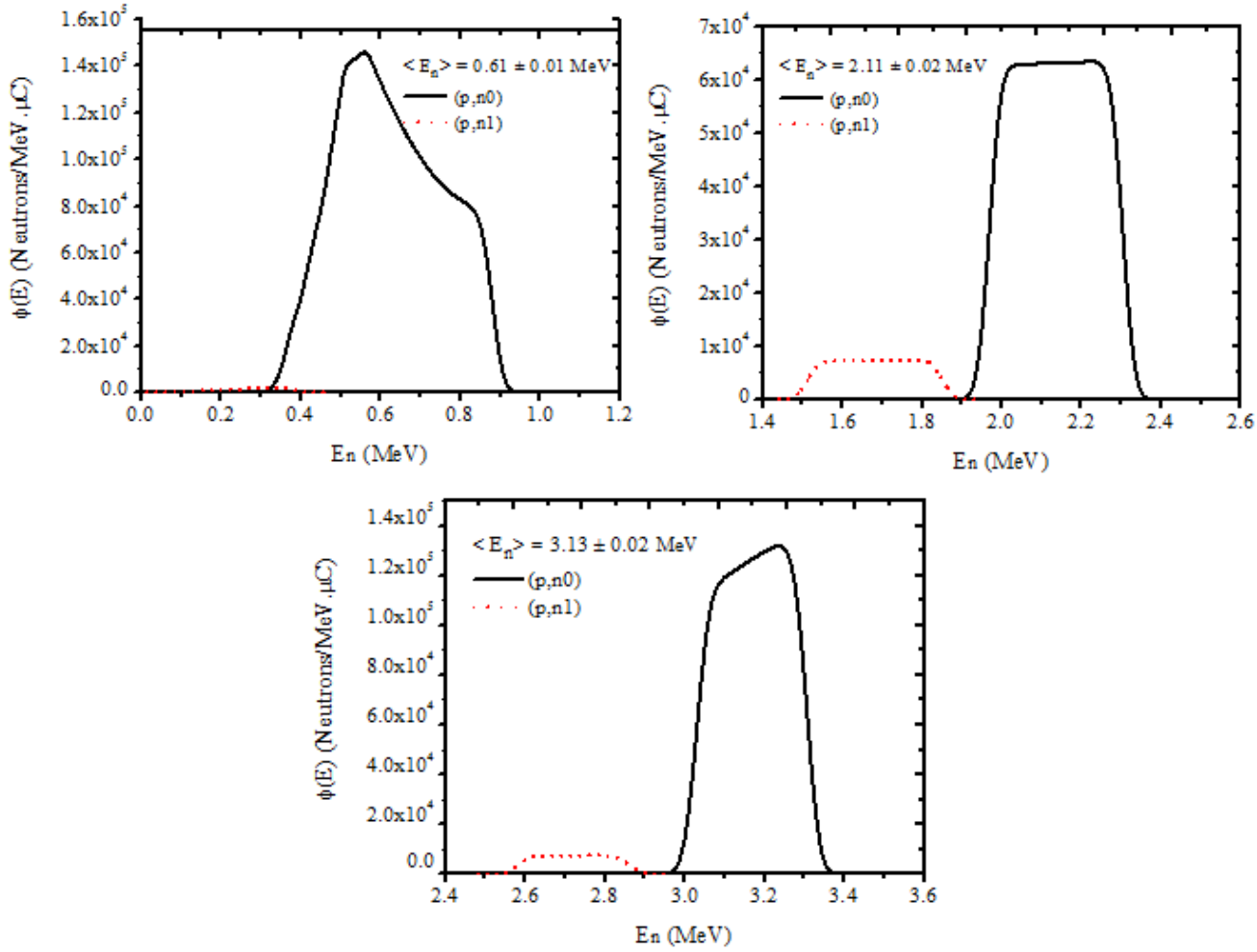

Figure 1 Neutron flux energy spectrum Φ(E), for (i) E_p = 2.6 MeV, (ii) E_p = 4.0 MeV and (iii) E_p = 5.0 MeV generated from EPEN code.

Table 1 Summary of present experimental sample details

Sample	Isotope	Isotope Abundance (%)	E_n (MeV)	Weight of isotope in sample (mg)	Number of atoms (10^{-4} atoms/b)
W-foil	^{186}W	28.43 ± 0.02	0.61 ± 0.01	283.4 ± 0.1	2.639
			2.11 ± 0.02	313.1 ± 0.1	2.916
			3.13 ± 0.02	299.2 ± 0.1	2.783
In-foil	^{115}In	95.17 ± 0.05	0.61 ± 0.01	250.1 ± 0.1	12.545
			2.11 ± 0.02	275.6 ± 0.1	9.611
			3.13 ± 0.02	257.0 ± 0.1	12.891

Table 2 The Experimental details of irradiation

Reaction	E_n (MeV)	Irradiation time (sec)	Cooling time (sec)	Counting time (sec)
$^{115}In(n,n')^{115m}In$	0.61±0.01	21660	4420	1380
	2.11±0.02	21600	2018	1420
	3.13±0.02	21660	5056	1272
$^{186}W(n,\gamma)^{187}W$	0.61±0.01	21660	31832	18600
	2.11±0.02	21600	67183	27854
	3.13±0.02	21660	48340	12262

Table 3 Nuclear spectroscopic data of sample and monitor reactions

Reaction	Product nuclei	Half-life (h)	E_γ (keV)	I_γ (%)
$^{115}In(n,n')$	^{115m}In	4.486 ± 0.004	336.24	45.9(1)
$^{186}W(n,\gamma)$	^{187}W	24.0 ± 0.4	479.53	26.6(4)

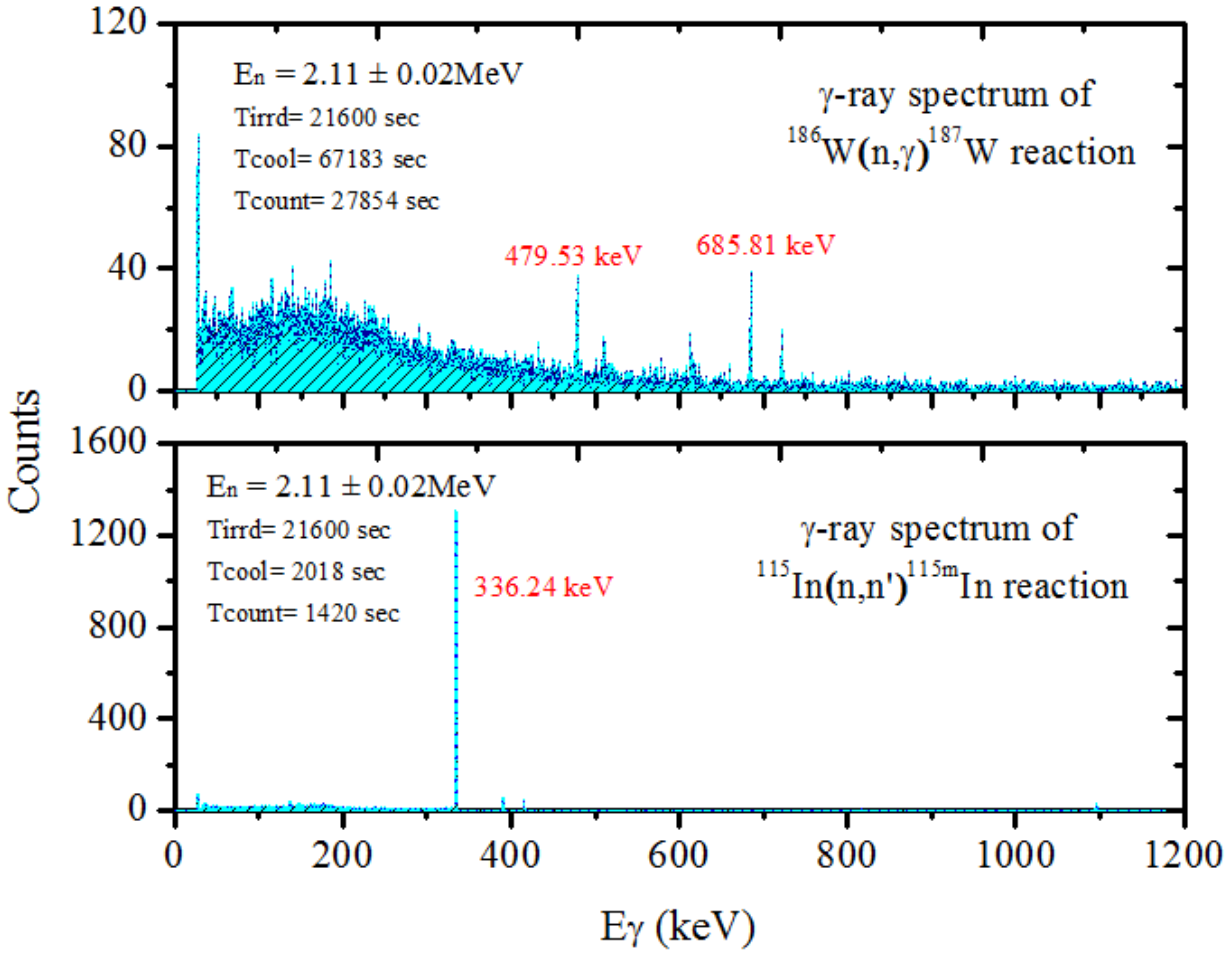

Figure 2 Typical γ-ray spectrum of $^{186}W(n,\gamma)^{187}W$ and $^{115}In(n,n')^{115m}In$ reaction recorded by HPGe detector

2.4 Off-line γ-ray spectroscopy

The In-W stack samples were irradiated for 6 hours to produce sufficient activity at three different neutron energies. After each irradiation, the irradiated W-target and In-monitor samples were cooled for sufficient time and then mounted on different Perspex plates for off-line γ-ray counting. The γ-ray counting was done for a longer period to get enough γ-ray activity to minimize the statistical errors and also counting was done multiple times to follow the half-lives of the radionuclides of present interest. The experimental timing details are given in Table 2. The γ-ray activity measurement of reaction products were carried out by a lead shielded 180cc high purity Ge (HPGe) detector having efficiency of 30% and an energy resolution of 1.8 keV for 1332 keV γ-ray energy of ^{60}Co. The recording and analysis of the γ-ray spectrum were carried out by using

the CAMAC-based LAMPS software. The recorded γ-ray spectra of the reaction produced from the $^{186}W(n,\gamma)^{187}W$ reaction with monitor reaction $^{115}In(n,n')^{115m}In$ is shown in Figure 2. The nuclear spectroscopic data are taken from Refs. [30-32] and given in Table 3. The product nuclei ^{115m}In of $^{115}In(n,n')$ reaction emits 336.24 keV γ-ray energy whereas the product nuclei ^{187}W of $^{186}W(n,\gamma)$ reaction emits 479.53 keV and 685.81 keV γ-ray energies. The photo-peak activity of 336.24 keV γ-ray energy of ^{115m}In was used for the neutron flux calculation, whereas 479.53 keV γ-ray energy of ^{187}W was used for estimation of $^{186}W(n,\gamma)$ reaction cross section.

Table 4 Details of measured HPGe detector efficiency for ^{152}Eu-source

Eγ (keV)	*Iγ*	*Counts (Cobs)*	*Kc*	*Efficiency (ε)*
121.78	0.2853 ± 0.0016	336620 ± 461	1.165	0.101078
344.27	0.2659 ± 0.0004	171402.4 ± 516.8	1.113	0.052850
778.90	0.1294 ± 0.0008	36409.4 ± 336.3	1.165	0.024143
964.07	0.1461 ± 0.0007	35981.7 ± 556.5	1.099	0.019945
1085.86	0.1021 ± 0.0005	26751.6 ± 370.2	0.915	0.017665
1408.01	0.2101 ± 0.0009	37819.5 ± 596.7	1.036	0.013741

The HPGe detector efficiency calibration was determined by using a multi γ-ray source-^{152}Eu ($\tau_{1/2}$ = 13.517±0.0009 years) having activity 6659.21 ± 82.1 Bq on 1 October 1999 [33]. The detector efficiency was determined by,

$$\varepsilon = \frac{CK_c}{A_0 I_\gamma e^{-\lambda T}\Delta t} \quad (2)$$

Where C is the number of count in time Δt (5484 sec), A_0 is the activity of ^{152}Eu-source at the manufacturing time, I_γ is the absolute intensity of desired γ-ray energy and λ is the decay constant. T is the difference between the source manufacturing to counting time. K_C is the coincidence summing correction factor is derived from the Monte Carlo simulation code EFFTRAN [34, 35]

using HPGe detector specifications such as material and dimension information of crystal, absorber and calibration source information. The measured efficiency of γ-ray energies are presented in Table 4. The comparison of measured efficiency and EFFTRAN code corrected detector efficiency is plotted in Figure 3.

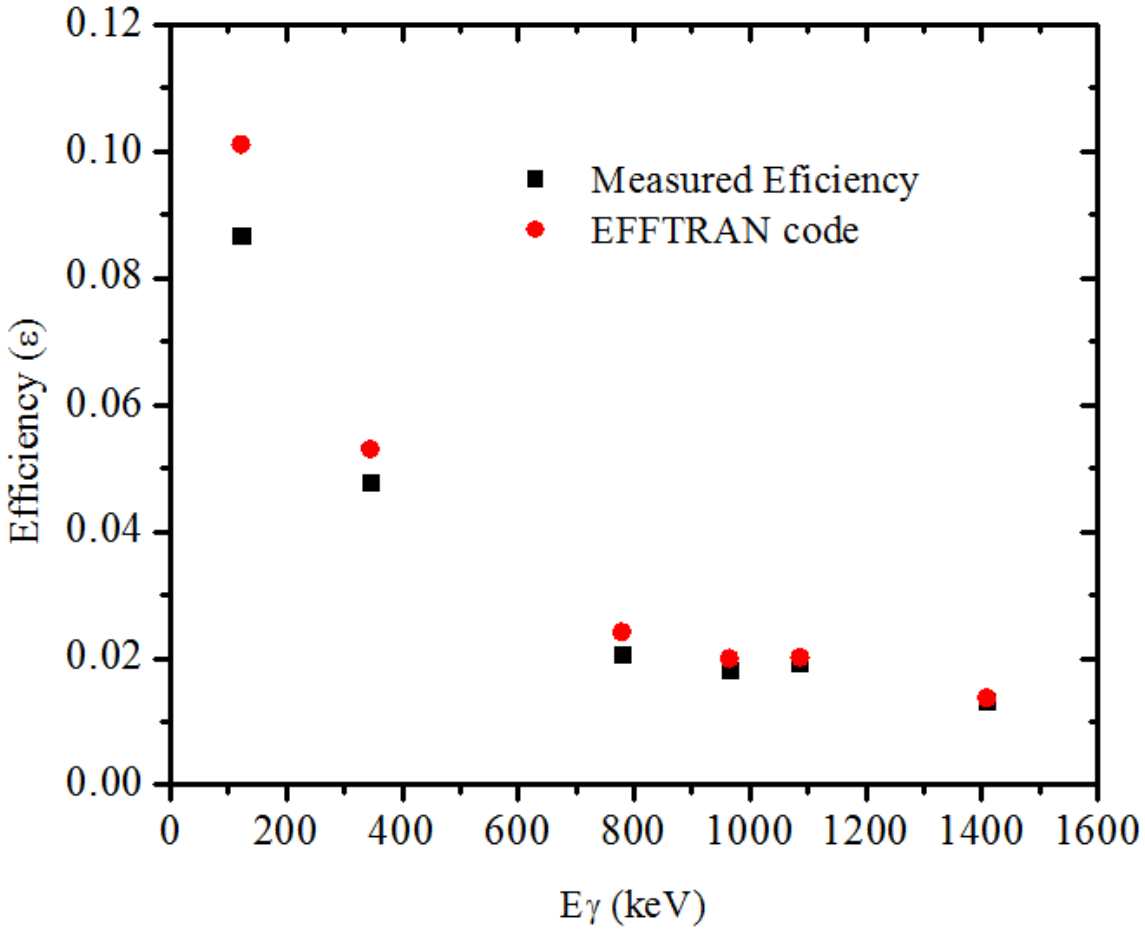

Figure 3 Comparison between the measured efficiency and EFFTRAN corrected efficiency

2.4.1 Covariance analysis and uncertainty propagation in detection efficiency

The covariance matrix for the detector efficiency was calculate from the partial uncertainties of attributes [36]. As seen in Eq. (1), the detector efficiency is a function of counts (C), the activity of source (A_0), γ-ray intensity (I_γ) and the decay constant (λ) therefore the uncertainties propagate due to these four attributes is given by,

$$\left(\frac{\Delta\varepsilon_i}{\varepsilon_i}\right)^2 = \left(\frac{\Delta C_i}{C_i}\right)^2 + \left(\frac{\Delta I_{\gamma i}}{I_{\gamma i}}\right)^2 + \left(\frac{\Delta A_0}{A_0}\right)^2 + (t\Delta\lambda)^2 \quad (3)$$

where, $(\Delta\lambda = 0.693 \times \tau_{1/2}/\tau_{1/2}^2)$ is the uncertainty in the decay constant. The covariance matrix for the detector efficiency is calculated from the partial uncertainties of the four attributes at corresponding energies using the formula,

$$(V_\varepsilon)_{ij} = \sum_r e_{ir} S_{ijr} e_{jr} \quad (4)$$

Where, S_{ijr} is the micro correlation matrix (n × n), e_{ir} and e_{jr} are diagonal matrices of partial uncertainties. The partial uncertainties of the attributes are given in Table 5. The covariance and the corresponding correlation matrix for the HPGe detector efficiency of γ-ray energies from ^{152}Eu-source is presented in Table 6. The total error in the measured efficiencies is determined by the formula, $\sigma_{\varepsilon ij} = \sqrt{(V_\varepsilon)_{ij}}$. The detection efficiency for the γ-ray energies from product nuclide ^{187}W and ^{115m}In are different which are estimated by interpolating the point-wise γ-ray efficiencies given in Table 4 using the function,

$$\ln \varepsilon_i = \sum_m P_m \ (\ln E_i)^{m-1} \quad (5)$$

Where, ε_i is the efficiency of the γ-ray energies E_i and P_m is the fitting parameter. The least square method is used to estimate the best fitting values for P that gives the minimum value for the Chi-square statistics given by, $\chi^2 = (Z - AP)^T V_Z^{-1} (Z - AP)$. The value for P is determined by the relation,

$$P = (A^T V_Z^{-1} A)^{-1} (A^T V_Z^{-1} Z) \quad (6)$$

Where, $V_Z = (V\varepsilon)ij/\varepsilon_i\varepsilon_j$, V_Z is the covariance matrix of the efficiencies ε, A = ln E_i and Z = ln ε_i [37]. In present work, the best fit model have the fitting values as P = -3.95367, -0.934269, -0.0592294, -0.147593 and -0.07223 with χ^2 = 0.177. The detection efficiency of the γ-ray energies of the sample (^{187}W, ε_r) and monitor (^{115m}In, ε_m) nuclides with uncertainties, covariance and correlation matrix is presented in Table 7. For the cross section measurement, the ration of the efficiencies ($\eta = \varepsilon_m/\varepsilon_r$) is required therefore the fraction uncertainty propagated from the η values is determined by the formula,

$$\frac{\nabla\eta_{m,r}}{\eta_{m,r}} = Var(\varepsilon_m) + Var(\varepsilon_r) - 2Cov(\varepsilon_m, \varepsilon_r) \quad (7)$$

and the obtained η value with its uncertainty is = 1.4128 ± 0.00112.

Table 5 Partial uncertainties of the attributed considered for HPGe detector efficiency

Eγ (keV)	Iγ ($\times 10^{-4}$)	Counts ($\times 10^{-4}$)	Activity ($\times 10^{-4}$)	Half-life ($\times 10^{-4}$)	Total Uncertainty ($\times 10^{-4}$)
121.78	5.659	1.384	12.39	8.890	16.33
344.69	3.729	3.256	6.476	4.648	9.484
778.90	1.492	2.230	2.959	2.123	4.523
964.07	0.956	3.085	2.444	1.754	4.414
1085.86	0.865	2.445	2.165	1.554	3.718
1408.01	0.589	2.168	1.684	1.208	3.057

Table 6 Covariance and Correlation matrix for the HPGe detector efficiencies

Eγ (keV)	Covariance matrix ($\times 10^{-7}$)						Correlation matrix					
121.78	26.66						1					
344.27	12.16	8.994					0.7852	1				
778.90	5.554	2.903	2.046				0.7521	0.6767	1			
964.07	4.587	2.398	1.095	1.948			0.6367	0.5729	0.5487	1		
1085.86	4.639	2.425	1.108	0.915	1.803		0.6694	0.6023	0.5769	0.4884	1	
1408.01	3.160	1.652	0.754	0.623	0.631	0.934	0.6334	0.5699	0.5459	0.4622	0.4859	1

Table 7 Interpolated detector efficiency of γ-ray energies of the monitor and sample reactions with uncertainties and correlation matrix

Reaction	Nuclei	Eγ (keV)	Efficiency	Correlation matrix	
^{115}In(n,n')	^{115m}In	336.24	0.05412 ± 0.00100	1	
^{186}W(n,γ)	^{187}W	479.53	0.03831 ± 0.00102	0.38703	1

3. Data analysis

3.1 Estimation of ^{186}W(n,γ)^{187}W reaction cross section and its uncertainties

The reaction cross section was measured by irradiating the target samples in the neutron energy range 0.6 MeV to 3.2 MeV and measuring the counts of the selected characteristic γ-ray energies using the standard activation formula,

$$< \sigma_r > = < \sigma_m > \eta \ \frac{A_r \lambda_r a_m N_m I_m f_m}{A_m \lambda_m a_r N_r I_r f_r} \ \times \ \frac{C_r * N_{Corr\,(r)}}{C_m * \ N_{Corr\,(m)}} \tag{8}$$

Where, *r* and *m* subscripts stands for sample and monitor reaction. $A_{r,m}$ is the photo-peak counts of product nuclei ^{187}W and ^{115m}In recorded by HPGe detector, $\lambda_{r,m}$ is the decay constant (cm^{-1}), $N_{r,m}$ is the total number of atoms , η ($\varepsilon_m/\varepsilon_r$) is the detector efficiency ratio, $\varepsilon_{r,m}$ is the efficiency of corresponding γ-ray energies, $I_{r,m}$ is the γ-ray intensity, $a_{r,m}$ is the isotopic abundance and $f_{r,m}$ is the timing factors given by:

$$f_{r,m} = \left(1 - e^{-\lambda t_{irr}}\right) e^{-\lambda t_{cool}} \left(1 - e^{-\lambda t_{count}}\right) \tag{9}$$

Where, t_{irr} is the irradiation time, t_{cool} is the cooling time which is the time difference when the irradiation stop and the counting started time and t_{count} is the counting time. $C_{r,m}$ is the total correction factor due to self-absorption of γ-rays, counting geometry and flux attenuation. $N_{corr\,(r,m)}$ is the low energy (p,n_1) neutron correction factor.

3.2 Reference monitor cross section

The spectrum averaged cross section for the monitor reaction $<\sigma_m>$ is determined by the equations,

$$< \sigma_m > = \frac{\int_{Ej,min}^{Ej,max} \Phi_i \sigma_m dE}{\int_{Ej,min}^{Ej,max} \Phi_i dE} \quad (10)$$

Where, σ_m is the $^{115}In(n,n')^{115m}In$ monitor reaction cross section taken from the IRDFF-1.05 (International Reactor Dosimetry and Fusion File) library [38] folded with the neutron flux values (Φ_i) from the neutron flux energy spectrum generated by simulation code EPEN [28, 29]. *Ej,min* and *Ej,max* are the lower and upper energy values of the energy spectrum. The neutron flux calculated from monitor reaction is 2.627×10^6 n cm^2 s^{-1} at 0.61 ± 0.01 MeV, 4.151×10^6 n cm^2 s^{-1} at 2.11 ± 0.02 MeV and 3.621×10^6 n cm^2 s^{-1} at 3.13 ± 0.02 MeV neutron energies, respectively by considering correction factors.

The correlation coefficients for the monitor reaction are obtained using the equation,

$$Corr\ (< \sigma_i >< \sigma_j >) = \frac{Cov(<\sigma_i><\sigma_j>)}{\sqrt{Var<\sigma_i>}\sqrt{Var<\sigma_j>}} \quad (11)$$

The monitor spectrum averaged cross section with uncertainties and correlation matrix is given in Table 8.

Table 8 Spectrum averaged cross section of ^{115}In(n,n')^{115m}In reaction with its uncertainty and correlation matrix

Reaction	En (MeV)	Cross section $<\sigma_m>$ (barn)	$\Delta<\sigma_m>$ (%)	Correlation matrix		
	0.61	0.01303 ± 0.00043	3.3001	1		
^{115}In(n,n')^{115m}In	2.11	0.29587 ± 0.00779	2.6329	0.2759	1	
	3.13	0.33842 ± 0.00804	2.3757	0.2982	0.3390	1

3.3 Correction factors

In order to get the actual cross section from the neutron photo-peak, the corrections are required in the cross section values. Many factors have their contribution to the final values of the measured cross section. The total correction factors of this neutron irradiation experiment mainly involved, the γ-ray self-absorption factor of the sample at a given γ-energy (C_s), the flux attenuation factor

(C_a), the counting geometry factor (C_g) and correction in measured cross section due to lower energy neutrons (N_{corr}) [39, 40].

3.2.1 Gamma ray self-attenuation factor: In the present experiments, the radio activities in irradiated samples are uniformly distributed. The characteristic γ-rays from the sample of a certain thickness causes the γ-ray self-absorption effect due to the Photoelectric effect, the Compton effect and the Electron pair production effect. The correction factor was measured by the equation,

$$C_s = \frac{\mu_s t_s}{1-exp^{(-\mu_s t_s)}} \tag{12}$$

Where, t_s is a sample thickness (cm); μ_s is a mass absorption co-efficient (cm^2gm^{-1}) which determined from NIST-XCOM [41].

3.2.3 Geometry correction factor: The irradiated samples were cooled for sufficient time and placed on a Perspex plate for γ-ray counting. The distance between the samples and the detector cap was kept in such a way that the coincidence summing effect will be minimized during the counting time. The counting geometry correction factor (C_g) was calculated by,

$$C_g = \frac{(h+ d/2)^2}{h^2} \tag{13}$$

Where, d is the sample thickness (cm); h is the distance from the sample surface to the effective detection cross section of the crystal in the HPGe detector (cm).

3.2.3 Flux attenuation correction factor: When the energetic neutrons travel through a sample of a certain thickness, because of the effect of flux attenuation these neutrons are absorbed by nuclear reactions. The correction factor for flux attenuation is measured by dividing the sample thickness into average k parts. Each part of the sample will produce the amount of radioactivity called N_1, N_2, N_3… N_k. The flux attenuation correction factor was derived by the following formula,

$$C_a = \frac{kN_1}{\sum_{i=1}^{i=k} N_i} \tag{14}$$

Where, N_i is the amount of radioactivity produced by i-th part of the sample. The correction factor due to experimental geometry is so insignificant that could be ignored. The total correction factor C_{tot} for sample reaction and monitor is calculated by the following formula and shown in Table 9.

$$C_{tot} = \frac{(C_s C_g C_a)_r}{(C_s C_g C_a)_m} \quad (15)$$

3.2.4 Low energy background correction factor: The proton beam energies in present work are above the threshold energy of the reaction therefore the contribution of lower energy background neutron from $^{7}Li(p,n_1)^{7}Be^*$ reaction was subtracted from actual measurement of $^{186}W(n,\gamma)^{187}W$ reaction cross section and is calculated by the equation:

$$N_{corr} = 1 - \frac{\int \Phi_1(E)\sigma_x(E)dE}{\int \Phi(E)\sigma_x(E)dE} \quad (16)$$

Where, $\Phi_1(E)$ is the neutron flux energy spectrum for (p,n_1) neutrons and $\Phi(E)$ is the total cross section [$\Phi(E) = \Phi_0(E) + \Phi_1(E)$] calculated by EPEN code. $\sigma_x(E)$ is the cross section values of $^{186}W(n,\gamma)^{187}W$ reaction taken from ENDF/B-VIII.0 [20] and $^{115}In(n,n')^{115m}In$ reaction cross section values taken from IRDFF-1.05 data library [38]. Table 10 shows the calculated values of low energy corrections and the γ-ray self-absorption correction factors of associated γ-ray energies of sample and monitor reactions.

Table 9 Correction factors in the present experiment

E_n (MeV)	$\frac{C_{s\,(r)}}{C_{S\,(m)}}$	$\frac{C_{g\,(r)}}{C_{g\,(m)}}$	$\frac{C_{a\,(r)}}{C_{a\,(m)}}$	C_r
0.61 ± 0.01	0.98374	0.98209	0.9999	0.96613
2.11 ± 0.02	0.98374	0.98209	0.9999	0.96613
3.13 ± 0.02	0.98374	0.98209	0.9999	0.96612

Table 10 Low neutron energy correction (N_{corr}) and γ-ray self-attenuation coefficient of sample and monitor reactions

Reaction	E_n (MeV)	N_{corr}	E_γ (keV)	C_s
$^{186}W(n,\gamma)^{187}W$	0.61 ± 0.01	0.98929	479.53	1.01416±0.00045
	2.11 ± 0.02	0.88682		
	3.13 ± 0.02	0.92766		
$^{115}In(n,n')^{115m}In$	0.61 ± 0.01	0.99998	336.241	1.02575±0.00130
	2.11 ± 0.02	0.92434		
	3.13 ± 0.02	0.94277		

3.4 Covariance analysis and uncertainty propagation in cross section

In covariance analysis, the covariance matrix ($V_{(\sigma)ij}$) for reaction cross section was determined by considering the fractional uncertainty (%) of different attributed involved in the calculations. The covariance matrix is for the measured cross section is determined by the formula,

$$(V_\sigma)_{ij} = \sum_r e_{ir} S_{ijr} e_{jr} \quad (17)$$

Where, S_{ijr} is micro-correlation matrix, e_{ir} and e_{jr} are the n×n diagonal matrix of partial uncertainties of the attributes involved in Eq. (7). The partial uncertainties of the attributes considered to estimate the reaction cross sections with correlation is shown in Table 11. The calculated $^{186}W(n,\gamma)^{187}W$ reaction cross section values with their uncertainties, covariance matrix and correlation matrix are shown in Table 12. The square root of the diagonal values of the covariance matrix are the error in the measured reaction cross section values. The uncertainties due to other parameters involved in the cross section values are count statistics (≤5%), reference cross section (≤1%), the detector efficiency (≤3%), weight of the sample (≤0.01%), isotopic abundance (≤1%), self -absorption of γ-rays (≤1%) and other parameters are neglected due to very small contributions.

Table 11 Fractional uncertainties (%) of different attributed involved in present experiment

Attributes	Fractional Uncertainty (%)			Correlation
	En = 0.61±0.01	En = 2.11±0.02	En = 3.13±0.02	
A_r	8.6678	7.0995	6.2248	0
A_m	4.5380	0.6080	0.5895	0
η	0.0789	0.0789	0.0789	1
I_r	1.5038	1.5038	1.5038	1
I_m	0.2179	0.2179	0.2179	1
f_r	0.0860	0.0889	0.0674	1
f_m	0.0054	0.0077	0.0014	1
W_r	0.0353	0.0319	0.0334	0
W_m	0.0400	0.0363	0.0423	0
σ_m	3.3001	2.6329	2.3757	1
a_r	0.0352	0.0352	0.0352	1
a_m	0.01045	0.01045	0.01045	1

Table 12 Measured cross section with uncertainties, covariance and correlation matrix

Reaction	En (MeV)	Cross section $\langle\sigma_s\rangle$ (barn)	Covariance matrix			Correlation matrix		
	0.61 ± 0.01	0.046618 ± 0.004877	0.0109			1		
$^{186}W(n,\gamma)^{187}W$	2.11 ± 0.02	0.026396 ± 0.002043	0.000232	0.005988		0.02877	1	
	3.13 ± 0.02	0.019474 ± 0.001335	0.000232	0.000232	0.004700	0.03244	0.04378	1

4. Theoretical calculations

The theoretical calculations of $^{186}W(n,\gamma)^{187}W$ reaction cross section were done by TALYS-1.96 and EMPIRE-3.2 nuclear codes [23, 24]. Both codes comprise various nuclear models, compound nucleus, level density and pre-equilibrium models, γ-ray strength functions over a broad range of energies and incident particles. In the present case, the theoretical reaction cross sections have been predicated by taking the combination of different input parameters like the optical models, nuclear level densities and γ-ray strength functions in neutron energy range from 0.4 to 5 MeV. Theoretically calculated cross sections are compared with the measured results, the available reported data from EXFOR database [18] and data available in ENDF/B-VIII.0, JEFF-3.3 and JENDL-5 [20-22].

In EMPIRE-3.2 nuclear code, the theoretical investigation of the $^{186}W(n,\gamma)^{187}W$ reaction cross section was done with optimized input parameters. The capture cross section was predicted by using parity dependent Hartree-Fock-Bogoliubov method (HFBM) doe level density parameter [42]. The default γ-ray strength function (GSTRFN=1) was used for γ-ray transmission coefficients [43]. The width fluctuation correction was applied with the Hofmann, Richert, Tepel and Weidenmuller (HRTW) model up to 5 MeV [44]. In EMPIRE code, the default values of the optical model potential (OMPOT=2408) and the exciton model (PCROSS=1.5) were used for the capture cross section [45].

The $^{186}W(n,\gamma)^{187}W$ reaction cross sections have been calculated by Talys-1.96 code taking into account the level density models with optimal values of input parameters in the neutron energy range from 0.4 to 5 MeV. In the present case, Skryme-Hartree-Fock-Bogoluybov different level density models (LDMODEL 4) was considered for estimation of reaction cross section with other optimized input parameters. [46] The code considers the direct, pre-equilibrium and compound components of the cross section in the calculations. The Brink-Axel Lorentzian model (strength-2) has been used for the γ-ray strength function [47]. In TALYS, in order to calculate the reaction cross sections, different input parameters like nuclear models, level densities, decay schemes and other input parameters are taken from the Reference Input Parameter Library RIPL-3 database [48].

5. Result and Discussion

The $^{186}W(n,\gamma)^{187}W$ reaction cross sections with uncertainties, covariance and correlation matrix were presented in Table 12 at spectrum averaged neutron energies of E_n=0.61 ± 0.01, 2.11 ± 0.02 and 3.13 ± 0.02 MeV using activation and off-line γ-ray spectrometric technique. The comparison between the measured cross sections with the previously published data was presented in Table 13 and the data from ENDF/B-VIII.0, JEFF-3.3, JENDL-5, TALYS-1.96 and EMPIRE-3.2 [20-24] were presented in Figure 4. The available data were published few decades ago have scarcity due to discrepancies in the decay data and monitor cross sections. The comparison with evaluated data shows that the cross section data with ENDF-V.III.0 [20] data library agrees at 0.61 ± 0.01 MeV (0.04649 barn) and 3.13 ± 0.02 MeV (0.017049) data and underestimates at 2.11 ± 0.02 MeV (0.02938). From Figure 4.5, it is observed that the measured cross section data are in good agreement with the data predicted by EMPIRE-3.2 at 0.61 ± 0.01 MeV (0.04387 barn); at 2.11 ± 0.02 MeV (0.02915 barns) and 3.13 ± 0.02 MeV (0.02545 barns) while the measured data are underestimates for TALYS-1.96 data except at 3.13 ± 0.02 MeV (0.02143 barns). The comparison with the previously reported data indicated that the measured cross section data agrees with reported data by M. Lindner et al. [10] at 0.6 MeV (0.048 barns) and data reported by G. G. Zaikin et al. [12] at 2.11 MeV (0.0291 barns) and 3.11 MeV (0.0231 barns).

Table 13 Comparison of measured $^{186}W(n,\gamma)^{187}W$ reaction cross section with previously reported data

En (MeV)	Cross section $<\sigma_s>$ (barn)	Literature		
		En (MeV)	$<\sigma_s>$ (barn)	References
0.61 ± 0.01	0.046618 ± 0.004877	0.6	0.048	M. Lindner et al. (1976)
		0.595	0.045	A.E. Johnsrud et al. (1959)
2.11 ± 0.02	0.026396 ± 0.002043	2.11	0.0291	G.G. Zaikin et al. (1968)
		3.11	0.0231	G.G. Zaikin et al. (1968)
3.13 ± 0.02	0.019474 ± 0.001335	3.1	0.016	J.A. Miskel et al. (1962)
		3.1	0.024	A.E. Johnsrud et al. (1959)

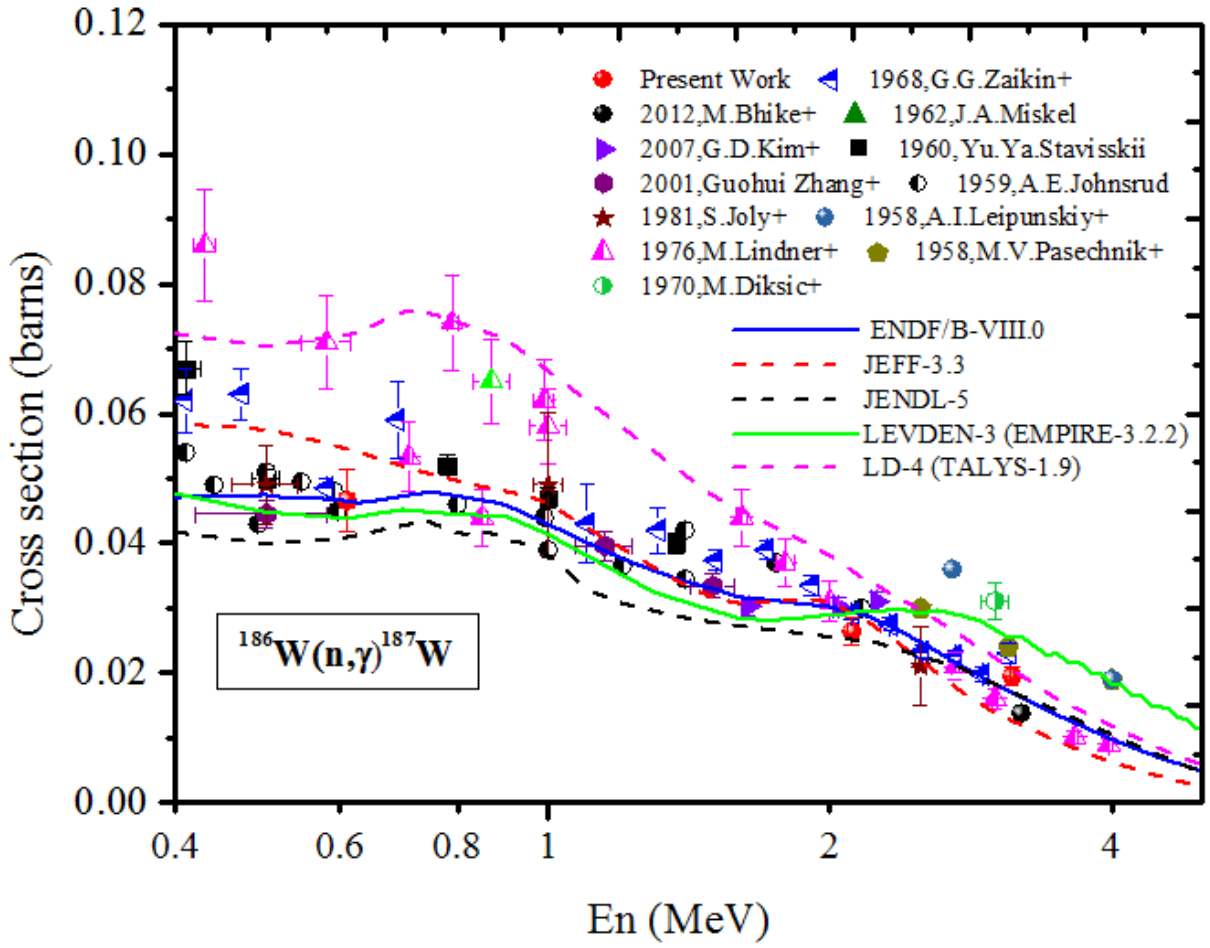

Figure 4 Comparison of $^{186}W(n,\gamma)^{187}W$ reaction cross section with previously published data, evaluated data and theoretical data

6. Conclusion

The cross section of $^{186}W(n,\gamma)^{187}W$ reaction was measured at spectrum averaged neutron energies 0.61 ± 0.01 MeV;2.11 ± 0.02 MeV and 3.13 ± 0.02 MeV, and the measured values are 0.046618 ± 0.004877 barns, 0.026396 ± 0.002043 barns and 0.019474 ± 0.001335 barns respectively. A detailed analysis of uncertainties propagate by various attributes was resented with covariance and correlation matrix. The measured values are compared with the literature data, theoretically predicted data by TALYS-1.96 and EMPIRE-3.2 codes and evaluated data from ENDF/B-VIII.0, JEFF-3.3 and JENDL-5. The measured results are in good agreement to the ENDF/B-VIII.0 and EMPIRE-3.2 data as well as the data reported earlier.

Acknowledgements

The authors are thankful to the staff members of the FOTIA facility for their support and help to run the experiments smoothly and also thankful to Alpesh Patel (IPR, Gandhinagar) for providing tungsten foil samples for the irradiation experiments.

Funding: This research did not receive any specific grant from funding agencies in the public, commercial, or not-for-profit sectors.

References

[1] Khripunov, B.I., Koidan, V.S., Ryazanov, A.I., et al. 2015. Physics Procedia 71, 63-67

[2] Gohar, Yousry, Bolshinsky, Igor, Karnaukhov, Ivan, 2015. KIPT accelerator-driven system design and performance, Report No. NEA/NSC/DOC (2015)7

[3] Forrest, R.A., 2006. Fusion Engineering and Design 81 (18) 2143-2156

[4] Kawano, T., Chadwick, M.B., Talou, P., Young, P.G., and Bonneau, L., 2008. Nuclear Reaction Data for Nuclear Technologies and Applications, AIP Conference Proceedings 1005, 17

[5] Marganiec, J., Dillmann, I., Domingo Pardo, C., and Kappeler, F., 2009. Physical Review C 80, 025804

[6] Bhike, M., Roy, B.J., Saxena, A., Choudhury, R.K., Ganesan, S., 2012. Nuclear Science and Engineering 170, 44

[7] Kim, G.D., Woo, H.J., Choi, H.W. et al., 2007. Journal of Radioanalytical and Nuclear Chemistry 271, 553

[8] Zhang, Guohui, Shi, Zhaomin, Tang, Guoyou, et al., 2001. Nuclear Science and Engineering 137, 107

[9] Voignier, J., Joly, S., Grenier, G., Drake, D.M., Nilsson, L., Report: Centre d`Etudes Nucleaires, Saclay ReportsNo.5089, NSR-Key No: 1981VOZW (1981)

[10] Lindner, M., Nagle, R.J., Landrum, J.H., 1976. Nuclear Science and Engineering 59, 381

[11] Diksic, M., Strohal, P., Peto, G., Bornemisza-Pauspertl, P., Hunyadi, I., Karolyi, J., 1970 Acta Physica Hungarica 28, 257

[12] Zaikin, G.G., Korzh, I.A., Sklyar, N.T., Totskii, I.A., 1968. Soviet Atomic Energy 25, 1362

[13] Miskel, J.A., Marsh, K.V., Lindner, M., Nagle, R.J., 1932. Physical Review 128, 2717

[14] Stavisskii, Yu.Ya., Tolstikov, V.A., 1960. Journal of Nuclear Energy A&B (Reactor Sci. and Technol.) 16, 496

[15] Johnsrud, A.E., Silbert, M.G., Barschall, H.H., 1959. Physical Review 116, 927

[16] Pasechnik, M.V., Barchuk, I.F., Totskiy, I.A., Strizhak, V.I. et al., 1958. Conf.: Second Internat. At. En. Conf., Geneva, Vol. 15, 18

[17] Leipunskiy, A.I., Kazachkovskiy, O.D., Artyukhov, G.Ja., Baryshnikov, A.I., et al., 1958. Conf.: Second Internat. At. En. Conf., Geneva, Vol.15, 50

[18] EXFOR, Cross Section Information Storage and Retrieval System (EXFOR), IAEA, Vienna, Austria, http://www.nds.iaea.or.at/exfor/(online)

[19] Otuka, N., et al., 2017. Radiation Physics and Chemistry 140, 502

[20] Brown, D.A., et al., 2018. Nucl. Data Sheets 148, 1

[21] JEFF 3.3, https://www.oecd-nea.org/dbdata/jeff/jeff33/

[22] Plompen, A.J.M. et al., 2020. Eur. Phys. J. A 56, 1

[23] Koning, A.J., Hilaire, S., Duijvestijn, M.C., 2008. TALYS-1.9, in Proceedings of the International Conference on Nuclear Data for Science and Technology, April 22–27, 2007, Nice, France, editors O. Bersillon, F. Gunsing, E. Bauge, R. Jacqmin, and S. Leray, (EDP Sciences, Les Ulis, France 2008) 211

[24] Herman, M., et al., 2013. EMPIRE-3.2 Malta modular system for nuclear reaction calculations and nuclear data evaluation User's Manual, No. BNL [101378-2013]. Brookhaven National Laboratory (BNL) National Nuclear Data Center, (2013)

[25] Singh, P., et al., 2002. Pramana Journal of Physics 59, 739

[26] Pope, C. H., et al, 1976. Phys. Rev. C 14, 438

[27] Lisken, H., and Paulsen, A., 1975. At. Data Nucl. Data Tables 15, 57

[28] Pachuau, R., et al., 2017. Nucl. Sci. Eng. 187, 70

[29] Pachuau, R., et al., 2017. EPJ Web Conf. 146, 12016

[30] NuDat 3 (2023) National Nuclear Data Center, Brookhaven National Laboratory. http://www.nndc.bnl.gov/nudat3

[31] Basunia, M.S., 2009. Nuclear Data Sheets, 110 (5), 999-1238

[32] Blachot, Jean, 2012. Nuclear Data Sheets, 113(10), 2391-2535

[33] Martin, M.J., 2013. Nuclear Data Sheets 114, 1497-1847

[34] Vidmar, T., 2005. Nuclear. Instrum. Methods A 550, 603

[35] Vidmar, T., Kanish, G., 2011. Applied Radiation and Isotope 908, 69

[36] Singh, R.K., Singh, N.L., et al., 2022. Chinese Physics C 46, 054002

[37] Geraldo, L. P., 1990. Nuclear Instrumentation and Methods in Physics Res. A, 290, 499-508

[38] Zsolnay, E. M., Capote, R., Nolthenius, H.K., Trkov, A., 2012. International Atomic Energy Agency Technical Report No. INDC(NDS)-0616

[39] Shen, Su, Yuan, Zhiling, Luo, Xiaobing, 2020. Nuclear Inst. and Methods in Physics Research B 476, 59-63

[40] Gandhi, A., Sharma, Aman, Pachuau, Rebecca, et al., 2021. Eur. Phys. J. A, 57 (1)

[41] Berger; M.J., Hubbell, J.H., Seltzer, S.M., Chang; J., et al., 2010. XCOM: photon cross sections database, NIST standard reference database (XGAM), 2010. Available at http://www.nist.gov/pml/data/xcom/index.cfm

[42] Goriely, S., Samyn, M. and Pearson, J.M, 2007. Phys. Rev. C 75, 064312

[43] Brink, D.M., 1955. Ph.D. thesis, Oxford University

[44] Hofmann, H. M., et al. 1975. Ann. Phys. 90, 403

[45] Griffin, J. J., 196. Phys. Rev. Lett. 17, 478

[46] Ignatyuk, A. V., Weil, J. L., Raman, S., Kahane, S., 1993. Phys. Rev. C, 47:1504

[47] Brink, D. M., 1957. Nucl. Phys. 4, 215 Axel, P., 1962. Phys. Rev. 126, 671

[48] Capote, R., Herman, M., Oblozinsky, P., et al., 2009. Nucl Data Sheets 110, 3107

Declaration of interests

This research did not receive any specific grant from funding agencies in the public, commercial, or not-for-profit sectors.

Measurement of 90Zr(n,2n)89Zr and 90Zr(n,p)90mY reaction cross-sections in the neutron energy range of 10.95 to 20.02 MeV

Article *in* Journal of Radioanalytical and Nuclear Chemistry · March 2021

DOI: 10.1007/s10967-021-07625-y

CITATIONS
0

READS
42

13 authors, including:

Mayur Mehta
Institute for Plasma Research
31 PUBLICATIONS **53** CITATIONS
SEE PROFILE

N.L. Singh
The Maharaja Sayajirao University of Baroda
183 PUBLICATIONS **1,440** CITATIONS
SEE PROFILE

R. K. Singh
The Maharaja Sayajirao University of Baroda
10 PUBLICATIONS **1** CITATION
SEE PROFILE

Siddharth Parashari
University of Zagreb
53 PUBLICATIONS **79** CITATIONS
SEE PROFILE

Journal of Radioanalytical and Nuclear Chemistry
https://doi.org/10.1007/s10967-021-07625-y

Measurement of ^{90}Zr(n,2n)^{89}Zr and ^{90}Zr(n,p)^{90m}Y reaction cross-sections in the neutron energy range of 10.95 to 20.02 MeV

Mayur Mehta[1,2] · N. L. Singh[2] · R. K. Singh[2] · Siddharth Parashari[2] · P. V. Subhash[3,4] · H. Naik[5] · R. D. Chauhan[2] · R. Makwana[2] · S. V. Suryanarayana[6] · S. Mukherjee[2] · A. Gandhi[7] · J. Varmuza[8] · K. Katovsky[8]

Received: 19 September 2020 / Accepted: 3 February 2021

Abstract
The (n,2n) and (n,p) reaction cross-sections of ^{90}Zr isotope have been measured in 10.95 to 20.02 MeV neutron energy range by using activation and off-line γ-ray spectrometric technique. ^{27}Al(n,α)^{24}Na and ^{115}In(n,n')^{115m}In monitor reactions have been used to measure the neutron fluence. The reaction cross-sections were estimated from TALYS-1.9 and EMPIRE-3.2.2 codes by making the selection of different input parameters. The uncertainties in the measurement were estimated using covariance analysis. The present results have been compared with the data measured previously by different authors and available in different evaluated nuclear data files.

Keywords ^{90}Zr(n,2n)^{89}Zr and ^{90}Zr(n,p)^{90m}Y reactions · Cross-section measurement · Off-line γ-ray spectrometry · TALYS-1.9 · EMPIRE-3.2.2 · Covariance analysis

Introduction

Zirconium (Zr) and its alloys have been extensively used as cladding material of fuel elements in fission reactors and structural materials in International Thermo-nuclear Experimental Reactor (ITER), like fusion reactors. These elements have also been used as nuclear fuel pellet in the design of accelerator-driven sub-critical system (ADSs), due to its unique properties of low neutron capture cross-section, good corrosion resistance and favorable chemical and mechanical properties. Zr is also used as a prime target material for the production of medical isotopes [1–4]. Thus accurate knowledge of nuclear reaction data of such materials is important for the design and operation of future nuclear systems and medical applications. The neutron induced reaction cross-sections data plays a vital role for the study of nuclear transmutation, induced activity and damage studies in a broad energy range [5–7].

The (n,2n) and (n,p) reaction cross-sections of ^{90}Zr isotope were measured by using the method of activation followed by off-line γ-ray spectrometric technique in fast neutron energy region where, there is a deficiency in cross-section data. In the present case, the cross-sections of ^{90}Zr(n,2n)^{89}Zr reaction were measured at average neutron energies of 13.97 ± 0.68, 16.99 ± 0.53 and 20.02 ± 0.58 MeV and the cross-sections of ^{90}Zr(n,p)^{90m}Y reaction were measured at 10.95 ± 0.45, 13.97 ± 0.68, 16.99 ± 0.53 and 20.02 ± 0.58 MeV. The measured cross-section values were compared with the data present in EXFOR compilation [8] and in Evaluated Nuclear Data Files (ENDF) [9]. For further comparison, the reaction cross-sections for both the

✉ Mayur Mehta
mayur@ipr.res.in

✉ N. L. Singh
nl.singh-phy@msubaroda.ac.in

1 Institute for Plasma Research, Gandhinagar 382428, India

2 Department of Physics, Faculty of Science, The M. S. University of Baroda, Vadodara 390002, India

3 ITER-India, Gandhinagar 382428, India

4 Homi Bhabha National Institute, Anushaktinagar, Mumbai 400094, India

5 Radiochemistry Division, Bhabha Atomic Research Centre, Mumbai 400085, India

6 Nuclear Physics Division, Bhabha Atomic Research Centre, Mumbai 400085, India

7 Department of Physics, Banaras Hindu University, Varanasi 221005, India

8 Department of Electrical Power Engineering, Brno University of Technology, Brno 61600, Czech Republic

Published online: 11 March 2021

reactions were theoretically estimated by using the TALYS-1.9 [10] and EMPIRE-3.2.2 [11] codes.

Experimental details

Details of irradiation and sample preparations

The experiment was performed by using the 14UD BARC-TIFR Pelletron facility at Mumbai, India. The neutrons of different energies were produced from ^{nat}Li(p,n) reaction at the 6 m height above the analyzing magnet of the main beam line in the Pelletron facility to utilize maximum proton current from accelerator. Natural lithium (Li) foil of thickness ≈6.8 mg/cm^2 was used as target, which was sandwich between two tantalum (Ta) foils of thickness ≈4 mg/cm^2 in front side and Ta foil of thickness 0.1 mm in back side of Li to stop the proton beams. Natural zirconium (Zr) metal foil (99.99% purity) having isotopic abundance of ^{90}Zr- 50.45%, ^{91}Zr-11.22%, ^{92}Zr-17.15%, ^{94}Zr-17.38% and ^{96}Zr-2.80% with dimensionof 10 × 10 mm^2 and 0.3 mm thick was used in all irradiation experiments. Aluminum (Al) and indium (In) metal foils (purity-99.99%) having isotopic abundance of ^{27}Al-100% and ^{115}In-95.71% with dimensions of 10 × 10 mm^2 and 0.1 mm thick have been used as monitors to measure the neutron flux. The dimensions of the target samples and monitors were kept same to avoid area corrections in the flux. The samples were wrapped in a 0.025 mm thick aluminum foil to prevent radioactive contamination during the experiment. All samples were stacked and wrapped additionally in aluminum foil of same thickness to avoid radioactive contamination to the surrounding. The Al-wrapped samples and monitors were kept one set at a time at a distance of 2.1 cm behind Ta-Li-Ta stack in 0° angle in forward direction. The In-Zr-Al stacks were irradiated with the neutron beam generated from the ^{7}Li(p,n)^{7}Be reaction with proton beam energies of 13, 16, 19 and 22 MeV, respectively. The proton beam current was monitored and recorded at regular interval during the experiments. The details of irradiations are given in Table 1. A schematic diagram of the irradiation set up is shown in Fig. 1.

Measurement of γ-ray activity

The irradiations of sample stacks were carried out for different times, depending on the neutron energy to build up sufficient activity in the samples. After the irradiation, the sample stacks were cooled for sufficient time to avoid the gamma dose of short-lived products. The samples were mounted on Perspex plates and taken for off-line γ-ray spectroscopy. The γ-ray counting of irradiated samples was performed by using HPGe detector coupled with a PC-based 4096 channel analyzer with GENIE spectroscopic software. The HPGe detector system had a resolution of 1.82 keV at 1332.50 keV

Table 1 Experimental parameters of the present work

	Irradiation 1	Irradiation 2	Irradiation 3	Irradiation 4
Proton energy (MeV)	13	16	19	22
Total irradiation time (hh:mm)	10:20	7:30	6:30	5:30
Beam current (nA)	175	180	200	160

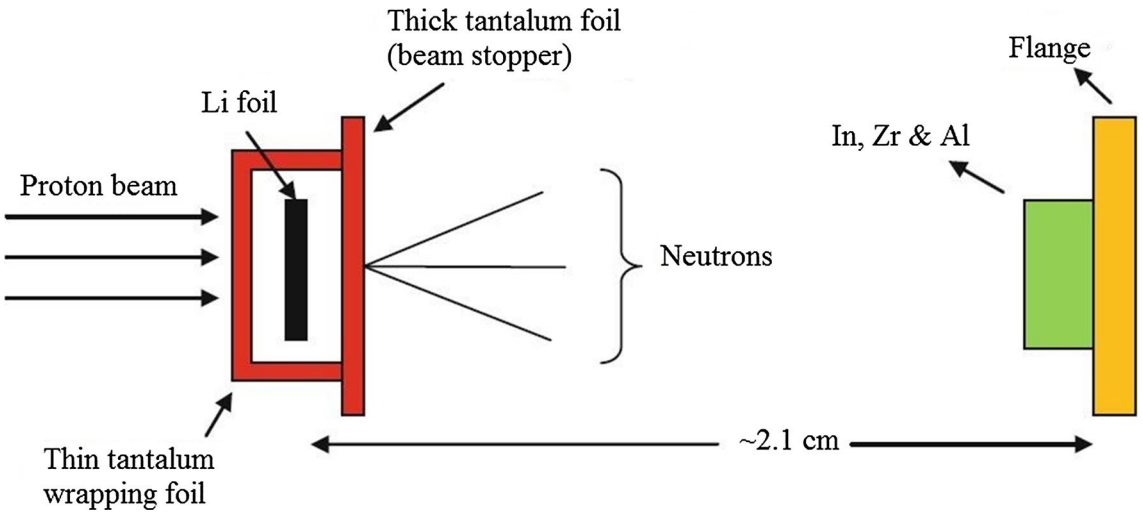

Fig. 1 A schematic diagram of experimental arrangements

γ-line of ^{60}Co. The detector dead time was kept below 5% throughout the counting. The efficiency calibration of the detector was carried out by using the characteristics γ-ray energies of ^{152}Eu ($T_{1/2} = 13.517 \pm 0.014$ year) source having activity $A_0 = 7767.73 \pm 86.99$ Bq on 1-October-1999. The nuclear spectroscopic data such as the γ-ray abundance and the γ-ray energies of ^{152}Eu source were retrieved from NuDat2.7 data [12, 13]. The distance between the Perspex plate and the end cap of the detector system was kept sufficient to minimize the summing effect. The respective γ-ray counting of target samples and monitors were recorded with increasing time for good counting statistics. A typical γ-ray spectrum of irradiated Zr target sample is shown in Fig. 2.

Data analysis

Estimation of average neutron energy and neutron flux

In the present experiment, the neutron energies were 10.95 ± 0.45, 13.97 ± 0.68, 16.99 ± 0.53 and 20.02 ± 0.58 MeV corresponding to proton beam energies of 13, 16, 19 and 22 MeV, respectively. The neutrons of different energies were generated by interaction of protons with ^{nat}Li target passing through Ta-Li-Ta stack. The degradation of the proton energy was calculated by SRIM software, which was 80–90 keV [14]. The threshold energy of ^{7}Li(p,n)^{7}Be reaction is $E_{th} = 1.881$ MeV, whereas for the first excited state $E_{th} = 2.37$ MeV. Therefore there is a contribution from a second group of neutrons from the ^{7}Li(p,n)^{7}Be reaction above 2.37 MeV proton energy. Above the proton energy of 4.5 MeV, there is a contribution from the three body interaction and other excited states in neutron production from main neutron group [15, 16]. Fig. 3 shows the neutron spectrum produced from the ^{7}Li(p,n) reaction, which consist contributions from sub neutron groups in the main peak as derived earlier [17–20]. The reaction cross-section was measured at the main neutron energy peak. The spectrum averaged neutron energy can be calculated using Eq. (1) [21].

$$E_{mean} = \frac{\int_{E_{ps}}^{E_{max}} E_i \Phi_i dE}{\int_{E_{ps}}^{E_{max}} \Phi_i dE} \quad (1)$$

where, E_{mean}: effective mean energy, E_{ps}: starting of peak neutron energy, E_{max}: maximum neutron energy, E_i: energy bin and Φ_i: neutron flux of energy bin E_i derived from literatures [17, 18]. As shown in Fig. 3, the neutron spectra have a quasi mono-energetic peak around E_p-1.881 MeV and a tail in a lower neutron energy region. The reaction cross-section due to the low energy neutrons from the tail part also contributes to the measured cross-section from the main neutron peak. Therefore this part must be removed, which is discussed in the next section.

In the present experiment, the ^{27}Al(n,α)^{24}Na and ^{115}In(n,n')^{115m}In reactions were used as monitor reactions to determine the neutron flux incident on the target samples.

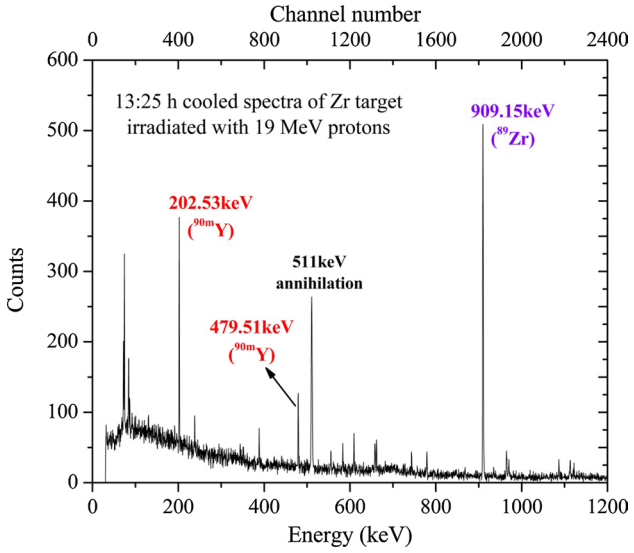

Fig. 2 Typical γ-ray spectrum for Zr target obtained by using HPGe detector

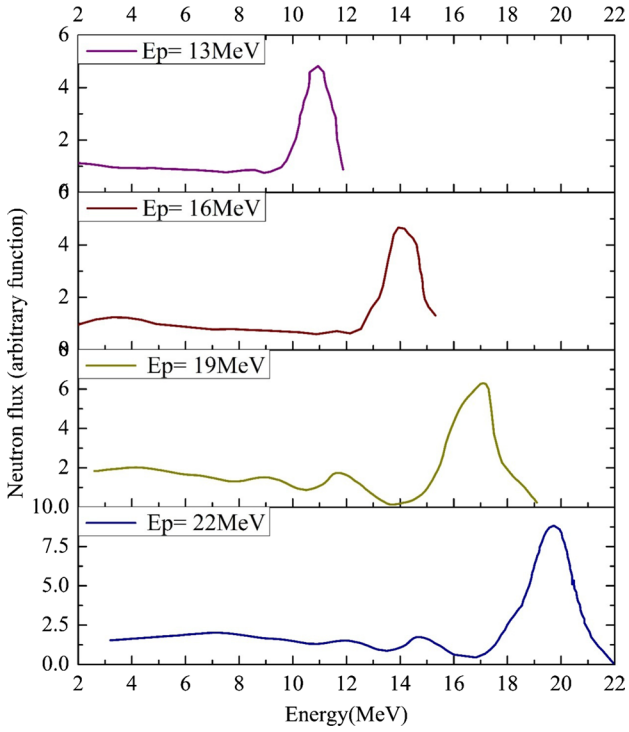

Fig. 3 Neutron spectra from the ^{7}Li(p,n)^{7}Be reaction with the proton energies of 13, 16, 19 and 22 MeV

The nuclear spectroscopic data of monitor reactions are given in Table 2 [12, 22, 23]. The measured neutron flux from the $^{27}Al(n,\alpha)^{24}Na$ and $^{115}In(n,n')^{115m}In$ monitor reactions for all four neutron energies are given in Table 3.

Estimation of $^{90}Zr(n,2n)^{89}Zr$ and $^{90}Zr(n,p)^{90m}Y$reactions cross-sections

The measurement of reaction cross-section was carried out by the method of neutron activation technique. The cross-section was measured from the recorded counts of the photo peak in the γ-ray spectrum using the activation formula-

$$\sigma = \frac{A_\gamma \lambda \left(\frac{CL}{LT}\right)}{NI_\gamma \varepsilon \left(1 - e^{-\lambda t_i}\right)\left(1 - e^{-\lambda t_c}\right) e^{-\lambda t_{CL}}} \quad (2)$$

where, Aγ: number of counts of photo peak, λ: decay constant (s^{-1}), CL and LT: clock time and live time for counting and CL/LT term is for dead time correction, N: number of atoms in target material,Φ: neutron flux, Iγ: absolute γ-ray intensity per decay of the residual nucleus (taken from Ref. [11]), ε: photo peak efficiency of the γ-rays, t_i: irradiation time and t_c: cooling time.

The nuclear spectroscopic data used for the calculation of $^{90}Zr(n,2n)^{89}Zr$ and $^{90}Zr(n,p)^{90m}Y$ reactions are given in Table 2 [12, 24, 25]. The threshold energy (E_{th}) of $^{90}Zr(n,2n)^{89}Zr$ reaction is 12.102 MeV, therefore, the reaction cross-sections were measured at average neutron energies of 13.97 ± 0.68, 16.99 ± 0.53 and 20.02 ± 0.58 MeV. Similarly, the threshold energy (E_{th}) of $^{90}Zr(n,p)^{90m}Y$ reaction is 1.512 MeV, therefore the reaction cross-sections were measured at 10.95 ± 0.45, 13.97 ± 0.68, 16.99 ± 0.53 and 20.02 ± 0.58 MeV neutron energies. The half-life of ^{89}Zr product nuclide is 78.41 ± 0.12 h, which decays by emitting γ-ray energy of 909.15 keV. The cross-section of $^{90}Zr(n,2n)^{89}Zr$ reaction was measured based on the observed activity of γ-ray energy of ^{89}Zr from the recorded γ-ray spectrum with sufficient cooling time. Similarly, for the $^{90}Zr(n,p)^{90m}Y$ reaction, the cross-section was measured from the observed activity of γ-ray energies of 202.53 keV and 479.51 keV emitted from ^{90m}Yproduct nuclide having half-life of 3.19 ± 0.06 h.

The $^{90}Zr(n,2n)^{89}Zr$ and $^{90}Zr(n,p)^{90m}Y$ reaction cross-sections measured in this experiment are given in Table 4. In this experiment, the actual reaction cross-section for the main peak neutrons was determined by subtracting the contribution from the lower energy neutrons. As shown in Fig. 3, it can be observed that these low energy neutrons have significant contribution in the actual measurement. The correction in the measured cross-section was carried out by tailing correction method by removing the contribution due to tail part as described in the literature [20, 21]. In order to do this, the cross-section due to the low energy tail part region was estimated by using TALYS-1.9 code [10] by folding the cross-section with the neutron flux distribution of neutron spectra as shown in Fig. 4. The cross-section due to tail part was calculated from the following relation.

Table 2 Nuclear spectroscopic data of monitor and target reaction products

Nuclear reaction	Threshold energy E_{th} (MeV)	Half-life of product	E_γ (keV)	I_γ (%)	Decay mode
$^{27}Al(n,\alpha)^{24}Na$	3.249	14.997 ± 0.012 h	1368.63 ± 0.05	99.9936 ± 0.0005	β^-(100%)
$^{115}In(n,n')^{115m}In$	–	4.486 ± 0.004 h	336.24 ± 0.25	46.0 ± 0.2	*IT (95.0%)* β^- *(5.00%)*
$^{90}Zr(n,2n)^{89}Zr$	12.102	78.41 ± 0.12 h	909.15 ± 0.15	99.04 ± 0.03	ε (100%)
$^{90}Zr(n,p)^{90m}Y$	1.512	3.19 ± 0.06 h	202.53 ± 0.03 479.51 ± 0.05	97.3 ± 0.4 90.74 ± 0.05	IT (*100%*)

Table 3 Spectrum averaged cross-section and neutron flux from different monitor reactions

	Set-1	Set-2	Set-3	Set-4
Proton energy (MeV)	13	16	19	22
Neutron energy from Eq. (1) (MeV)	10.95 ± 0.45	13.97 ± 0.68	16.99 ± 0.53	20.02 ± 0.58
Measured neutron flux based onthe $^{27}Al(n, \alpha)^{24}Na$ reactionmonitor (n cm^{-2} s^{-1})	1.3237×10^6	1.1706×10^6	2.4549×10^6	3.3569×10^6
Measured neutron flux based onthe $^{115}In(n,n')^{115m}In$ reaction monitor (n cm^{-2} s^{-1})	1.3343×10^6	1.1980×10^6	2.4621×10^6	3.3939×10^6

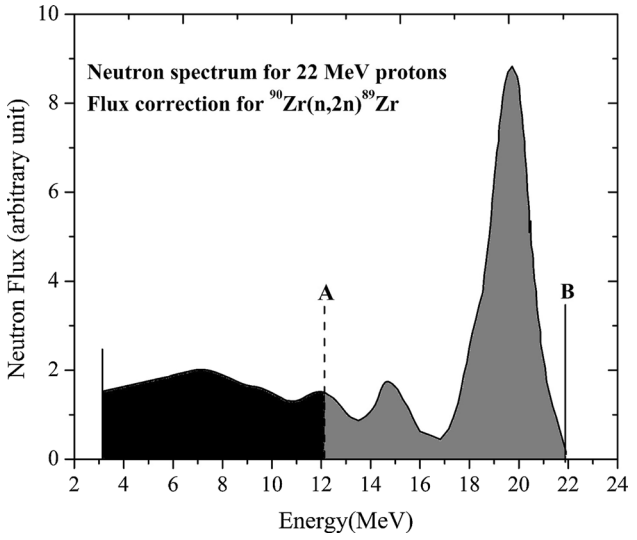

Fig. 4 Neutron flux correction for threshold energy reactions, A labeled as ^{90}Zr(n,2n)^{89}Zr reaction threshold energy of 12.102 MeV and B labeled as maximum neutron energy

$$\langle \sigma_{tail} \rangle = \frac{\int_{E_{th}}^{E_{ps}} \sigma(E)\Phi(E)dE}{\int_{E_{th}}^{E_{ps}} \Phi(E)dE} \quad (3)$$

where, E_{th}: threshold energy of the corresponding reaction and E_{ps}: minimum energy of the main peak region for the proton energies of 13, 16, 19 and 22 MeV.

In the present case, both the reactions have threshold energy; therefore the corrected neutron flux has been used tomeasurethe actual cross-section. The threshold energy (E_{th}) of ^{90}Zr(n,2n)^{89} Zr reaction is 12.102 MeV, therefore the neutron flux for this reaction must be the area under the curve which is from A (E_{th}) to B (E_{max}) as shown in Fig. 4. By using this flux, the cross-section of ^{90}Zr(n,2n)^{89}Zr reaction for all neutron energies have been calculated. To remove the tailing part, the cross-section was estimated by TALYS-1.9 from threshold energy—E_{th} (A) to the minimum energy of the main peak started—E_{ps} (B). By using Eq. (3), the spectrum averaged cross-section was calculated, which was subtracted from the measured cross-sections. This gives the final cross-section value for the main peak neutron energy. Similarly, for the ^{90}Zr(n,p)^{90m}Y reaction, final cross-sections has been determined at 10.95 ± 0.45, 13.97 ± 0.68, 16.99 ± 0.53 and 20.02 ± 0.58 MeV neutron energies.

Table 4 Basic keywords and the corresponding values used in the input file of the TALYS-1.9 and EMPIRE-3.2.2 code in order to reproduce the cross-sections of present work

TALYS-1.9	EMPIRE-3.2.2
ldmodel 3	LEVDEN 3
widthmode 1	HRTW 3
widthfluc 11.968	GSTRFN 1
gammax 2	OMPOT 2411 1(n)
strength 1	OMPOT 5411 2(p)
localomp y	DIRECT 0
preeqmode 2	PCROSS 1.5

Theoretical calculations

Theoretically, the ^{90}Zr(n,2n)^{89}Zr and ^{90}Zr(n,p)^{90m}Y reaction cross-sections were predicated by TALYS-1.9 [10] and EMPIRE-3.2.2 [11] codes over the neutron energy range from reaction threshold to 22 meV. TALYS code is basically used for the analysis and to generate nuclear data for all reaction channels involving projectiles like neutrons, protons, photons, deuterons, tritons, ^{3}He- and α- particles with target nuclides of mass 5 and heavier in the energy range of 1 keV to 200 eMeV [26]. In TALYS, different nuclear models are used to generate reaction cross-sections with various buildup parameter options including those compiled in the Reference Input Parameter Library RIPL-3 database [27]. In the present case, for the prediction of reactions cross-sections, the local optical model potential (OMP) proposed by Koning and Delaroche [28] was used for the outgoing neutrons and protons. For the compound nucleus contributions, TALYS uses the Hauser–Feshback model [29]. For the pre-equilibrium contribution, the two-component exciton model proposed by Koning and Duijvestijn was used [30]. In addition, TALYS have six different level density models to predict reaction cross-section.The cross-section was predicted by all six level density models define as ldmodel-1 to ldmodel-6 [31–36].

EMPIRE-3.2.2 code was also used for the ^{90}Zr(n,2n)^{89}Zr and ^{90}Zr(n,p)^{90m}Y reaction cross-sections calculation over a neutron energy range from threshold to 22 MeV. This code provides the complete and precise information of reaction cross-sections on the basis of different reaction mechanisms [11, 37, 38]. The Hauser-Feshbach statistical model was taken in account for the calculation of the compound nucleus reaction cross-sections. In EMPIRE code, different formulations (LEVDEN 0–3) of the nuclear level densities have been provided with different parameterization. In the present case, the calculations have been done with all available LEVDEN options [11]. The transmission coefficients were determined through optical model routines, which were implemented via the ECIS06 code [39, 40] and for the direct reactions; spherical optical model calculations were performed. The optical model parameters proposed by Koning and Delaroche [28] and Morillon and Romain [41] were used in the present calculations for the outgoing protons and neutrons. The width fluctuation corrections were carried out by considering the Hofmann,

Table 5 Comparison of reaction cross-section from present work with the available data from literature

Energy (MeV)	Measured	Tailing correction [10]	Final	EXFOR*	
^{90}Zr(n,2n)^{89}Zr reaction cross-section (mb)					
13.97 ± 0.68	515.24	–	515.2 ± 37.4	539.7 ± 11.9	Jiuzi et al. [53]
16.99 ± 0.53	1118.88	107.08	1011.8 ± 72.94	1086 ± 36	Pavlik et al. [54]
20.02 ± 0.58	1633.88	542.78	1091.1 ± 78.66	1200 ± 80	Semkova et al. [52]
^{90}Zr(n,p)^{90m}Y reaction cross-section (mb)					
10.95 ± 0.45	6.72	0.83	5.89 ± 0.41	5.41 ± 0.07	Raics et al. [62]
13.97 ± 0.68	9.71	0.86	8.85 ± 0.64	11.8 ± 0.6	Filatenkov [51]
16.99 ± 0.53	13.74	1.51	12.23 ± 0.88	12.1 ± 0.2	Marcinkowski et al. [63]
20.02 ± 0.58	10.69	3.24	7.45 ± 0.54	8.4 ± 0.8	Semkova et al. [52]

*Literature data are near to the values of present work

Richert, Tepel, and Weiden muller (HRTW) model up to incident neutron energy of 3 meV [42]. Gamma emission was described by using the Modified Lorentzian (MLO1) γ-ray strength functions given by Plujko [43], with parameters taken from the RIPL-3 database [27]. The classical exciton model [44] was used by means of the PCROSS code [11] with the default mean free path parameter (PCROSS-1.5) for the pre-equilibrium emission mechanism. The basic input parameters used in TALYS-1.9 and EMPIRE-3.2.2 input file to reproduce the cross-sections of present work are given in Table 5.

Covariance analysis

Covariance analysis is a technique to calculate the uncertainties in the measured data. The error propagation technique [18] has been used by several authors to estimate the true uncertainties in the measured cross-sections. The technique allows us to propagate errors from each individual quantity, which has been used in the measurement, into the final measured data. The flow of the calculations is rather simple and has two stages. Firstly, we calculate the covariance and correlations among the detector efficiencies and then we use the information from first stage into the second to calculate the covariance and correlations in the measured data.

Covariance analysis in the detector efficiencies

The geometry dependent efficiency of a detector is given by the following relation.

$$\epsilon_g = K_c \frac{A_{obs}}{N_o I_\gamma e^{-\lambda T} \nabla t} \tag{4}$$

where, A_{obs}: the observed count of the γ-ray with branching ratio I_γ, N_o: strength of the calibration source at the time of manufacturing, T: time between the manufacture of calibration source and date of experiment, ∇t: counting time for calibration source, and K_c: summing factors for the detector efficiencies calculated using the EFFTRAN code [45].

The above equation is expended in terms of four attributes, $\epsilon = f\left(A_{obs}, N_0, I_\gamma, t_{1/2}\right)$. The complete process of the calculations is similar to that of adopted by the others [17–19]. The present experiment was performed using a common detector setup for the cross-section measurement of two reactions; therefore, the two data sets are correlated by the efficiencies of the detector. The partial uncertainties in four attributes mentioned above are listed in Table 6. The covariance $\left(V_{\epsilon_{ij}}\right)$ of the efficiencies of the calibration source are given in Table 7. Now that we have found the correlating factors in the detector efficiencies for calibration source, we must now use this information to find the efficiencies, their uncertainties, and correlations among the γ-rays of sample and monitor reaction residues. This can easily be done by considering a model,

$$\ln \epsilon_i = \sum_m P_m (\ln E_i)^{m-1} \tag{5}$$

where, ϵ_i are efficiencies considered in the cross-section calculations, P_m are fitting parameters of order m and E_i iscorresponding γ-ray energies. The above equation can be written as Z = AP, with fitting parameters $P_m$and the corresponding covariance matrix V_p, is given as,

$$P_m = V_p\left(A' V_Z^{-1} A\right) \tag{6}$$

where, V_z matrix can be obtained as,

Table 6 Partial uncertainties in the efficiency

Energy (keV)	A_{obs}	I_γ	N_0	$T_{1/2}$	Total uncertainty
121.8	0.000816	0.000572	0.001155	4.83E−06	1.743638
244.7	0.000783	0.000329	0.000703	2.94E−06	1.221808
443.9	0.000688	0.002138	0.000488	2.04E−06	0.946682
964	0.000265	0.000107	0.00025	1.05E−06	0.425977
1112	0.000258	0.000117	0.000226	9.43E−07	0.396565
1408	0.000182	7.13E−05	0.000187	7.83E−07	0.308867

Table 7 Covariance matrix ($V_{\epsilon_{ij}} \times 100$) for the detector efficiencies

0.0030938					
0.0008305	0.0015126				
0.0005763	0.0003507	0.0009057			
0.0002955	0.0001798	0.0001248	0.000184		
0.0002664	0.0001621	0.0001125	0.0000577	0.0001593	
0.0001346	0.0001346	0.0009340	0.00004790	0.0000432	9.68×10^{-5}

$$V_Z = \frac{\left(V_{\epsilon_{ij}}\right)}{\langle \epsilon_i \rangle \langle \epsilon_j \rangle}$$

The goodness of the fit can be obtained as,

$$\chi_m^2 = (Z - AP)' V_Z^{-1} (Z - AP) \tag{7}$$

By using above definitions, the fitting parameters for the detector efficiencies of sample and monitor reaction residues γ-rays were found to be

$$P_m = (-0.38370; -0.8694; 0.1693; 0.3208; -0.10); \chi_m^2 = 0.72$$

Now the calculated detector efficiencies, covariance and corresponding correlation parameters [17–19] are given in Table 8.

Covariance analysis in the uncertainty of measured cross-sections

The covariance analysis in the uncertainty of the measured cross-sections was calculated by using the ratio method [46], modifying the definition given in Eq. (2). The ratio method is a simple technique, which enable us to use the error of each quantity used in the calculations into the final uncertainty of the result. We rewrite the Eq. (2) as,

$$\sigma_R = \sigma_W \frac{A_s N_m \Phi_m I_{\gamma_m} \eta_{m,s} f_{\lambda_m}}{A_m N_s \Phi_s I_{\gamma_s} f_{\lambda_s}} \tag{8}$$

where, the terms have the meanings similar to Eq. (2). The subscript 's' and 'm' denotes quantities for sample and monitor reactions, respectively and the time factor '*f*' and '$\eta_{m,s}$' are defined as

$$f = \left(1 - e^{-\lambda t_i}\right)\left(1 - e^{-\lambda t_c}\right)\left(e^{-\lambda t_r}\right)/\lambda \tag{9}$$

$$\eta_{m,s} = \frac{\epsilon_m}{\epsilon_s}; \frac{\nabla \eta_{m,s}}{\eta_{m,s}} = Var(\epsilon_m) + Var(\epsilon_s) - 2Cov(\epsilon_m, \epsilon_s) \tag{10}$$

The partial uncertainties from each attribute in above equation can be communicated directly to the sample cross-section using the quadratic sum formula not for the decay constant because of its relation to the cross-sectionby an exponential function, therefore, the uncertainty in f can be denoted as,

Table 8 Detector efficiencies, their covariance and correlation factors for the γ-rays of sample and monitor residues

γ-Energy (keV)	Efficiency	Error	Covariance ($\times 10^5$)					Correlations				
202.53	0.069118	0.001639	0.268647					1				
336.24	0.051709	0.000963	0.056928	0.092827				0.360	1			
479.51	0.040575	0.000891	−0.00937	0.075224	0.079363			−0.064	0.876	1		
909.15	0.023447	0.000397	0.018138	0.016666	0.019337	0.015724		0.279	0.436	0.547	1	
1386.6	0.016727	0.000295	0.013596	0.011913	0.008049	0.004203	0.008685	0.281	0.419	0.306	0.359	1

Table 9 Partial uncertainties of the ^{90}Zr(n,2n)^{89}Zr reaction cross-section measurements with respect to the ^{27}Al(n, α)^{24}Na monitor reaction

C_r	C_m	I_r	f(r)	f(m)	w_r	w_m	σ_W	a_r	A_r	A_m	I_m	$\eta_{m,s}$
0.005073	0.0515	0.000303	0.114215	0.000639	0.011205	0.014230	0.088126	0.000583	2.19×10^{-5}	4.45×10^{-9}	1.5×10^{-5}	0.000285
0.002098	0.0669	0.000303	0.113844	0.000369	0.012162	0.019950	0.071952	0.000583	2.19×10^{-5}	4.45×10^{-9}	1.5×10^{-5}	0.000285
0.011467	0.0706	0.000303	0.114509	0.000336	0.01923	0.024890	0.086428	0.000583	2.19×10^{-5}	4.45×10^{-9}	1.5×10^{-5}	0.000285

$$\left(\frac{\nabla f}{f}\right)^2 = \left(\frac{\lambda t_i e^{-\lambda t_i}}{1-e^{-\lambda t_i}} - \lambda t_c + \frac{\lambda(LT)e^{-\lambda(LT)}}{1-e^{-\lambda(LT)}} - 1\right)\left(\frac{\nabla \lambda}{\lambda}\right)^2 \tag{11}$$

The covariance matrix,$V_{(CS)_{ij}}$, for the cross-section values were calculated by using the method similar to the step one. The cross-sections for the (n,p) and (n,2n) reactions were treated independent due to the use of different monitors in the calculations. The partial uncertainties for the two combinations of reactions ^{90}Zr(n,2n)^{89}Zr with ^{27}Al(n,α)^{24}Na monitor and ^{90}Zr(n,p)^{90m}Y with ^{115}In(n,n')^{115m}In monitor are given in Tables 9 and 10. The covariance and correlations for the same sets of the measurements are given in Tables 11 and 12. The final uncertainty in the measured data can now be found out by taking the square root of the diagonal elements of the covariance matrix for respective neutron energy.

Results and discussion

In the present experiment, the ^{90}Zr(n,2n)^{89}Zr and ^{90}Zr(n,p)^{90m}Y reaction cross-sections were measured in neutron energy range from 10.95 to 20.02 MeV. The quasi-monoenergetic neutrons were produced from the ^{7}Li(p,n) reaction. The efficiency calibration of HPGe detector was performed by using standard ^{152}Eu source. The neutron fluxes at different energies were measured by using the ^{27}Al(n,α)^{24}Na and ^{115}In(n,n')^{115m}In monitor reactions and the correction factor in the neutron flux was incorporated for the measurement of cross-sections at all neutron energies. As mentioned earlier, the ^{90}Zr(n,2n)^{89}Zr and ^{90}Zr(n,p)^{90m}Y reaction cross-sections measured in this experiment are given in Table 5. The uncertainties in the present measurements shown in Table 5 were calculated by using covariance analysis and were found to be 15–26%.

For comparison, the literature data [47–52] of comparable neutron energies of present work are also given in Table 4. The comparison of present experimental results along with previously measured data by different authors from EXFOR [8], predicted cross-section data by TALYS-1.9 [10] and EMPIRE-3.2.2 [11] codes with optimized parameters as well as the cross-sections from evaluated data libraries [47, 48, 53, 54] are presented in Figs. 5 and 6. The comparison of ^{90}Zr(n,2n)^{89}Zr reaction cross-section with TALYS-1.9 is show in Fig. 5a and with EMPIRE -3.2.2 code is shown in Fig. 5b. From Table 5 and Fig. 5, it can be seen that the cross-section of ^{90}Zr(n,2n)^{89}Zr reaction at the neutron energies of 13.97 ± 0.68 and 16.99 ± 0.53 MeV are in good agreement with previously published cross-section by Jiuzi et al. [55] and Pavlik et al. [56]. However, the ^{90}Zr(n,2n)^{89}Zr reaction cross-section at the neutron energy of 20.02 ± 0.58 MeV from the present work is slightly lower than the data reported by Semkova et al. [50] at 20.1 ± 0.1 MeV. It can be also seen from Fig. 5 that the experimental ^{90}Zr(n,2n)^{89}Zr reaction cross-section from the present work and the EXFOR [8] based literature data are in excellent agreement with the evaluated data from ENDF/B-VIII.0 [53], JENDL-4.0 [54], JEFF-3.3 [47] and ROSFOND-2010 [48] libraries.

Similarly, it can be also seen from Table 4 and Fig. 6 that the ^{90}Zr(n,p)^{90m}Y reaction cross-sections are in good agreement with cross-section measured previously by Raics et al. [57], Marcinkowski et al. [58] and Semkova et al. [50] at 10.95 ± 0.45, 16.99 ± 0.0.53 and 20.02 ± 0.58 MeV neutron energies, respectively. Similarly, the^{90}Zr(n,p)^{90m}Y reaction cross-sections from the present work at the neutron energy of 13.97 ± 0.68 MeV is slightly lower than the data reported by Filatenkov [49] at 13.96 meV. Besides this, it can be seen from Figs. 5 and 6 that the data from the present work fill the gaps and follow the trend line of the previous experimental data [49, 50, 55–68].

The experimental data from the present work and EXFOR [8] based literature data for ^{90}Zr(n,2n)^{89}Zr and ^{90}Zr(n,p)^{90m}Y

Table 10 Partial uncertainties for the ^{90}Zr(n,p)^{90m}Y reaction cross-section measurements with respect to the ^{115}In(n, n')^{115m}In monitor reaction

C_r	C_m	I_r	f(r)	f(m)	w_r	w_m	σ_W	a_r	a_m	A_r	A_m	I_m	$\eta_{m,s}$
0.099	0.012	0.000404	0.114215	0.00097	0.013	0.011	0.035611	0.000583	0.000522	2.19×10^{-5}	4.35×10^{-8}	0.002179	0.117725
0.163	0.0094	0.000551	0.143867	0.00074	0.014	0.016	0.09713	0.000583	0.000522	2.19×10^{-5}	4.35×10^{-8}	0.002179	0.036589
0.15095	0.0071	0.000551	0.11314	0.00021	0.012	0.022	0.160262	0.000583	0.000522	2.19×10^{-5}	4.35×10^{-8}	0.002179	0.036589
0.204	0.0094	0.000551	0.11128	0.00027	0.012	0.013	0.10467	0.000583	0.000522	2.19×10^{-5}	4.35×10^{-8}	0.002179	0.036589

reactions within the neutron energies from threshold to 22 MeV follow the trend of theoretical values of based on TALYS-1.9 [10] and EMPIRE-3.2.2 [11] codes. However, for both the reactions, TALYS-1.9 with the generalized superfluid model matches the present data, whereas EMPIRE-3.2.2 with the Morillon et al. [41] and RIPL-3 microscopic HFB nuclear level density model (Fitted-EMPIRE) also matches the cross-sections of present work.

Conclusions

1. The ^{90}Zr(n,2n)^{89}Zr and ^{90}Zr(n,p)^{90m}Y reaction cross-sections were measured by the method of neutron activation and off-line γ-ray spectrometry in the neutron energy range of 10.95 to 20.02 meV.
2. The cross-section of ^{90}Zr(n,2n)^{89}Zr reaction at average neutron energies of 13.97 ± 0.68 and 16.99 ± 0.53 meV within uncertainties are in good agreement with the literature data. Similarly, the ^{90}Zr(n,p)^{90m}Y reaction cross-sections at the neutron energies of 10.95 ± 0.45, 16.99 ± 0.53 and 20.02 ± 0.58 meV within uncertainties are in good agreement with the literature data. Few data with discrepanciesare reported for both the reaction cross-sections within the neutron energy range of 16–22 meV in literature, therefore the present work will add the cross-sections points in this energy range and will enhance the IAEA-EXFOR database in this neutron energy range.
3. Theoretically, the reaction cross-sections were calculated by TALYS-1.9 and EMPIRE-3.2.2 codes with optimized input parameters from threshold to 22 meV. The results estimated by TALYS-1.9 and EMPIRE-3.2.2 based on suitable parameters for the ^{90}Zr(n,2n)^{89}Zr and ^{90}Zr(n,p)^{90m}Y reactions are in good agreement with the results of present work and literature.

Table 11 The measured data and the uncertainties along with the covariance and correlations for the $^{90}Zr(n,2n)^{89}Zr$ reaction

Energy (MeV)	Cross-section (mb)	Error	Covariance			Correlations		
13.97 ± 0.68	515.173	79.5072	0.0238			1		
16.99 ± 0.53	1011.788	153.992	0.0130	0.0232		0.553	1	
20.02 ± 0.58	1091.078	178.243	0.0131	0.0130	0.0267	0.518	1	1

Table 12 The measured data and the uncertainties along with the covariance and correlations for the $^{90}Zr(n,p)^{90m}Y$ reaction

Energy (MeV)	Cross-section(mb)	Error	Covariance				Correlations			
10.95 ± 0.45	5.897	1.014	0.0296				1			
13.97 ± 0.68	8.854	2.140	0.0162	0.0584			0.389	1		
16.99 ± 0.53	12.232	3.069	0.0127	0.0162	0.0630		0.293	0.267	1	
20.02 ± 0.58	7.452	1.922	0.0124	0.0159	0.0125	0.0665	0.280	0.255	0.193	1

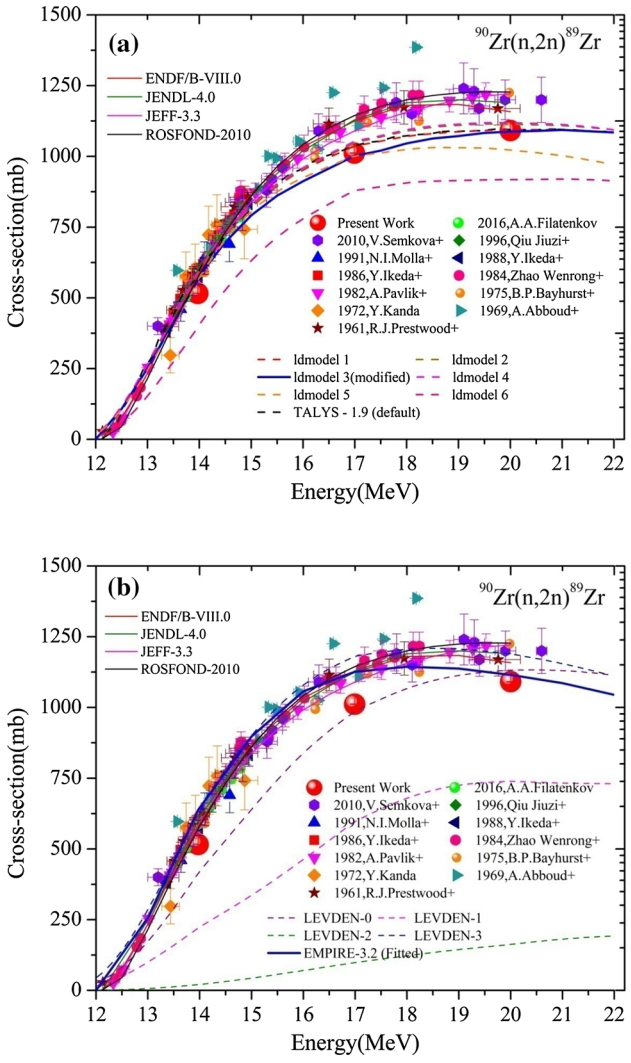

Fig. 5 **a** Comparison of experimental results of present work along with previously reported data in EXFOR [8], evaluated data in ENDF [9] and theoretically calculated data by TALYS-1.9 code [10] for the $^{90}Zr(n,2n)^{89}Zr$ reaction. **b** Comparison of experimental results of present work along with previously reported data in EXFOR[8], evaluated data in ENDF[9] and theoretically calculated data byEMPIRE-3.2.2[11] code for the$^{90}Zr(n,2n)^{89}Zr$ reaction

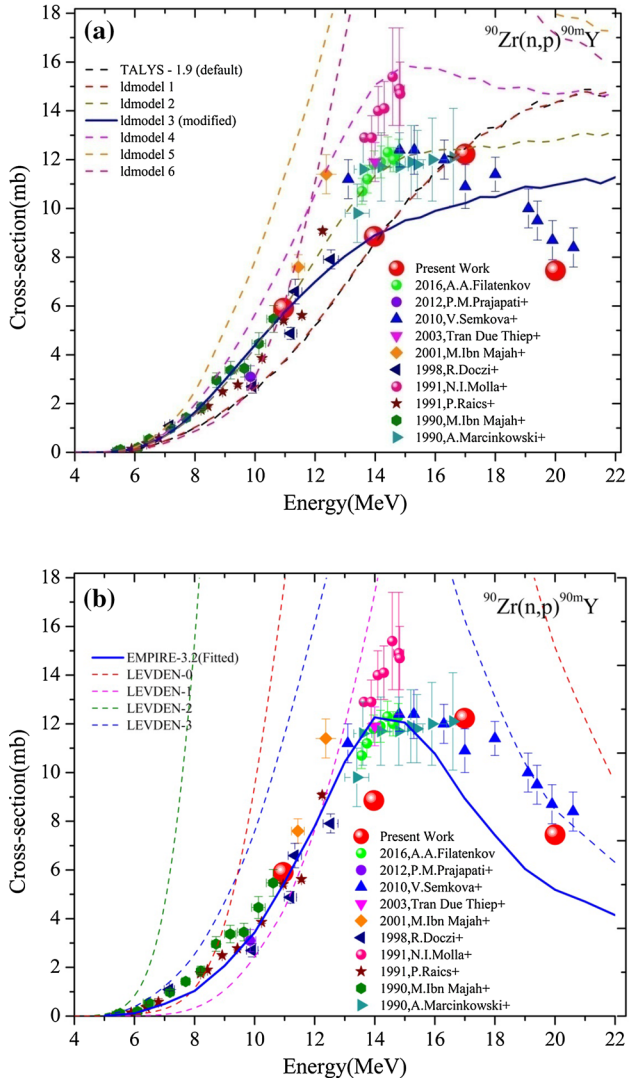

Fig. 6 **a** Comparison of experimental results of present work along with previously reported data in EXFOR [8], evaluated data in ENDF [9] and theoretically calculated data by TALYS-1.9 code [10] for the $^{90}Zr(n,p)^{90m}Y$ reaction. **b** Comparison of experimental results of present work along with previously reported data in EXFOR[8], evaluated data in ENDF[9] and theoretically calculated data by EMPIRE-3.2.2 [11] code for the$^{90}Zr(n,p)^{90m}Y$ reaction

Acknowledgements The authors would like to thank Dr. S.C. Sharma for his help in experimental set up. The author is grateful to the staff of BARC-TIFR Pelletron facility for allowing to use the Pelletron facility for the irradiation of experimental samples.

References

1. Krishnan R, Asundi MK (1980) Proc Indian Aead Sci (Eng Sci) 4:41–56
2. Lemaignan C, Motta AT (2006) Mater Sci Technol 15:4–47. https://doi.org/10.1002/9783527603978.mst0111,retrievedon8thMay2020
3. Kostal M, Schulc M, Rypar V et al (2017) Appl Radiat Isot 128:92–100
4. Uddin MS, Khandaker MU, Kim KS et al (2008) Nucl Instr Methods Phys Res B 266:13–20
5. Forrest RA (2006) Fusion Eng Des 81:2143
6. Aliberti G, Palmiotti G, Salvatores M (2006) Ann Nucl Energy 33:700
7. Shusterman JA, Scielzo ND, Thomas KJ et al (2019) Nature 565:328–330
8. EXFOR, Experimental Nuclear Reaction Data, http://www-nds.iaea.org/exfor, retrieved 8th May 2020
9. ENDL, Evaluated Nuclear Data Libraries, http://www-nds.iaea.org/endf/, retrieved 8th May 2020
10. Koning AJ (2018) TALYS-1.9, A Nuclear reaction program, user's manual, NRG-1755 ZG Petten, The Netherlands
11. Herman M et al (2007) Nucl Data Sheets 108:2655
12. NuDat 2.8 (2020) National Nuclear Data Center, Brookhaven National Laboratory. http://www.nndc.bnl.gov/nudat2, retrieved 8th May 2020
13. Martin MJ (2013) Nuclear data sheets for A = 152*. Nucl Data Sheets 114:1497–1847
14. Ziegler JF (2004) Nucl Instrum Methods Phys Res Sect B 219–220:1027–1036
15. Poppe CH, Anderson JD, Davis JC et al (1976) Phys Rev C 14:438
16. Mashnik SG, Chadwick MB, Hughes HG et al (2008) Los Alamos National Laboratory, Los Alamos, NM 87545, USA. arXiv:nucl-th/0011066v1
17. Soni B, Parashari S, Mukherjee S et al (2020) Eur Phys J Plus 135:300
18. Parashari S, Mukherjee S, Suryanarayana SV et al (2019) Phys Rev C 99:044602
19. Parashari S, Mukherjee S, Naik H et al (2019) Eur Phys J A 55:51
20. Makwana R, Mukherjee S, Mishra P et al (2017) Phys Rev C 96:024608
21. Smith DL et al. Corrections for Low Energy Neutrons by Spectral Indexing, retrieved from, https://www.oecdnea.org/science/docs/2005/nsc-wpec-doc2005-357.pdf, retrieved 8th May 2020
22. Firestone RB (2007) Nuclear Data Sheets for A = 24. Nucl Data Sheets 108(11):2319–2392
23. Blachot J (2012) Nuclear Data Sheets for A = 115. Nucl Data Sheets 113(10):2391–2535
24. Singh B (2013) Nuclear data sheets for A = 89. Nucl Data Sheets 114(1):1–208
25. Browne E (1997) Nuclear Data Sheets for A = 90. Nucl Data Sheets 82(3):379–546
26. Koning AJ, Rochman D (2012) Nucl Data Sheets 113(12):2841–2934
27. Capote R, Herman M, Oblozinsky P et al (2009) Nucl Data Sheets 110:3107
28. Koning AJ, Delaroche JP (2003) Nucl Phys A 713:231
29. Hauser W, Feshbach H (1952) Phys Rev 87:366
30. Koning AJ, Duijvestijn MC (2007) Nucl Phys A International Conference on Nuclear Data for Science and Technology 211–214
31. Gilbert A, Cameron AGW (1965) Can J Phys 43:1446
32. Dilg W, Schantl W, Vonach H, Uhl M (1973) Nucl Phys A 217:269
33. Ignatyuk AV, Istekov KK, Smirenkin GN (1979) Sov J Nucl Phys 29:450
34. Ignatyuk AV, Weil JL, Raman S, Kahane S (1993) Phys Rev C 47:1504
35. Goriely S, Hilaire S, Koning AJ (2008) Phys. Rev. C 78:064307
36. Hilaire S, Girod M, Goriely S, Koning AJ (2012) Phys Rev C 86:064317
37. Gandhi A et al (2019) J Radioanal Nucl Chem 322:89
38. Kalamara A et al (2019) Eur Phys J A 55:187
39. Raynal J, IAEA unpublished, SMR-9/8. 28
40. Raynal J (1972) Computing as a language of physics, in ICTP International Seminar Course, Trieste, Italy, IAEA, p 281
41. Morillon B, Romain P (2007) Phys. Rev. C 76:044601
42. Hofmann HM et al (1975) Ann Phys 90:403
43. Plujko VA (2000) Acta Phys Pol B 31:435
44. Griffin JJ (1966) Phys Rev Lett 17:478
45. Vidmar T, Kanish G, Vidmar G (2011) Appl Radiat Isot 69:908
46. Otsuka N et al (2017) Radiat Phys Chem 140:502
47. Koning AJ, Bauge E, Dean CJ et al (2011) J Korean Phys Soc 59:1057–1062
48. Zabrodskaya SV, Ignatyuk AV, Koscheev VN (2007) Nuclear constants, ROSFOND-2010, p. 1–2
49. Filatenkov AA (2016) Neutron activation cross sections measured at KRI in neutron energy region 13.4 - 14.9 MeV, Report: USSR report to the I.N.D.C.No.0460
50. Semkova V, Bauge E, Plompen AJM et al (2010) Nucl Phys A 832:149
51. Bayhurst BP, Gilmore JS, Prestwood RJ et al (1975) Phys Rev C 12:451
52. Abboud A, Decowski P, Grochulski W et al (1969) Nucl Phys A 139:42
53. Herman M, Trkov A (2018) Nucl Data Sheets 148:214–253
54. Shibata K, Iwamoto O, Nakagawa T et al (2011) J Nucl Sci Technol 48:1–30
55. Jiuzi Q, Junqian Y, Jingkang Y (1997) J Lanzhou Univ Nat Sci Ed 32:57
56. Pavlik A, Winkler G, Vonach H et al (1982) J Phys Part G (Nucl Part Phys) 8:1283
57. Raics P, Nagy S, Szegedi S, Kornilov NV, Kagalenko AB (1991) Conference on Nuclear Data for Science and Technology, Juelich, p 660
58. Marcinkowski A, Garuska U, Hoang HM et al (1990) Nucl Phys A 510:93
59. Kanda Y (1972) Nucl Phys A 185:177
60. Zhao Wenrong Lu, Hanlin FP (1984) Chin J Nucl Phys (Beijing) 6(1):80
61. Molla NI, Miah RU, Rahman M et al (1991) Conference on Nuclear Data for Science and Technology, Juelich, p 355
62. Ikeda Y, Konno C, Oishi K et al (1988) Report: JAERI Reports No.1312
63. Ikeda Y, Maekawa H, Nakamura T et al (1986) Radiat Eff 92:175
64. IbnMajah M, Chiadli A, Sudar S et al (2001) Appl Radiat Isot 54:655
65. Doczi R, Semkova V, Fenyvesi A et al (1998) Nucl Sci Eng 129:164
66. IbnMajah M, Qaim SM (1990) Nucl Sci Eng 104:271
67. Prajapati PM, Mukherjee S, Naik H et al (2012) Nucl Sci Eng 171:78
68. Thiep TD, Do NV, An TT, Son NN (2012) Nucl Phys A 722(2003):569

Applied Radiation and Isotopes 182 (2022) 110142

Contents lists available at ScienceDirect

Applied Radiation and Isotopes

journal homepage: www.elsevier.com/locate/apradiso

Cross-section of (n,2n) reaction for niobium and strontium isotopes between 13.97 to 20.02 MeV neutron energies

Mayur Mehta [a,b,*], N.L. Singh [a,h], Ratankumar Singh [a], Rakesh Chauhan [a], Rajnikant Makwana [a], S.V. Suryanarayana [c], H. Naik [d], P.V. Subhash [e,f], S. Mukherjee [a], Jan Varmuza [g], Karel Katovsky [g]

[a] Department of Physics, Faculty of Science, The M. S. University of Baroda, Vadodara, 390002, India
[b] Institute for Plasma Research, Gandhinagar, 382428, India
[c] Nuclear Physics Division, Bhabha Atomic Research Centre, Trombay, Mumbai, 400085, India
[d] Radiochemistry Division, Bhabha Atomic Research Centre, Trombay, Mumbai, 400085, India
[e] ITER-INDIA, Institute for Plasma Research, Gandhinagar, 382428, India
[f] Homi Bhabha National Institute, Anushaktinagar, Mumbai, 400094, India
[g] Department of Electrical Power Engineering, Brno University of Technology, Brno, 61600, Czech Republic
[h] Department of Physics, Netaji Subhas University of Technology, Delhi, 110078, India

ARTICLE INFO

Keywords:
^{93}Nb(n,2n)^{92}Nb^{m} and ^{88}Sr(n,2n)^{87}Sr^{m} reaction cross-sections
Activation and off-line γ-ray spectrometry
TALYS-1.9 code

ABSTRACT

The activation cross-sections of ^{93}Nb(n,2n)^{92}Nb^{m} and ^{88}Sr(n,2n)^{87}Sr^{m} reactions were measured using the activation and off-line γ-ray spectrometry technique in the neutron energy range 13.97–20.02 MeV. The present measurements have been done at the neutron energies where there are deficiencies and scarcity in the reaction cross-section data. The neutron flux was determined using the ^{27}Al(n,α)^{24}Na monitor reaction. The γ-ray self-attenuation effect and the low energy background neutron corrections were done in this experiment. The results of the present work were compared with the previously published data and evaluated nuclear data libraries. Theoretically, the cross-section for ^{93}Nb(n,2n)^{92}Nb^{m} and ^{88}Sr(n,2n)^{87}Sr^{m} reactions was predicted by TALYS-1.9 nuclear code and compared with the present results.

1. Introduction

The precise measurement of (n,2n) reaction cross-section of the reactor and structural materials is important for several applications in the areas of fusion-fission reactor technology, accelerator technologies, medical applications and nuclear waste management studies in the energy range from eV to MeV (Forrest, 2006; Wenrong et al., 1989; Kiraly et al., 2001; Ganesan, 2007; Padamsee, 1998). Moreover, the knowledge of model-based reaction cross-sections of fusion-fission materials is also important for better understanding and validation of experimental measurements (Yiğit, 2020a,b; Luo et al., 2018). and for the analysis of reaction Q-value (Yiğit, 2020a,b). Niobium (Nb) and strontium (Sr) are the structural materials for fusion and fission reactors and are important for their superconductive properties. Nb and Sr are prominent materials also used as superconducting magnets in the reactors. The ^{93}Nb(n,2n)^{92}Nb^{m} reaction cross-section was also used as a flux monitor and is important in neutron dosimetry within the energy range of 10–20 MeV (Pasha and Basavanna, 2019; Majerle et al., 2016; Honusek et al., 2011; Uno et al., 1996; Fessler et al., 2000; Santry and Werner, 1990; Filatenkov, 1999; Ikeda, 1993; Nethaway, 1978; Wenrong et al., 1989). The cross-section of ^{88}Sr(n,2n)^{87}Sr^{m} reaction was measured previously by different authors around 14 MeV energy but very few data with discrepancies are available in the neutron energy range between 15 and 20 MeV (Filatenkov, 2016; Guozhu et al., 2006; Konno, 1993; Bormann et al., 1976; Bormann, 1965; Srinivasa Rao et al., 1978; Molla, 1983; Salaita and Eapen, 1974; Hyvoenen-Dabek et al., 1978; Minetti and Pasquarelli, 1968). Therefore there is a need to obtain accurate cross-sections data in this energy region. In the present case, the cross-section of ^{93}Nb(n,2n)^{92}Nb^{m} reaction was measured at 13.97 ± 0.68 MeV and 20.02 ± 0.58 MeV whereas the ^{88}Sr(n,2n)^{87}Sr^{m} reaction cross-section was measured at 13.97 ± 0.68 MeV and 16.99 ± 0.53 MeV energies using activation and off-line γ-ray spectrometry technique. The experimentally measured results were compared with the literature data available in EXFOR (http://www.nds.iaea.or.at/exfor/(online)) and ENDF nuclear data libraries (https://www-nds.iaea.org/exfor/endf.htm (online)). The theoretical cross-sections were predicted by using

* Corresponding author. Institute for Plasma Research, Near Indira bridge, Bhat village, Gandhianagar, 382428, Gujarat, India.
E-mail address: mayur@ipr.res.in (M. Mehta).

https://doi.org/10.1016/j.apradiso.2022.110142
Received 1 December 2021; Received in revised form 4 February 2022; Accepted 4 February 2022
Available online 10 February 2022

TALYS-1.9 nuclear code (Koning et al., 2011).

The experimental details of the present work are given in Section II. The calculation of spectrum average neutron energy and reaction cross-section is provided in Section III. It also contains the calculation of correction factors to estimate the corrected reaction cross-sections. Section IV describes the theoretical calculations by using different nuclear models. The result and discussions are given in Section V followed by conclusions in Section VI.

2. Experimental details

The experimental work was carried out at 6-meter height of the 14UD BARC-TIFR (Bhabha Atomic Research Center-Tata Institute of Fundamental Research) Pelletron facility in Mumbai-India (Mehta, 2020). A lithium foil of thickness ~6.8 mg/cm^2 was wrapped in between ~4 mg/cm^2 thick tantalum (Ta) foil in the front and 0.1 mm Ta foil in the back. Then the accelerated proton beam energies of 16, 19 and 22 MeV were bombarded on natural lithium (^{nat}Li) foil, which generates neutron beams energies of 13.97 ± 0.68 MeV, 16.99 ± 0.53 MeV and 20.02 ± 0.58 MeV by the ^{7}Li(p,n)^{7}Be reaction. The energy spread for the proton beam at this port was 50–90 keV and the degradation of proton beam energy was calculated by SRIM code (Ziegler, 2004). The beam current was recorded during the experiments and it was in the range between 120 and 200 nA. A lithium foil was wrapped in between tantalum (Ta) foil of thickness ~4 mg/cm^2 in the front and 0.1 mm Ta foil in the back. The natural Nb-foil of dimension 10 × 10 mm^2 area and 0.8 mm thickness and natural Sr-foil of 10 × 10 mm^2 area and 0.3 mm thickness were kept at a distance of 2.1 cm after the Ta–Li–Ta stack in the forward direction. Aluminum (Al) foil of thickness 0.1 mm and 10x10 mm^2 area was used as flux monitor via the ^{27}Al(n,α)^{24}Na reaction (Mehta et al., 2020). The Nb and Sr samples were wrapped in 0.025 mm thick Al-foil to avoid radioactive contamination from one another during the irradiation. A schematic diagram of the experimental setup is shown in Fig. 1. Table 1 gives the details of proton energies, irradiation time and recorded beam current of the present experiment. The details of samples and monitor are given in Table 2.

The Al–Nb–Sr stack samples were irradiated for 5–7 hours at 16, 19 and 22 MeV proton beam energies of corresponding neutron beam energies 13.97 ± 0.68, 16.99 ± 0.53 and 20.02 ± 0.58 MeV to get sufficient activity in the irradiated samples for off-line γ-ray counting. After each irradiation, the target samples were cooled for sufficient time depending on the half-life of product nuclides. The stack was dismantled and the individual irradiated samples were mounted on different Perspex plates for offline γ-ray spectrometry. The γ-ray counting of the activated target samples was done by a pre-calibrated 80 cm^3 High Purity Germanium (HPGe) detector coupled to a PC-based 4K channel analyzer with GENIE software. The detector resolution had an FWHM of 1.82 keV at the photo-peak of 1332 keV γ-line of ^{60}Co. To keep the detector dead time within 5% and to avoid the pile-up effect, the samples were placed at a suitable distance from the end cap of the detector during γ-ray counting. The γ-ray counting of each sample was done with increasing time to have good counting statistics and to follow the half-life of the radionuclide of interest. The energy and efficiency calibration of the detector was carried out by using the characteristics γ-ray energies of standard ^{152}Eu source (Martin, 2013). The recorded γ-ray spectrum of the products from the ^{93}Nb(n,2n)^{92}Nb^m and ^{88}Sr(n,2n)^{87}Sr^m reactions with ^{27}Al(n,α)^{24}Na monitor reaction are shown in Fig. 2.

Table 1
Experimental details.

	Set-1	Set-2	Set-3
E_P (MeV)	16	19	22
E_n (MeV)	13.97 ± 0.68	16.99 ± 0.53	20.02 ± 0.58
Total irradiation time (hh:mm)	07:25	06:30	05:15
Beam current (nA)	120	200	160

Table 2
Details of irradiated samples in present experiment.

Isotope	E_n (MeV)	Sample	Isotopic abundance (%)	Density (g/cm^3)	Weight (mg)	Number of target atoms (× 10^{-4}atoms/b)
^{27}Al	13.97 ± 0.68	Al-foil	100	2.7	27.97	6.243
	16.99 ± 0.53				30.99	6.917
	20.02 ± 0.58				31.3	6.986
^{88}Sr	13.97 ± 0.68	Sr-foil	82.58	2.64	74.7	4.226
	16.99 ± 0.53				76.9	4.354
^{93}Nb	13.97 ± 0.68	Nb-foil	100	8.57	638.6	40.951
	20.02 ± 0.58				701.8	45.494

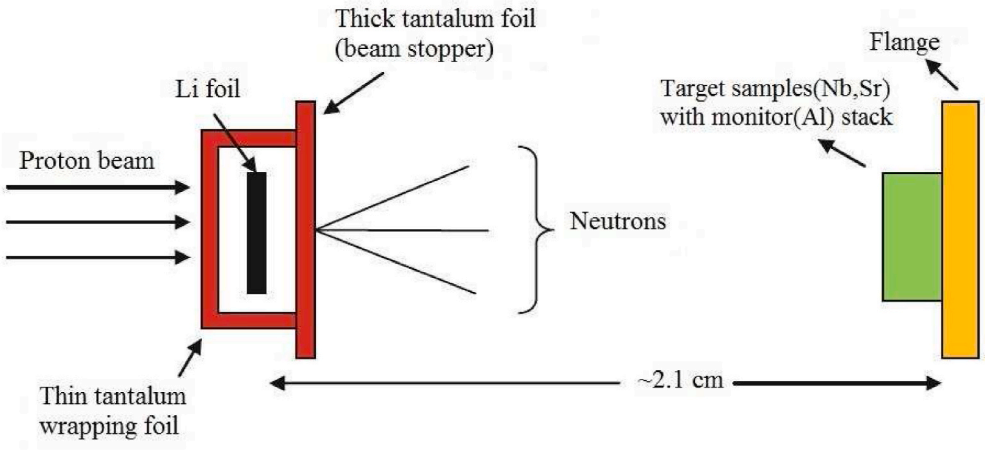

Fig. 1. A schematic diagram of irradiation set up.

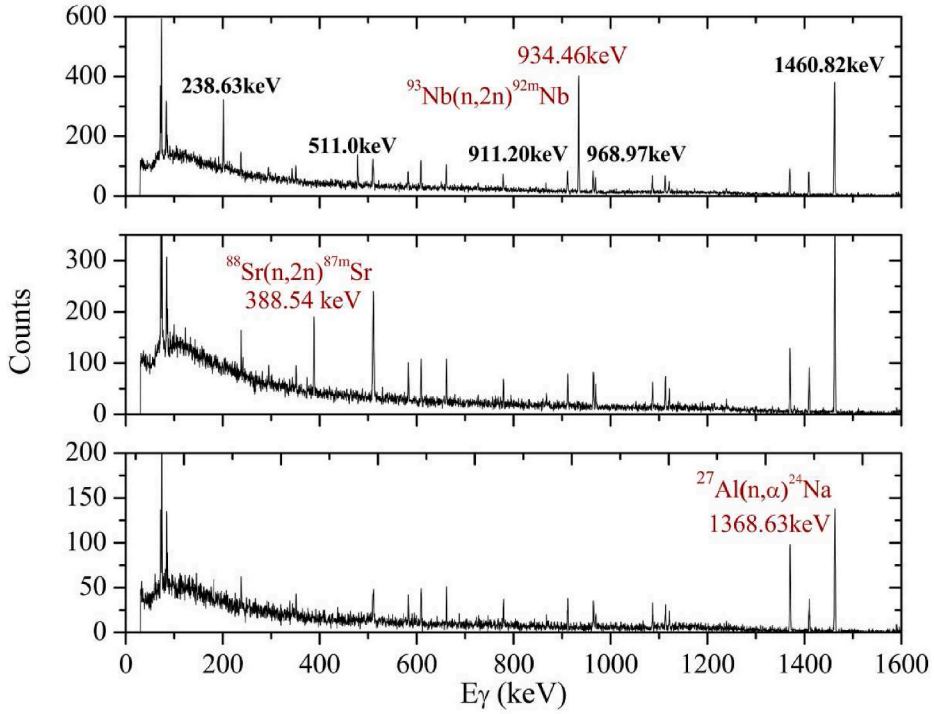

Fig. 2. Typical γ-ray spectra of $^{93}Nb(n,2n)^{92}Nb^{m}$, $^{88}Sr(n,2n)^{87}Sr^{m}$ and $^{27}Al(n,\alpha)^{24}Na$ reactions for $E_n = 13.97 \pm 0.68$ MeV recorded by HPGe detector.

3. Data analysis

3.1. Measurement of average neutron energy

In the present experiment, neutrons of desired energies were produced from the $^{7}Li(p,n)^{7}Be$ reaction. The proton beam energies of 16, 19 and 22 MeV were bombarded on the Ta–Li–Ta stack and respective average neutron beam energies of 13.97 ± 0.68 MeV, 16.99 ± 0.53 MeV and 20.02 ± 0.58 MeV were produced. When these high energy protons interact with ^{nat}Li, different reactions take place, which results in the generation of continuous neutron spectra as mentioned by Poppe and Anderson (1976) and Mashnik (2008). The threshold energy for production of ground state of ^{7}Be through the $^{7}Li(p,n)$ reaction is 1.88 MeV, therefore for proton energies of 16, 19 and 22 MeV, the corresponding first group (n_0) neutron energies were 14.12, 17.12 and 20.12 MeV. The threshold energy of the first excited state of ^{7}Be is 2.37 MeV, thus the energies of the second group of neutrons (n_1) were 13.63, 16.63 and 19.63 MeV. At high proton energies, $^{7}Li(p,\gamma)^{8}Be \rightarrow {}^{4}He + n$ (Q = −3.23 MeV) reaction channel also opens up which gives a continuous neutron energy distribution. The resulting neutron spectra for all three proton energies are shown in Fig. 3, which were derived from various available publications (Poppe and Anderson, 1976; Mashnik, 2008; Smith et al., 2005; Soni et al., 2020; McNaughton, 1975; Anderson et al., 1970). In fact, the neutron spectra for the proton energies of 16, 19 and 22 MeV based on the experimental arrangement of present work were generated by Soni et al. (2020) by using MCNP-6.1 code (Goorley et al., 2012). Thus in the present work, we have used the neutron spectra of Fig. 3. The spectrum averaged neutron energy can be given by the formula Smith et al. (2005):

$$E_{mean} = \frac{\int_{E_{ps}}^{E_{max}} E_i \Phi_i dE}{\int_{E_{ps}}^{E_{max}} \Phi_i dE} \quad (1)$$

where E_{mean} is the effective mean neutron energy, E_{ps} is the beginning of the neutron energy peak, E_{max} is the maximum neutron energy, E_i is the energy bin and Φ_i is a neutron flux of energy bin E_i. As shown in Fig. 3, E_{ps} = 12.1, 13.7, 16.9 and E_{max} = 15.3, 19.1 and 21.9 are the integration limit for the incident proton energies of 16, 19 and 22 MeV, respectively.

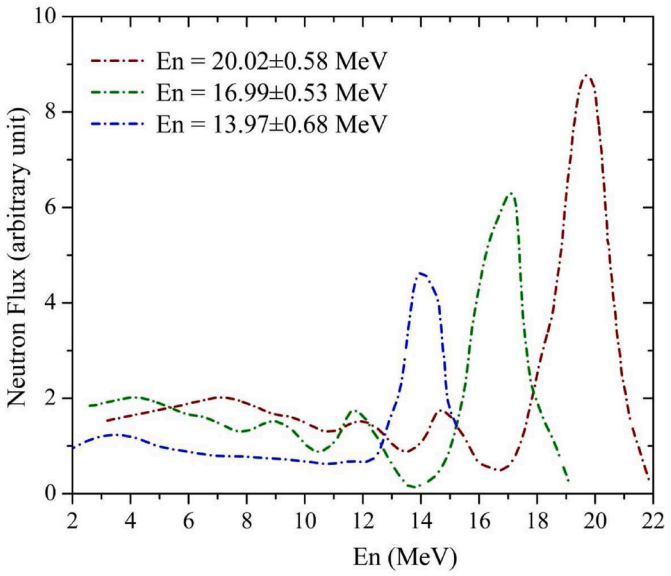

Fig. 3. Neutron spectra from the $^{7}Li(p,n)$ reaction with the proton energies of 16, 19 and 22 MeV.

3.2. Estimation of $^{93}Nb(n,2n)^{92}Nb^{m}$ and $^{88}Sr(n,2n)^{87}Sr^{m}$ reaction cross-sections

The cross-sections of $^{93}Nb(n,2n)^{92}Nb^{m}$ reaction at the neutron energies of 13.97 ± 0.68 MeV and 20.02 MeV ± 0.58 MeV and the cross-sections of $^{88}Sr(n,2n)^{87}Sr^{m}$ reaction at neutron energies of 13.97 ± 0.68 MeV and 16.99 ± 0.53 MeV were estimated by the ratio method using the formula:

$$\sigma_s(E_n) = \ < \sigma_m(E_n) > \eta \frac{C_s \lambda_s I_m a_m A_s W_m f_m}{C_m \lambda_m I_s a_s A_m W_s f_s} \times \frac{C_{attn.(s)}\ N_{corr.(s)}}{C_{attn.(m)}\ N_{corr.(m)}} \quad (2)$$

where, s and m subscript stands for sample and monitor, σ_s and σ_m are sample and monitor reaction cross-sections at the neutron energy E_n. The ^{27}Al(n,α)^{24}Na monitor cross-sections ($<\sigma_m>$) determined by the linear interpolation method using IRDFF-1.05 data (Zsolnay and Capote, 2012) which are 122.54 ± 0.59 mb, 76.457 ± 0.62 mb and 38.061 ± 0.50 mb corresponding to the neutron energies of 13.97 ± 0.68 MeV, 16.99 ± 0.53 MeV and 20.02 ± 0.58 MeV, respectively. η $(=\frac{\varepsilon_m}{\varepsilon_s})$ is the detector efficiency ratio for the characteristic γ-ray energies of monitor and sample reaction products, $C_{s,m}$ is the recorded photo-peak counts of the reaction products ^{92}Nb^m, ^{88}Sr^m and ^{24}Na, $\lambda_{s,m}$ is the decay constant, $a_{s,m}$ is the isotopic abundance of target nuclei, $A_{s,m}$ is the average atomic mass and $W_{s,m}$ is the weight of the sample and monitor foils. The needed parameters and nuclear spectroscopic data like half-life, γ-ray intensity, isotopic abundance with uncertainties used in Eq. (2) are given in Tables 2 and 3, respectively. The timing factor $f_{s,m}$ is given by the equation:

$$f_{s,m} = (1 - e^{-\lambda t_{irr}}) e^{-\lambda t_{cool}} (1 - e^{-\lambda t_{count}}) \quad (3)$$

where t_{irr}, t_{cool} and t_{count} are irradiation, cooling and counting time. $C_{attn.(s,m)}$ is the self-attenuation correction factor and $N_{corr.(s,m)}$ is the correction for non-primary neutrons determined in the following section.

In the present experiment, the primary neutrons produce from the ^{7}Li(p,n$_0$)^{7}Be reaction are not mono-energetic but have energy spread therefore the averaged monitor reaction cross-section was measured by the formula:

$$< \sigma_m > = \frac{\int_{E_{min}}^{E_{max}} \Phi_0(E)\sigma_m(E)dE}{\int_{E_{min}}^{E_{max}} \Phi_0(E)dE} \quad (4)$$

where the point wise monitor cross-section $\sigma_m(E)$ was taken from IRDFF-1.05 (Zsolnay and Capote, 2012) and folded with the neutron energy flux spectrum $\Phi_0(E)$. The corrected neutron flux determined by considering γ-ray self-attenuation and background low energy neutron correction is given in Table 6.

3.3. Corrections

The γ-ray self-attenuation correction is required in γ-ray spectrometry analysis due to the interaction of γ-rays in samples. The γ-ray self-attenuation correction factor for γ-ray energies of ^{92}Nb^m, ^{87}Sr^m and ^{24}Na radio-nuclide is given by:

$$C_{attn.(s,m)} = \frac{(1 - e^{-\mu t})}{\mu t} \quad (5)$$

where, μ is the mass-absorption coefficient retrieved from XMuDat version 1.01 (Nowotny, 1998) and t is the thickness of the sample foils. Similarly, the low energy background neutron correction is calculated by the formula:

$$N_{corr(s,m)} = 1 - \frac{\int_{Emin}^{Emax} \Phi_1(E)\sigma_x(E)dE}{\int_{Emin}^{Emax} \Phi(E)\sigma_x(E)dE} \quad (6)$$

where, $\Phi(E) = \Phi_0(E) + \Phi_1(E)$, in which $\Phi_1(E)$ is the secondary neutron flux energy spectrum and $\Phi_0(E)$ is the primary neutron flux energy spectrum. σ_x is the ^{93}Nb(n,2n)^{92}Nb^m and ^{88}Sr(n,2n)^{87}Sr^m reaction cross-sections taken from JEFF-3.3 (Plompen et al., 2020) and ^{27}Al(n,α)^{24}Na monitor cross-section taken from IRDFF-1.05 (Zsolnay and Capote, 2012). Table 4 summarizes the γ-ray self-attenuation and low energy correction factor for monitor and sample reactions at the neutron energies of 13.97 ± 0.68, 16.99 ± 0.53 and 20.02 ± 0.58 MeV.

Table 3
Nuclear spectroscopic data with uncertainties taken from Refs (http://www.ndc.bnl.gov/nudat2/index.jsp).

Reaction	Product	Half-life	Eγ (keV)	Iγ(%)
^{27}Al(n,α)	^{24}Na	14.997 ± 0.012 h	1368.63	99.9936 ± 0.0015
^{93}Nb(n,2n)	^{92}Nb^m	10.15 ± 0.02 d	934.44	99.15
^{88}Sr(n,2n)	^{87}Sr^m	2.815 ± 0.012 h	388.53	82.19 ± 0.22

Table 4
Correction factors applied in the estimation of reaction cross-sections.

Reaction	E_n	Eγ(keV)	$C_{attn.}$	N_{corr}
^{27}Al(n,α)^{24}Na	13.97 ± 0.68	1368.626	1.00071	0.81309
	16.99 ± 0.53			0.63229
	20.02 ± 0.58			0.43170
^{88}Sr(n,2n)^{87}Sr^m	13.97 ± 0.68	388.531	1.00397	1
	16.99 ± 0.53			0.97818
^{93}Nb(n,2n)^{92}Nb^m	13.97 ± 0.68	934.44	1.0190	0.92783
	20.02 ± 0.58			0.69330

Table 5
The fractional (%) partial uncertainties in the measured cross-section due to different attributes of the present experiment.

Attributes		E_n = 13.97 ± 0.68 MeV	E_n = 16.99 ± 0.53 MeV	E_n = 20.02 ± 0.58 MeV
Counts	Nb	0.49955	–	1.47569
	Sr	0.0786	0.5341	–
	Al	3.1101	2.8917	1.2321
Weight	Nb	0.01566	–	0.01425
	Sr	0.13385	0.12992	–
	Al	0.3575	0.3227	0.3195
Intensity	Nb	0.01009	–	0.01009
	Sr	0.26767	0.26767	–
	Al	0.0015	0.0015	0.0015
Half-life	Nb	0.19704	0.19704	0.19704
	Sr	0.42629	0.42629	0.42629
	Al	0.08002	0.08002	0.08002
Efficiency	Nb	2.78571	–	2.78571
	Sr	2.22120	2.22120	–
	Al	1.70238	1.70238	1.70238
Monitor cross-section	$\sigma_{m\text{-}Al}$	0.48148	0.81091	1.3189
Total	Nb	5.0029	–	5.2114
	Sr	6.2254	6.9369	–

The uncertainties in the measured cross-sections of ^{92}Nb^m and ^{87}Sr^m isotopes were determined by considering the fractional partial uncertainties propagated from various attributes like the photo-peak counts ($C_{s,m}$), spectrum averaged monitor cross-section (σ_m), the detector efficiency (η), γ-ray intensity ($I_{s,m}$), the weight of samples ($W_{s,m}$) and timing factor ($f_{s,m}$). The uncertainty due to isotopic abundance of ^{93}Nb and ^{27}Al was not considered as their value is 100%. The fractional partial uncertainties of different attributes are given in Table 5. The neutron energies have an uncertainty of about 3%–5% and the cross-sections about 5% for the ^{93}Nb(n,2n)^{92}Nb^m reaction and about 6%–7% for the ^{88}Sr(n,2n)^{87}Sr^m reaction.

4. Nuclear model based calculations of reaction cross-section

TALYS is a software for the analysis and prediction of nuclear reaction cross-sections induced by neutrons, photons, protons, deuterons, tritons, ^{3}He- and alpha-particles within the energy range of 1 keV–200 MeV and for target nuclides of mass 12 and heavier (Koning et al., 2011; Koning and Rochman, 2012). The calculations are performed by ECIS06 code (Raynal, 1994). In the present case, TALYS-1.9 code is used for the calculations of ^{93}Nb(n,2n)^{92}Nb^m and ^{88}Sr(n,2n)^{87}Sr^m reaction cross-sections by considering default nuclear reaction models and various level density models (LD-models) between 13.97 and 20.02 MeV neutron energies. There are six different level density models available

Table 6
Comparison of $^{93}Nb(n,2n)^{92}Nb^{m}$ reaction cross-section.

E_n (MeV)	Flux ($\times 10^6$)	Cross-section (barn).									
		Measured	LD-1	LD-2	LD-3	LD-4	LD-5	LD-6	TENDL-2019	JENDL/AD-2017	JEFF-3.3
13.97 ± 0.68	1.361 ± 0.068	0.39875 ± 0.01983	0.51688	0.49607	0.46571	0.43454	0.42568	0.35075	0.45902	0.44799	0.45903
20.02 ± 0.58	5.466 ± 0.285	0.21660 ± 0.01126	0.28575	0.30573	0.29876	0.26342	0.25953	0.24358	0.32254	0.31928	0.32272

in TALYS-1.9 code, The constant temperature model (CTM) at low energies and Fermi gas model at high energies (Glibert and Cameron, 1965), the Back-shifted Fermi gas level density model (BFM) (Dilg et al., 1973), the Generalized Super-fluid Model (GSM) (Ignatyuk et al., 1979; Ignatyuk et al., 1993) and the models of microscopic level densities. (Goriely et al., 2001; Goriely et al., 2008; Hilaire et al., 2012). The comparison of present results with predicted cross-sections for the $^{93}Nb(n,2n)^{92}Nb^{m}$ reaction was shown in Fig. 4 for 10–24 MeV neutron energy and 12–20 MeV for the $^{88}Sr(n,2n)^{87}Sr^{m}$ reaction as shown in Fig. 5. The calculated reaction cross-sections using various level density models for both the reactions have significant difference, which are shown in Tables 6 and 7 at neutron energies of present interest.

5. Results and discussion

The experimental reaction cross-sections from this work along with the previously measured data, the available evaluated data from TENDL-2019, JENDL/AD-2017 and JEFF-3.3 and predicted data by TALYS-19 are shown in Figs. 4 and 5. Table 6 shows the comparison of $^{93}Nb(n,2n)^{92}Nb^{m}$ reaction cross-section measured at 13.97 ± 0.68 MeV and 20.02 ± 0.58 MeV neutron energies. The predicted data from TALYS-1.9 overestimate the present data at 13.97 ± 0.68 MeV by about ~14%–20% for LD-1 to LD-3 models and ~ 6%–12% for LD-4 to LD-6 models while the evaluated data from TENDL-2019, JENDL/AD-2017 and JEFF-3.3 libraries overestimate the present data by ~11%–13% at 13.97 ±

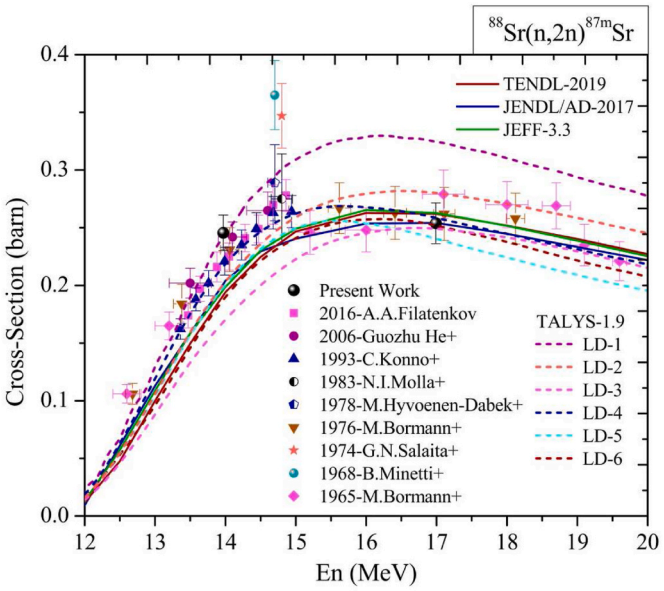

Fig. 5. Comparison of $^{88}Sr(n,2n)^{87}Sr^{m}$ reaction cross-section with the previously published data, evaluated data and predicated data by TALYS-1.9 code.

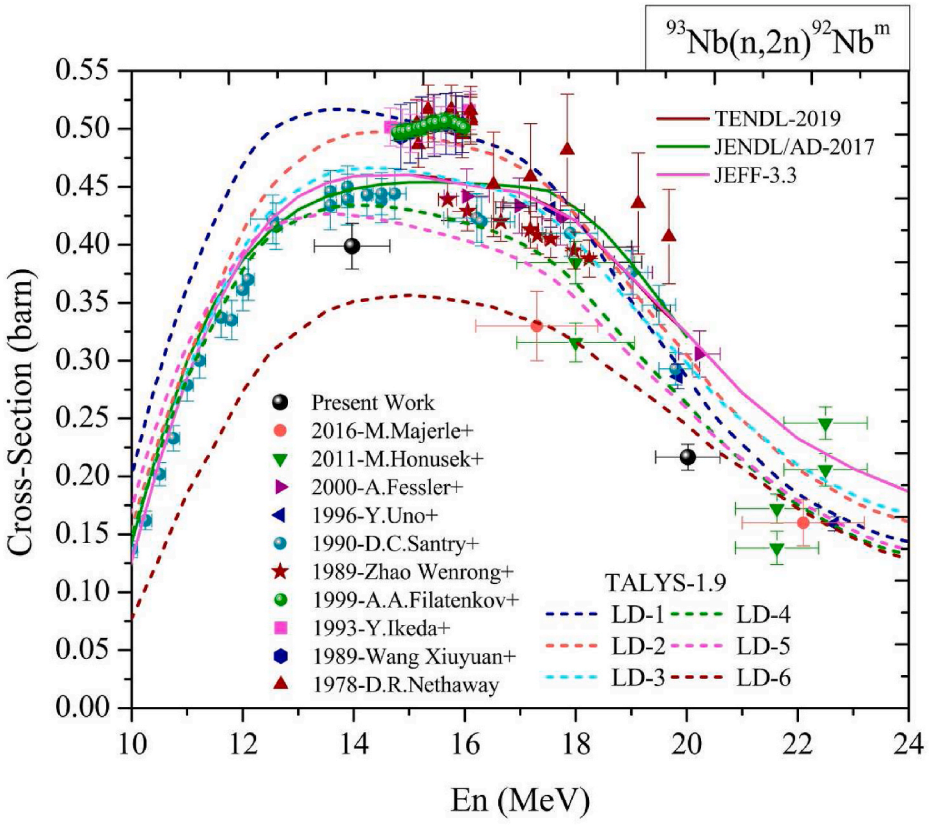

Fig. 4. Comparison of $^{93}Nb(n,2n)^{92}Nb^{m}$ reaction cross-section with the previously published data, evaluated data and predicated data by TALYS-1.9 code.

Table 7
Comparison of $^{88}Sr(n,2n)^{87}Sr^{m}$ reaction cross-section.

E_n (MeV)	Flux ($\times 10^6$)	Cross-section (barn)									
		Measured	LD-1	LD-2	LD-3	LD-4	LD-5	LD-6	TENDL-2019	JENDL/AD-2017	JEFF-3.3
13.97 ± 0.68	1.445 ± 0.091	0.24562 ± 0.01545	0.22484	0.20274	0.16903	0.21893	0.20078	0.18975	0.19200	0.20216	0.19647
16.99 ± 0.53	3.803 ± 0.264	0.25387 ± 0.01765	0.28956	0.28103	0.25000	0.25914	0.24116	0.25214	0.26200	0.25420	0.26276

0.68 MeV. For 20.02 ± 0.58 MeV, the predicated data overestimated the present data by ~11%–27% for LD-1 to LD-6 models and the evaluated data overestimate the present data by ~31–33%.

Table 7 shows the comparison of $^{88}Sr(n,2n)^{87}Sr^{m}$ reaction cross-sections at 13.97 ± 0.68 MeV and 16.99 ± 0.53 MeV energies. The predicted data from TALYS-1.9 underestimate the present data by 17%–30% for LD-2 to LD-6 models and ~8% for LD-1 model while the evaluated data from TENDL-2019, JENDL/AD-2017 and JEFF-3.3 libraries underestimate the present data by ~17%–21% at 13.97 ± 0.68 MeV. For 16.99 ± 0.53 MeV, the predicated data overestimate by ~9%–12% for LD-1 and LD-2 models and ~0.7%–5% for LD-3 to LD-6 models. The evaluated data overestimated the present data by ~0.1–3% at 16.99 ± 0.53 MeV.

6. Conclusion

The formation cross-sections of $^{92}Nb^{m}$ and $^{87}Sr^{m}$ isotopes from the (n,2n) reaction of ^{93}Nb and ^{88}Sr were determined within the neutron energy range of 13.97 MeV–20.02 MeV by using the activation and off-line γ-ray spectroscopic method. The $^{93}Nb(n,2n)^{92}Nb^{m}$ reaction cross-sections have discrepancies around 12% compared to the previously measured data (Xiuyuan et al., 1989) at 13.97 ± 0.1 MeV and around 29% compared to the previously published data (Fessler et al., 2000) at 20.229 ± 0.375 MeV. Similarly, the $^{93}Nb(n,2n)^{92}Nb^{m}$ reaction cross-section data predicted by TALYS-1.9 have discrepancies with present data around ~6% for LD-5 model at 13.97 MeV and around ~11% for LD-6 model at 20.02 MeV neutron energies. The $^{88}Sr(n,2n)^{87}Sr^{m}$ reaction cross-section have the discrepancy is about 10% in between the present data and the earlier reported data by (Konno et al., 1993) at 13.99 MeV and about 3%–9% with the reported data by (Bormann et al., 1976) at 17.11 ± 0.15 MeV. Similarly for the cross-section data predicated by TALYS-1.9, the discrepancies with the present data is around ~8% with LD-1 model at 13.97 MeV and around <1% with LD-6 model at 16.99 MeV. Very few cross-section data with large discrepancies are available from threshold to 18 MeV neutron energies. Above that, there is a deficiency in cross-section data for both the reactions; therefore the future work will be focused to carry out the experiments in the high neutron energy region to obtain the data with better accuracy to improve the nuclear data libraries.

CRediT authorship contribution statement

Mayur Mehta: Writing – review & editing, Writing – original draft. **N.L. Singh:** Writing – review & editing, Supervision, Conceptualization. **Ratankumar Singh:** Formal analysis. **Rakesh Chauhan:** Data curation. **Rajnikant Makwana:** Formal analysis. **S.V. Suryanarayana:** Formal analysis. **H. Naik:** Writing – review & editing, Methodology. **P.V. Subhash:** Writing – review & editing. **S. Mukherjee:** Writing – review & editing. **Jan Varmuza:** Software. **Karel Katovsky:** Software.

Declaration of competing interest

The authors declare that they have no known competing financial interests or personal relationships that could have appeared to influence the work reported in this paper.

Acknowledgment

The authors thank the staff of BARC-TIFR Pelletron facility-Mumbai for allowing us to use the irradiation facility and their continuous support to carry out the experiments smoothly. The authors also thank the staff of the target lab facility of TIFR for helping in sample preparation, which was used for irradiations.

References

Yiğit, Mustafa, 2020a. Investigation of (n,2n) reaction cross sections on Pd and Cd isotopes using equilibrium and pre-equilibrium models. Appl. Radiat. Isot. 166, 109399.
Anderson, J.D., Wong, C., Madsen, V.A., 1970. Charge exchange part of the effective two-body interaction. Phys. Rev. Lett. 24, 1074.
Bormann, M., 1965. Some excitation functions of neutron induced reactions in the energy range 12.6-19.6 MeV. Nucl. Phys. 63, 438.
Bormann, M., et al., 1976. (n,2n) excitation functions for Fe-54, Ge-70, Se-74,Rb-85, Sr-86,88, Y-89, Mo-92, and Hg-204 in the neutron energy region 13-18 MeV. Z. Phys. A: Hadrons Nucl. 277, 203.
Dilg, W., Schantl, W., Vonach, H., Uhl, M., 1973. Level density parameters for the back-shifted fermi gas model in the mass range 40 <A< 250. Nucl. Phys. 217 (2), 269–298.
Fessler, A., et al., 2000. Neutron activation cross-section measurements from 16 to 20 MeV for isotopes of F, Na, Mg, Al, Si, P, Cl, Ti, V, Mn, Fe, Nb, Sn, and Ba. Nucl. Sci. Eng. 134 (2), 171.
Filatenkov, A.A., 2016. Neutron Activation Cross Sections Measured at KRI in Neutron Energy Region 13.4-14.9 MeV, Report: USSR Report to the I. N.D.C.No.0460.
Filatenkov, A.A., et al., 1999. Systematic Measurement of Activation Cross Sections at Neutron Energies from 13.4 to 14.9 MeV, Report. Khlopin Radiev. Inst., Leningrad. Reports No.252.
Forrest, R.A., 2006. Data requirement for neutron activation: Part I : cross-section. Fusion Eng. Des. 81 (18), 2143–2156.
Ganesan, S., 2007. Nuclear data requirements for accelerator driven sub-critical systems - a roadmap in the Indian context. Pramana - J. Phys. 68, 257.
Glibert, A., Cameron, A.G.W., 1965. A composite nuclear-level density formula with shell corrections. Can. J. Phys. 43, 1446.
Goorley, T., et al., 2012. Initial MCNP6 release overview. Nucl. Technol. 180 (3), 298–315.
Goriely, S., Tondeur, F., Pearson, J.M., 2001. A Hartree-Fock nuclear mass table. Atomic Data Nucl. Data Tables 77, 311.
Goriely, S., Hilaire, S., Koning, A.J., 2008. Improved microscopic nuclear level densities within the Hartree-Fock-Bogoliubov plus combinatorial method. Phys. Rev. C 78, 064307.
Guozhu, He, et al., 2006. Cross-section measurements for (n,2n), (n,p) and (n,a) reactions on strontium at the neutron energy about 14MeV. Ann. Nucl. Energy 33, 37.
Hilaire, S., Girod, M., Goriely, S., et al., 2012. Temperature-dependent combinatorial level densities with the D1M Gogny force. Phys. Rev. C 86, 064317.
Honusek, M., Bem, P., Burjan, V., et al., 2011. Neutron activation experiments on niobium in NPI p-^{7}Li quasi-monoenergetic neutron field. J. Kor. Phys. Soc. 59, 1374.
Hyvoenen-Dabek, M., Tarvainen, M., Holmberg, P., 1978. 14 MeV neutron cross sections on Mg, Cl and Sr. J. Radioanal. Chem. 46, 357.
Ignatyuk, A.V., Istekov, K.K., Smirenkin, G.N., 1979. The role of collective effects in the systematics of nuclear level densities. Sov. J. Nucl. Phys. 29, 450.
Ignatyuk, A.V., Weil, J.L., Raman, S., Kahane, S., 1993. Density of discrete levels in 116Sn. Phys. Rev. C 47, 1504.
Ikeda, Y., et al., 1993. Absolute measurements of activation cross sections of 27-Al(n, p) 27-Mg, 27-Al(n,alpha)24-Na, 56-Fe(n, p)56-Mn, 90-Zr(n,2n)89-Zr-m+g and 93-Nb (n,2n)92-Nb-m at energy range of 13.3 - 14.9 MeV. J. Nucl. Sci. Technol. 30, 870.
Kiraly, B., Csikai, J., Doczi, R., 2001. Validation of neutron data libraries by differential and integral cross sections. J. Architect. Educ. 6, 283–288.
Koning, A.J., Rochman, D., 2012. Modern nuclear data evaluation with the TALYS code system. Nucl. Data Sheets 113, 2841–2934.
Koning, A.J., et al., 2011. TALYS-1.9, A Nuclear Reaction Program, User's Manual. NRG-1755 ZG Petten, The Netherlands.
Konno, C., 1993. Activation Cross Section Measurements at Neutron Energy from 13.3 to 14.9 MeV. Report: JAERI ReportsNo.1329.
Luo, Junhu, Jiang, Li, He, Long, 2018. Isomer ratios and cross sections for the isomeric pair ^{122m}Sb and ^{122g}Sb in the ^{123}Sb(n,2n) reaction. Appl. Radiat. Isot. 140, 115–120.
Majerle, M., Bem, P., Novak, J., Simeckova, E., et al., 2016. Au, Bi, Co and Nb cross-section measured by quasi monoenergetic neutrons from p+^{7}Li reaction in the energy range of 18-36 MeV. Nucl. Phys., Section A 953, 139.

Martin, M.J., 2013. Nuclear data sheets for A = 152. Nucl. Data Sheets 114, 1497–1847.
Mashnik, S.G., et al., 2008. ^{7}Li(p,n) Nuclear Data Library for Incident Proton Energies to 150 MeV. Los Alamos National Laboratory, Los Alamos, NM 87545, USA retrieved from. https://arxiv.org/abs/nucl-th/0011066.
McNaughton, M.W., et al., 1975. Measurements of ^{7}Li(p,n) and ^{9}Be(p,n) cross sections at 15, 20 and 30 MeV. Nucl. Instrum. Methods 130, 555.
Mehta, Mayur, et al., 2020. Indian J. Pure Appl. Phys. 58 (5), 392–396.
Minetti, B., Pasquarelli, A., 1968. Isomeric cross section ratio for (n,2n) reactions induced by 14.7 MeV neutrons. Nucl. Phys. Sect. A 118, 449.
Molla, N.I., 1983. Measurement of cross section for neutron induced reactions at 14 MeV via activation technique. In: Prog. Rep.: Bangladesh Report to the I.N.D.C.No.002, p. 1.
Nethaway, D.R., 1978. The 93Nb(n,2n)92(m)Nb cross section. J. Inorg. Nucl. Chem. 40, 1285.
Nowotny, R., 1998. XMuDat: Photon Attenuation Data on PC. IAEA Report No. IAEA-NDS 195.
Padamsee, H., 1998. RF Superconductivity for Accelerators. John Wiley & Sons.
Pasha, Imran, Basavanna, Rudraswamy, et al., 2019. J. Radioanal. Nucl. Chem. 320, 561–568.
Plompen, A.J.M., et al., 2020. The joint evaluated fission and fusion nuclear data library, JEFF-3.3. Eur. Phys. J. A 56, 181.
Poppe, C.H., Anderson, J.D., 1976. Cross sections for the ^{7}Li(p,n)7Be reaction between 4.2 and 26 MeV. Phys. Rev. C 14, 438.
Raynal, J., 1994. Notes on ECIS94, CEA Saclay Report No.CEA-N-2772.
Retrieved from. http://www.nndc.bnl.gov/nudat2/index.jsp.
Retrieved from ENDF/B-VIII.0, Cross Section Information Storage and Retrieval System (ENDF), IAEA, Vienna, Austria, retrieved from https://www-nds.iaea.org/exfor/endf.htm(online).
Retrieved from EXFOR, Cross Section Information Storage and Retrieval System (EXFOR), IAEA, Vienna, Austria, retrieved from http://www.nds.iaea.or.at/exfor/(online).
Salaita, G.N., Eapen, P.K., 1974. Production of isomers by the cyclic activation method. In: Conf. On Nucl.Meth.in Envir. Res., p. 95. Columbia.
Santry, D.C., Werner, R.D., 1990. Cross sections for the ^{93}Nb(n,2n)^{92m}Nb reaction. Can. J. Phys. 68, 582.
Smith, D.L., et al., 2005. Corrections for low energy neutrons by spectral indexing. retrieved from. https://www.oecdnea.org/science/docs/2005/nsc-wpec-doc2005-357.pdf.
Soni, Bhargav, Parashari, Siddharth, Mukherjee, S., et al., 2020. Measurement of (n,xn) reaction cross sections on ^{113,115}In isotopes using quasi-monoenergetic neutrons within 10-20 MeV. Eur. Phys. J. Plus 135, 300.
Srinivasa Rao, C.V., et al., 1978. Fluctuations in the systematics of (n,2n) reaction cross sections in the low mass region; Fast neutron cross-sections of fusion reactor interest. In: Conf.: 21. Nucl. Phys. And Solid State Phys. Symp-1978., Bombay, vol. 2, p. 113.
Uno, Y., Meigo, S., Chiba, S., Fukahori, T., et al., 1996. Measurements of activation cross sections for the neutron dosimetry at an energy range from 17.5 to30 MeV by using the ^{7}Li(p,n) quasi-mono-energetic neutron source. In: Conf.: 9th Internat. Symposium on Reactor Dosimetry, p. 465. Prague.
Wenrong, Zhao, et al., 1989. Compilation of Measurements and Evaluations of Nuclear Activation Cross Sections for Nuclear Data Application, Report: Chinese Report to the I. N.D.C.No.16.
Xiuyuan, Wang, Fanhua, Hao, Zhengtong, Li, Ruiliang, Huang, 1989. Measurements of Activation Cross Section, Private Communication. W, WANG, p. 712.
Yĭğĭt, M., 2020b. Analysis of the reaction Q-value effect using newly evaluated empirical formulas of (n,2n) cross sections near 14.6 MeV. Int. J. Mod. Phys. E 29 (2), 2050005.
Ziegler, J.F., 2004. SRIM-2003. Nucl. Instrum. Methods Phys. Res., Sect. B 219–220, 1027–1036.
Zsolnay, E.M., Capote, R., et al., 2012. Technical Report No. INDC (NDS)-0616. IAEA, Vienna.

Journal of Radioanalytical and Nuclear Chemistry
https://doi.org/10.1007/s10967-024-09682-5

Activation cross section for $^{85}Rb(n,2n)^{84m}Rb$ and $^{85}Rb(n,p)^{85m}Kr$ reactions with uncertainty propagation and covariance analysis

Mayur Mehta[1,2] · N. L. Singh[1,3] · Ratankumar Singh[1] · R. Makwana[1] · P. V. Subhash[2,4] · Rakesh Chauhan[1] · S. V. Suryanarayana[5] · K. Katovsky[6]

Received: 21 June 2024 / Accepted: 24 July 2024

Abstract
The cross section of $^{85}Rb(n,2n)^{84m}Rb$ and $^{85}Rb(n,p)^{85m}Kr$ reactions were measured at neutron energy range 12–20 MeV using activation analysis followed by off-line γ-ray spectroscopic technique. The quasi mono-energetic neutrons were produced through $^{7}Li(p,n)^{7}Be$ reaction. The measurements were done relative to $^{27}Al(n,\alpha)^{24}Na$ reference monitor reaction cross section. The detailed uncertainty propagation from the attributes present in measurements was performed using covariance analysis. The γ-ray self-attenuation and background low neutron energy corrections were performed in the measurement studies. Theoretical calculations were performed by TALYS-1.96 nuclear code. The comparison of measured values with the available data in EXFOR database and evaluated data from JENDL-5 and EAF-2010 shows the measured cross section values of $^{85}Rb(n,p)^{85m}Kr$ reaction were slightly higher than the published values, evaluated data and theoretical data while for $^{85}Rb(n,2n)^{84m}Rb$, the measured values were consistent with the published data.

Keywords Rubidium · (n,2n) and (n,p) reaction cross section · Activation analysis · Covariance analysis · Correlation matrix

Introduction

An accurate knowledge of neutron activation cross sections are important for understanding and selection of suitable materials in nuclear technology applications and nuclear theory investigation [1]. The applications of activation cross sections are also important for neutron activation analysis, isotope production, medical technology and others. In present study, the cross section measurements have been carried out for rubidium isotopes for the reasons as follows: (i) K. Heyde et al. [2] reported in their theoretical studies that for the nuclei lie between the magic numbers of 28 and 50, shape coexistence plays a prominent role in their structure. (ii) Otuka et al. [3] reported in their theoretical work that many kinds of cross sections have been measured and published but due to large discrepancies and lack of sufficient information of the uncertainties in measurements users face difficulties. For (n,p) and (n,2n) reactions, multiple cross section studies have been carried out by different authors presented in Table 1 and Table 2. The experimental cross section values are published in EXFOR database [4] for both the reactions but no report had been found with detailed analysis of uncertainties using covariance analysis method. The purpose of the present work is to measure the cross section of $^{85}Rb(n,2n)^{84m}Rb$ and $^{85}Rb(n,p)^{85m}Kr$ reactions in the neutron energy range 12–20 MeV and to report the cross section data with uncertainties propagate from all attributes involved in the activation equation and covariance and correlation matrix. The cross section for both the reactions has

✉ Mayur Mehta
mayur@ipr.res.in

N. L. Singh
nl.singh-phy@msubaroda.ac.in

1 Department of Physics, Faculty of Science, The M.S. University of Baroda, Vadodara 390002, India

2 Institute for Plasma Research, Gandhinagar 382428, India

3 Department of Physics, Netaji Subhas University of Technology, Dwarka, New Delhi 110078, India

4 Homi Bhabha National Institute, Anushaktinagar, Mumbai 400094, India

5 Nuclear Physics Division, Bhabha Atomic Research Centre, Trombay, Mumbai 400085, India

6 Department of Electrical Power Engineering, Brno University of Technology, 61600 Brno, Czech Republic

Published online: 05 September 2024

Table 1 Summary of $^{85}Rb(n,p)^{85m}Kr$ reaction cross section from the previous measurements

Sample form	Neutron source	Monitor reaction	Decay data	Detector	Reference
RbCl powder	$T(d,n)^4He$	$^{93}Nb(n,2n)^{92m}Nb$	$E_\gamma = 304.87$, $I_\gamma = 14.0$, $\tau_{1/2} = 4.48$ h	HPGe	1993, C. Konno
RbCl powder	$T(d,n)^4He$	$^{27}Al(n,\alpha)^{24}Na$	$E_\gamma = 151.$, $I_\gamma = 16.1$, $\tau_{1/2} = 4.48$ h	Ge(Li)	1990, Y. Xialin
Rb_2O powder	$T(d,n)^4He$	$^{27}Al(n,\alpha)^{24}Na$	$E_\gamma = 151.2$, 304.9 $I_\gamma = 75,14$ $\tau_{1/2} = 4.48$ h	Ge(Li)	1986, R. Pepelnik
Rb_2CO_3 powder	$T(d,n)^4He$	$^{27}Al(n,\alpha)^{24}Na$	$E_\gamma = 304$, $I_\gamma = 13.5$, $\tau_{1/2} = 4.48$ h	Ge(Li)	1979, B. Erlandsson
Natural Rb	$T(d,n)^4He$	$^{27}Al(n,\alpha)^{24}Na$	$E_\gamma = 151$, $I_\gamma = 79.6$, $\tau_{1/2} = 4.4$ h	Ge(Li)	1977, N.I. Molla
RbCl powder	$T(d,n)^4He$	$^{56}Fe(n,p)^{56}Mn$	$E_\gamma = 305$, $I_\gamma = 23$, $\tau_{1/2} = 4.48$ h	Ge(Li)	1976,W. Augustyniak
Rb_2SO_4 powder	$T(d,n)^4He$	$^{56}Fe(n,p)^{56}Mn$	$E_\gamma = 150$, $I_\gamma = 78$, $\tau_{1/2} = 4.4$ h	Ge(Li)	1971, P. Venugopala Rao
Natural Rb	$T(d,n)^4He$	$^{27}Al(n,\alpha)^{24}Na$	$E_\gamma = 305$, $I_\gamma = 13$, $\tau_{1/2} = 4.4$ h	Ge(Li)	1970, L. Hussain
Powder of pure element	$T(d,n)^4He$	$^{1}H(n,el)^{1}H$	$E_\gamma = 304$, $I_\gamma = 14$, $\tau_{1/2} = 4.48$ h -	NaI(Tl)	1966, M. Bormann

*E_γ in keV and I_γ in percentage (%)

Table 2 Summary of $^{85}Rb(n,2n)^{84m}Rb$ reaction cross section from the previous measurements

Sample form	Neutron source	Monitor reaction	Decay data	Detector	Reference
RbCl powder	$T(d,n)^4He$	$^{93}Nb(n,2n)^{92m}Nb$	$E_\gamma = 248.02$, $I_\gamma = 63$, $\tau_{1/2} = 20.26$min	HPGe	2018, Junhua Luo
RbCl powder	$T(d,n)^4He$	$^{93}Nb(n,2n)^{92m}Nb$	$E_\gamma = 247$, $I_\gamma = 64.5$, $\tau_{1/2} = 20.5$ min	HPGe	1993, C. Konno
RbCl powder	$T(d,n)^4He$	$^{27}Al(n,\alpha)^{24}Na$	$E_\gamma = 248$, $I_\gamma = 63$, $\tau_{1/2} = 20.5$ min	Ge(Li)	1990, Y. Xialin
RbCl powder	$T(d,n)^4He$	$^{56}Fe(n,p)^{56}Mn$	$E_\gamma = 464$, $I_\gamma = 32$, $\tau_{1/2} = 20$ min	NaI(Tl) & Ge(Li)	1976,W. Augustyniak
Rb_2CO_3 powder	$T(d,n)^4He$	$^{1}H(n,el)^{1}H$	$E_\gamma = NA.$, $I_\gamma = NA$, $\tau_{1/2} = 21.2$ min	NaI(Tl)	1976, M. Bormann
Rb_2CO_3 powder	$T(d,n)^4He$	$^{27}Al(n,\alpha)^{24}Na$	$E_\gamma = 250.$, 464 $I_\gamma = 65,32$ $\tau_{1/2} = 20$ min	Ge(Li)	1974,S.K. Ghorai
Rb_2CO_3 powder	$T(d,n)^4He$	$^{1}H(n,el)^{1}H$	$E_\gamma = 463.9$, $I_\gamma = 63.3$, $\tau_{1/2} = 20.26$ min	NaI(Tl)	1968, M. Bormann
Natural Rb	$T(d,n)^4He$	$^{63}Cu(n,2n)^{62}Cu$	$E_\gamma = 465$, $I_\gamma = 35$, $\tau_{1/2} = 20$ min	NaI(Tl)	1968, B. Minetti

*E_γ in keV and I_γ in percentage (%)

been calculated using TALYS-1.96 [5] nuclear reaction model code. The measured cross section values are compared with the reported literature data and evaluated data from JENDL-5 and EAF 2010 library [6, 7].

Experimental details

Neutron irradiation facility

The 6 m 14UD BARC-TIFR Pelletron facility at Mumbai-India was used for neutron irradiation experiments [8]. The quasi monoenergetic neutrons were produced by bombarding proton beam of energies 15, 18, 19 and 21 MeV on natural lithium (Li) foil of thickness 8.0 mg/cm^2. The neutrons were produced via $p + {}^7Li \rightarrow n + {}^7Be$ reaction. Lithium foil was sandwiched between the two tantalum foils of thickness 0.1 mm thick in back side to stop the proton beam and 4.0 mg/cm^2 in the front side. The energy degradation of proton beam in lithium and tantalum foil was 80–90 keV calculated by SRIM software [9]. The target samples with monitor were kept at a 21 mm distance from Ta-Li-Ta stack at 0^o with respect to the proton beam direction as shown in Fig. 1. The proton beam current was monitored and recorded at a time interval during the irradiation. The experimental details are presented in Table 3.

Estimation of averaged neutron energy

In present experiment, the proton beam of energies 15, 18, 19 and 21 MeV bombarded on the lithium target to produce quasi-monoenergetic neutrons in the forward direction via $^7Li(p,n)$ reaction. The threshold energy of $^7Li(p,n)^7Be$ reaction is 1.881 MeV for the ground state of ^7Be and corresponding neutron energy for the ground state is E_p –1.881 likewise the threshold energy for the first excited state is 2.37 MeV and corresponding neutron energy for the first excited state is E_p –2.37. Below proton energy of 2.37 MeV, monoenergetic neutrons produces from $^7Li(p,n)$ reaction and above the proton energy of 4.5 MeV, three body interaction and other excited states contribute in the neutron production from the main neutron group [11, 12]. The main group neutrons are used for cross section measurements. The neutron spectrum for 15, 18, 19 and 21 MeV energies were generated by interpolation from the spectra reported by M.W. McNaughton et al. [13, 14] having a long tail towards lower

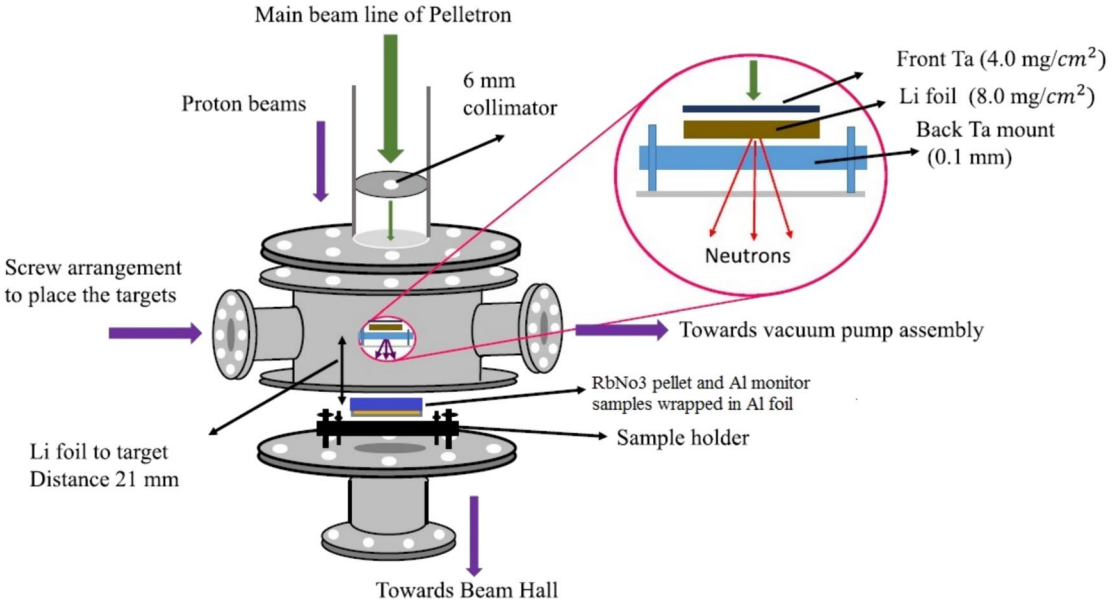

Fig. 1 A schematic diagram of experimental set up for irradiation [10]

Table 3 Details of irradiation experiments

	Irradiation 1	Irradiation 2	Irradiation 3	Irradiation 4
E_p (MeV)	15	18	19	21
En (MeV)	12.97 ± 0.51	15.72 ± 0.59	16.73 ± 0.66	18.99 ± 0.74
Irradiation time (hh:mm)	9:00	7:00	3:00	7:00
Beam current (nA)	175	180	180	160

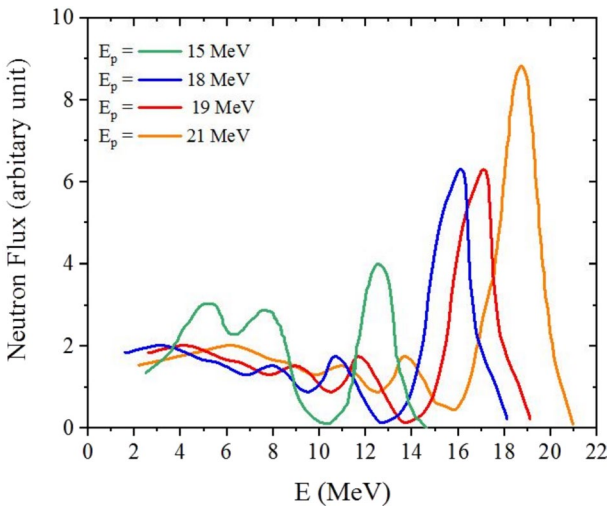

Fig. 2 Neutron spectra from ^{7}Li(p,n).^{7}Be reaction of proton energies 15, 18, 19 and 21 MeV generated from M.W. McNaughton et al. [13]

energies and a peak near E_p–1.88 as presented in Fig. 2. The spectrum averaged neutron energy is calculated from the spectrum using equation,

$$\langle E_{mean} \rangle = \frac{\int_{E_{ps}}^{E_{\max}} E_i \Phi_i dE}{\int_{E_{ps}}^{E_{\max}} \Phi_i dE} \quad (1)$$

where, E_{mean} is effective mean energy, E_{ps} is starting of peak neutron energy, E_{max} is maximum neutron energy, E_i is energy bin and Φ_i is neutron flux of energy bin E_i. The corresponding neutron energies are 12.97 ± 0.51, 15.72 ± 0.59, 16.73 ± 0.66 and 18.99 ± 0.74 MeV for proton energies 15, 18, 19 and 21 MeV respectively. The reaction cross-section due to the low energy neutrons from the tail part also contributes to the measured cross-section from the main neutron peak. The correction due to low energy background neutrons is done as discussed in Sect. "Low energy background correction".

Sample preparations

In the irradiation experiments, rubidium sample was in the form of pellet while aluminum was used as a thin metal foil of thickness 0.1 mm. A $RbNO_3$ powder form of known amount was used to prepare circular pellet of diameter 1 cm packed into the polyethylene bag. The ^{27}Al(n,α)^{24}Na

reaction was used to determine the absolute neutron flux. The reference monitor cross section was taken from the standard IRDFF-II data library [15]. The sample details are given in Table 4. The AFCOSET ER-182A make micro balance was used for the sample weight measurements have the least count of 0.1 mg. The samples for irradiation were placed as "Rb-Al" stack in the 0^0 to the beam direction.

Gamma ray spectroscopy

The irradiated experiments were carried out for the sufficient time to produce enough activity in the samples. After the irradiation stops, the samples were transferred to the counting room. The target sample and the monitor sample were mounted on the Perspex plate and taken for the off-line γ-ray spectroscopy. The emitted γ-rays from the product nuclides (^{84m}Rb, ^{85m}Kr and ^{24}Na) were recorded by a pre-calibrated 80 cm^3 high purity germanium (HPGe) detector having 40% relative efficiency and a 1.82 keV energy resolution at 1332.50 keV γ-energy of ^{60}Co. The detector was coupled with a PC-based 4096 channel analyser with CMAC based Linux Advanced Multi-Parameter System LAMPS software and the dead time of the detector was < 5% throughout the counting time. The nuclear spectroscopic data with uncertainties of the sample and monitor reactions are given in Table 5 [16–19].

The efficiency calibration of the HPGe detector was determined for different γ-ray energies using a standard ^{152}Eu source ($\tau_{1/2} = 13.517 \pm 0.009$ year) of known activity ($A_0 = 7767.73 \pm 88.1$ Bq as on 1-October-1999) [20]. The HPGe detector efficiency was determined using the relations,

$$\varepsilon = \frac{C_{obs}K_c}{A_o I_\gamma e^{-\lambda T}\nabla t} \quad (2)$$

where, C_{obs} is the photo peak counts measured in time ($\Delta t = 3754$ s), A_0 is the ^{152}Eu-source activity at the time of manufacturing, I_γ is the γ-ray intensity, T is the time interval between the source manufacturing to the experiment date. Kc is the coincidence summing correction factor. The irradiated samples were kept at a distance of 3 cm from the detector end cap, the correction for the coincidence summing effects of γ-ray energy lines was made in the detector efficiency measurements. The Monte Carlo simulation code EFFTRAN [21] was used to calculate the correction factor (Kc). The code required the material and dimension details of crystal, cavity, housing, window and mounting holder of the HPGe detector and calibration source [22]. The comparison of measured efficiency with the EFFTRAN code is presented in Fig. 3.

Covariance analysis and uncertainty propagation in efficiency

The covariance matrix for the detector efficiency was determined which gives the complete information of the uncertainties in the measurements. From Eq. (2), the efficiency is the function of counts, γ-ray intensity, activity and the decay constant. In the measured efficiency the uncertainties propagate from these four attributes $\varepsilon = \Delta\varepsilon$ (ΔC_{obs}, ΔI_γ, ΔA_0, $\Delta\lambda$). Therefore the total uncertainties were calculated using the formula,

Table 4 Sample details used for the irradiation experiments

Sample	Isotope	Isotopic abundance (%)	Density (g/cm^3)	E_n (MeV)	Weight (gm)	Number of target atoms ($\times 10^{-4}$ atoms/b)
Al-foil	^{27}Al	100	2.7	12.97 ± 0.51	0.0125	2.79
				15.72 ± 0.60	0.0134	2.99
				16.73 ± 0.66	0.0125	2.79
				18.99 ± 0.74	0.0134	2.99
$RbNO_3$ powder	^{85}Rb	72.17	3.11	12.97 ± 0.51	0.3007	15.29
				15.72 ± 0.60	0.3017	15.34
				16.73 ± 0.66	0.3007	15.29
				18.99 ± 0.74	0.2996	15.24

Table 5 Nuclear spectroscopic data with uncertainties used in present experiments [16–19]

Reaction	Product	Half-life	Decay Mode	Eγ (keV)	I_γ (%)
^{85}Rb(n,2n)	^{84m}Rb	20.26 ± 0.04 (min)	IT	463.62	33.10 ± 0.24
^{85}Rb(n,p)	^{85m}Kr	4.408 ± 0.008 (hour)	β^-	151.195	75.5 ± 0.5
^{27}Al(n,α)	^{24}Na	14.997 ± 0.012 (hour)	β^-	1368.625	99.9940 ± 0.0020

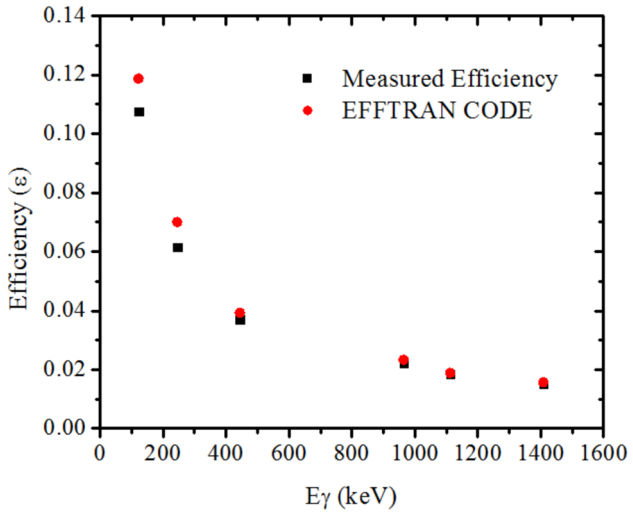

Fig. 3 Comparison of measured efficiency with EFFTRAN Code corrected efficiency

$$\left(\frac{\Delta\varepsilon_i}{\varepsilon_i}\right)^2 = \left(\frac{\Delta C_i}{C_i}\right)^2 + \left(\frac{\Delta A_0}{A_0}\right)^2 + \left(\frac{\Delta I_{\gamma i}}{I_{\gamma i}}\right)^2 + (t\Delta\lambda)^2 \quad (3)$$

where, ΔC_i, A_0 and $\Delta I_{\gamma i}$ are the uncertainties in counts, source activity and the γ-ray intensities respectively, and $\Delta\lambda = 0.693 \times \Delta\tau_{1/2}/\tau_{1/2}^2$ is the uncertainty in the decay constant. The partial uncertainties values of all four attributes are important to create the covariance matrix for the detector efficiencies which is determined by,

$$\left(V_\varepsilon\right)_{ij} = \sum_r e_{ir} S_{ijr} e_{jr} \quad (4)$$

where, e_{ir} and e_{jr} are the n × n diagonal matrices and S_{ijr} are the n × n micro-correlation matrix. The covariance matrix and the correlation matrix for the HPGe detection efficiency is presented in Table 6. The total error in the measured efficiency is the variance of the diagonal covariance matrix given by $(\sigma_\varepsilon)_{ii} = ((V_\varepsilon)_{ii})^{1/2}$ [23]. The detector efficiency of γ-ray energies from ^{84m}Rb, ^{85m}Kr and ^{24}Na nuclides were determined by the interpolation method through the linear parametric function [24, 25],

$$\ln(\varepsilon_i) = \sum_m P_m (\ln E_i)^{m-1} \quad (5)$$

where, ε_i and E_i is the efficiency and corresponding γ-ray energy of ^{152}Eu source and P_m is the fitting parameter. The above Eq. (5) can be written as Z = AP, with fitting parameters P_m and the corresponding covariance matrix V_p, is given as,

$$P_m = V_p\left(A^T V_Z^{-1} A\right) \quad V_p = \left(A^T V_Z^{-1} Z\right) \quad (6)$$

where, V_z matrix can be obtained as,

$$V_Z = \frac{\left(V_{\varepsilon_{ij}}\right)}{\langle\varepsilon_i\rangle\langle\varepsilon_j\rangle}$$

The goodness of the fit can be obtained as,

$$\chi_m^2 = (Z - AP)' V_Z^{-1} (Z - AP) \quad (7)$$

By using above definitions, the fitting parameters for the detector efficiencies of sample and monitor reaction residues γ-rays were found to be,

$$P_m = (-3.90622, -0.746071, 0.116215, -0.024697, -0.027535); \chi_m^2 = 2.29$$

From above fitting parameters, the fitted efficiency curve and the measured efficiency is shown in Fig. 4. The calculated detector efficiencies with uncertainties for ^{84m}Rb, ^{85m}Kr and ^{24}Na nuclides and corresponding correlation matrix are given in Table 7.

^{85}Rn(n,p)^{85m}Kr and ^{85}Rb(n,2n)^{84m}Rb cross sections

The neutron averaged spectrum average cross section ($<\sigma_r>$) for both reactions were measured relative to ^{27}Al(n,α)^{24}Na reference monitor reaction cross sections ($<\sigma_m>$) using standard activation formula as,

Table 6 Covariance and Correlation matrix for HPGe detector efficiency of ^{152}Eu-source

Eγ (keV)	Covariance matrix (×10^{-7})						Correlation matrix					
121.78	25.97						1					
244.69	8.545	11.98					0.484	1				
443.96	5.161	2.953	5.645				0.426	0.359	1			
964.079	3.067	1.755	1.059	1.442			0.501	0.422	0.371	1		
1112.07	2.561	1.465	0.885	0.526	1.131		0.474	0.398	0.350	0.412	1	
1408.006	2.093	1.197	0.723	0.429	0.358	0.609	0.526	0.443	0.390	0.458	0.432	1

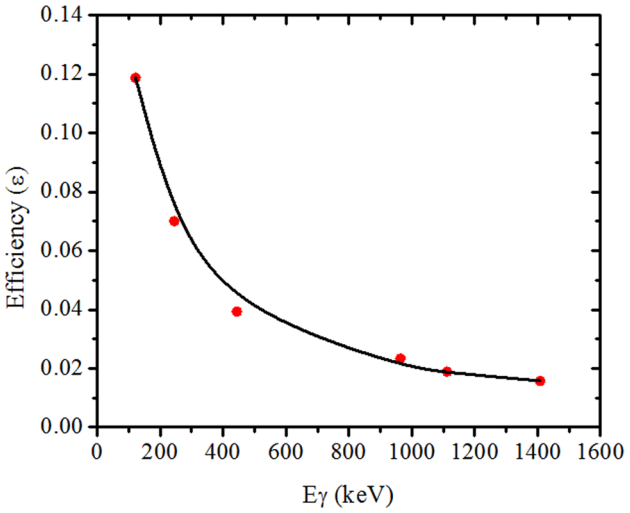

Fig. 4 Efficiency fitted curve and the measured efficiency

Table 7 Interpolated detection efficiencies with uncertainties and correlation matrix for sample and monitor reactions

Reaction	Eγ (keV)	Efficiency	Correlation matrix		
^{85}Rb(n,p)^{85m}Kr	151.195	0.10371 ± 0.00172	1		
^{85}Rb(n,2n)^{84m}Rb	463.62	0.03829 ± 0.00071	0.237	1	
^{27}Al(n,α)^{24}Na	1368.625	0.01608 ± 0.00024	0.579	0.376	1

$$< \sigma_r >= \langle \sigma_m \rangle \eta \frac{A_r \lambda_r a_m N_m I_m f_m}{A_m \lambda_m a_r N_r I_r f_r} \times \frac{C_{attn(r)} * N_{Corr(r)}}{C_{attn(m)} * N_{Corr(m)}} \quad (8)$$

where, η ($\varepsilon_m/\varepsilon_r$) is the detector efficiency ratio, $\varepsilon_{r,m}$ is the efficiency of corresponding γ-ray energies of sample and monitor reaction, $A_{r,m}$ is the counts of photo-peak recorded by HPGe detector, $\lambda_{r,m}$ is the decay constant (cm^{-1}), $N_{r,m}$ is the total number of atoms, $I_{r,m}$ is the γ-ray intensity, $a_{r,m}$ is the isotopic abundance of the target and monitor nuclei. The nuclear spectroscopic data are given in Table 4 and 5. $f_{r,m}$ is the timing factors of the sample and monitor reaction are given by,

$$f_{r,m} = \left(1 - e^{-\lambda t_{irr}}\right) e^{-\lambda t_{cool}} \left(1 - e^{-\lambda t_{count}}\right) \quad (9)$$

where, t_{irr} is the irradiation time, t_{cool} is the cooling time which is the time difference when the irradiation stop and the counting start time and t_{count} is the counting time. $C_{attn(r,m)}$ is γ-ray self-attenuation correction factor. $N_{corr\ (r,m)}$ is the low energy neutron correction factor.

Correction factors

Gamma ray self-attenuation factor

In γ-ray spectroscopy method, the γ-rays from the nuclides make interactions within the sample due to self-attenuation effect. Therefore in cross section measurement, the correction factor for self-attenuation of γ-rays need to be determine using formula,

$$C_{attn} = \frac{\mu_m \rho d}{1 - exp^{(-\mu_m \rho d)}} \quad (10)$$

where, ρ and d is the sample density and thickness. μ_m is the mass attenuation coefficient calculated from the XMuDat version 1.0.1. [26]

Low energy background correction

As discussed above (Sect. "Estimation of averaged neutron energy"), the proton energies for the irradiation are above the threshold energies of the first excited state of the ^{7}Li(p,n)^{7}Be reaction. Therefore contribution from the low energy background neutrons from ^{7}Li(p,n$_1$)^{7}Be* reactions needs to be subtract to determine the correct cross sections. Hence, the correction factor due to low energy background neutron is calculated by,

$$N_{corr} = 1 - \frac{\int_{E_{low}}^{E_{high}} \Phi_1(E)\sigma_x(E)dE}{\int_{E_{low}}^{E_{high}} \Phi(E)\sigma_x(E)dE} \quad (11)$$

where, Φ_1(E) is the neutron flux energy spectrum for (p,n$_1$) neutrons and $\Phi(E) = \Phi_0(E) + \Phi_1(E)$ $\sigma_x(E)$ is the cross section values of sample reactions taken from JENDL-5 [6] and ^{27}Al(n,α)^{24}Na reaction cross section values taken from IRDFF-II data library [15]. The calculated values of low energy corrections and the γ-ray self-attenuation correction factors of associated γ-ray energies of sample and monitor reactions are given in Table 8.

Reference monitor reaction cross section and its correlation matrix

In present work, the neutrons produced from ^{7}Li(p,n) reaction are not monoenergetic therefore the spectrum averaged monitor reaction cross section ($< \sigma_m >$) was calculated by,

$$\langle \sigma_m \rangle = \frac{\int_{E_{low}}^{E_{high}} \Phi_0(E)\sigma_m(E)dE}{\int_{E_{low}}^{E_{high}} \Phi_0(E)dE} \quad (12)$$

Table 8 γ-ray self-attenuation correction and low energy background correction factors used to measure cross sections

Reaction	Eγ (keV)	Cattn	En (MeV)	Ncorr
^{85}Rb(n,p)^{85m}Kr	151.195	1.04888 ± 0.00248	12.97 ± 0.51	0.8144
			15.72 ± 0.60	0.7711
			16.73 ± 0.66	0.7198
			18.99 ± 0.74	0.6907
^{85}Rb(n,2n)^{84m}Rb	463.62	1.01348 ± 0.00068	12.97 ± 0.51	-
			15.72 ± 0.60	0.9885
			16.73 ± 0.66	0.9429
			18.99 ± 0.74	0.8681
^{27}Al(n,α)^{24}Na	1368.625	1.00071 ± 0.00004	12.97 ± 0.51	0.8418
			15.72 ± 0.60	0.7267
			16.73 ± 0.66	0.6256
			18.99 ± 0.74	0.5144

where, σ_m is the monitor ^{27}Al(n,α)^{24}Na monitor reaction cross section from IRDFF-II folded with the neutron flux spectrum shown in Fig. 2. The spectrum averaged monitor cross section at nearest point energies with uncertainties and correlation matrix is given in Table 9.

Covariance analysis and uncertainty propagation in cross section

Nuclear data with statistics are important for researcher for precise and accurate evaluation. As a result, the reported experimental data are important with uncertainties and covariance matrix. In present study, the ^{85}Rb(n,2n)^{84m}Rb and ^{85}Rb(n,p)^{85m}Kr reaction cross section were measures at averaged neutron energies 12.97 ± 0.51, 15.72 ± 0.60, 16.73 ± 0.66 and 18.99 ± 0.74 MeV respectively. The cross section was measured by a ratio method. In the covariance analysis, the covariance matrix for the measured cross section was calculated by the formula,

$$\left(V_\sigma\right)_{ij} = \sum_r e_{ir} S_{ijr} e_{jr} \tag{13}$$

where, e_{ir} and e_{jr} are the n × n diagonal matrices of the partial uncertainties of i^{th} and j^{th} attributes and S_{ijr} are the n × n micro-correlation matrix. The partial uncertainties of the various attributes such as monitor cross section ($<\sigma_m>$), γ-ray photo peak counts (A_s, A_m), efficiency ratio (η), γ-ray intensity (I_γ) and isotopic abundance of sample and monitor,timing factor (f_s, f_m) and number of atoms (N_s, N_m) were used to calculate the uncertainties in the cross section. The partial uncertainties and the cross section with uncertainties and correlation matrix for ^{85}Rb(n,p)^{85m}Kr reaction is presented in Table 10 and Table 11. Similarly for the ^{85}Rb(n,2n)^{84m}Rb reaction, the partial uncertainties and the cross section with uncertainties and correlation matrix is presented in Table 12 and Table 13.

Theoretical calculations

Theoretically, the ^{85}Rb(n,p)^{85m}Kr and ^{85}Rb(n,2n)^{84m}Rb reactions cross section from threshold to 20 MeV neutron energies were calculated using TALY (version 1.96) code [5]. In present study, the input parameters were used as a default only the level density models were taken for the cross section measurements. There are six level density models are present for the selections as follows: (i) ldmodel 1 (Constant and Fermi-gas model); (ii) ldmodel 2 (Back-shifted Fermi-gas model); (iii) ldmodel 3 (Generalized super-fluid model); (iv) ldmodel 4 (microscopic level densities from (Skyrme force) Goriely's tables) [27]; (v) ldmodel 5 (microscopic level densities Skyrme force) from Hilaire's combinatorial tables) [27]; and (vi) ldmodel 6 (microscopic level densities (temperature dependent HFB, Gogny force) from Hilaire's combinatorial tables [27]. The cross section for both the reactions were compared with the measured cross section values, available published data and also with the evaluated data from JENDL 5and EAF 2010 data in Fig. 5 and Fig. 6.

Table 9 ^{27}Al(n,α)^{24}Na reaction cross section with uncertainties and correlation matrix

<En> (MeV)	Cross section $<\sigma_m>$ (mb)	Δ σ_m (%)	Correlation matrix			
12.97 ± 0.51	123.64 ± 1.280	1.04	1			
15.72 ± 0.60	96.91 ± 0.4846	0.50	0.0731	1		
16.73 ± 0.66	80.69 ± 0.5245	0.65	0.1436	0.8022	1	
18.99 ± 0.74	48.63 ± 0.5350	1.10	0.6699	0.0389	0.4024	1

Table 10 Partial uncertainties of $^{85}Rb(n,p)^{85m}Kr$ reaction cross-section measurements with respect to the $^{27}Al(n,\alpha)^{24}Na$ monitor reaction

Parameters	Partial Uncertainty (%)				Correlation
	En = 12.97 MeV	En = 15.72 MeV	En = 16.73 MeV	En = 18.99 MeV	
A_r	5.018	3.841	4.573	3.848	0
A_m	6.057	5.395	3.554	5.431	0
I_r	0.665	0.665	0.665	0.665	1
I_m	0.002	0.002	0.002	0.002	1
f_r	0.055	0.032	0.005	0.045	1
f_m	0.003	0.006	0.008	0.001	0
W_r	0.033	0.033	0.033	0.033	0
W_m	0.800	0.746	0.800	0.746	0
σ_m	1.037	0.600	0.750	1.100	1
a_r	0.014	0.014	0.014	0.014	1
$C_{att\text{-}r}$	0.236	0.236	0.236	0.236	1
$C_{att\text{-}m}$	0.004	0.004	0.004	0.004	1
$\eta_{m,r}$	1.026	1.026	1.026	1.026	1

*subscript *r* stands for reaction and *m* for monitor reaction

Table 11 The measured $^{85}Rb(n,p)^{85m}Kr$ reaction cross section data with uncertainties and correlations matrix

En (MeV)	Cross section (barns)	Correlations			
12.97 ± 0.51	0.00431 ± 0.00035	1			
15.72 ± 0.60	0.00538 ± 0.00037	0.0275	1		
16.73 ± 0.66	0.00469 ± 0.00028	0.0310	0.0368	1	
18.99 ± 0.74	0.00336 ± 0.00023	0.0270	0.0322	0.0362	1

Result and discussions

The $^{85}Rb(n,p)^{85m}Kr$ and $^{85}Rb(n,2n)^{84m}Rb$ reactions cross section measured at neutron energies 12.97 ± 0.51, 15.72 ± 0.60 16.73 ± 0.66 and 18.89 ± 0.74 MeV with their uncertainties and correlation matrix are presented in Table 11 and Table 13. Several authors measured (n,p) and (n,2n) reaction cross section of ^{85}Rb isotope presented in Table 1 and 2 by preferring different monitor reactions and γ-ray energies of product nuclide. In present experiment, the cross section is measured by 151.195 keV γ-ray energy for $^{85}Rb(n,p)^{85m}Kr$ reaction and 463.62 keV γ-ray energy for $^{85}Rb(n,2n)^{84m}Rb$ reaction.

The comparison of the $^{85}Rb(n,p)^{85m}Kr$ reaction cross section with the reported data [28–36], evaluated data [6, 7] and theoretically predicted data from TALYS-1.96 [5] was plotted in Fig. 5. For the comparison of the measured cross sections results with the published data, the nearest energy point values were considered. The comparison results indicate that the cross section at 12.97 ± 0.51 MeV agrees with the ldmodel 2 and ldmodel 3, at 15.72 ± 0.60 MeV agrees

Table 12 Partial uncertainties of $^{85}Rb(n,2n)^{84m}Rb$ reaction cross-section measurements with respect to the $^{27}Al(n,\alpha)^{24}Na$ monitor reaction

Parameters	Partial Uncertainty (%)				Correlation
	En = 12.97 MeV	En = 15.72 MeV	En = 16.73 MeV	En = 18.99 MeV	
A_r	4.794	3.783	3.604	3.124	0
A_m	6.057	5.395	3.554	5.431	0
I_r	0.725	0.725	0.725	0.725	1
I_m	0.002	0.002	0.002	0.002	1
f_r	0.065	0.086	0.089	0.067	1
f_m	0.003	0.005	0.008	0.001	0
W_r	0.033	0.033	0.033	0.033	0
W_m	0.800	0.746	0.800	0.746	0
σ_m	1.037	0.600	0.750	1.100	1
a_r	0.014	0.014	0.014	0.014	1
$C_{att\text{-}r}$	0.067	0.067	0.067	0.067	1
$C_{att\text{-}m}$	0.004	0.004	0.004	0.004	1
$\eta_{m,r}$	0.157	0.157	0.157	0.157	1

Table 13 The measured ^{85}Rb(n,2n)^{84m}Rb reaction cross section data with uncertainties and correlations matrix

En (MeV)	Cross section (barns)	Correlations			
12.97 ± 0.51	0.47476 ± 0.03735	1			
15.72 ± 0.60	0.58063 ± 0.03889	0.0107	1		
16.73 ± 0.66	0.64504 ± 0.03372	0.0137	0.0162	1	
18.99 ± 0.74	0.63007 ± 0.04062	0.0111	0.0131	0.0167	1

with the JENDL-5, at 16.73 ± 0.66 MeV agrees with the ldmodel 4, respectively. At 18.99 ± 0.74 MeV the result is agreed with the reported data by M. Bormann et al. [33] at 18.89 MeV (0.003 barns).

Similarly, the comparison of the measured ^{85}Rb(n,2n)^{84m}Kr reaction cross section with the reported data [34–42], evaluated data [6, 7] and theoretically predicted data from TALYS-1.96 [5] was plotted in Fig. 6. For the ^{85}Rb(n,2n)^{84m}Rb reaction, the cross section values were overestimate with the evaluated data and theoretically predicted data by TALYS 1.96. The cross section values at 12.97 ± 0.51 MeV and 18.99 ± 0.74 MeV were overestimated with the reported data by M. Bormann et al. [39] at 12.94 MeV (0.231 barns) and 18.89 MeV (0.466 barns), respectively. The cross section results at 15.72 ± 0.60 MeV and 16.73 ± 0.66 MeV were consistent with in 10% with the reported data by W. Augustyniak et al. [35] at 15.4 MeV (0.525 barns) and 16.6 MeV (0.6 barns), respectively. In case of ^{85}Rb(n,2n)^{84m}Rb reaction, 463.62 (33.1%) keV γ-ray energy was used for the cross section measurements which was earlier used by S.K. Ghorai et al. [40] and B. Minetti et al. [42] earlier. The comparison of measured values at 15.72 ± 0.60 MeV and 16.73 ± 0.66 MeV indicate that the values were agreed within 12% and 6% to the reported values by S.K. Ghorai et al. [40] at nearest energy points at 15 MeV (0.662 barns) and 16.2 MeV (0.688 barns).

Conclusions

The ^{85}Rb(n,p)^{85m}Kr and ^{85}Rb(n,2n)^{84m}Rb reactions cross sections were calculated in the energy range from 12 to 20 MeV using the offline γ-ray spectroscopic method. The absolute neutron flux was determined using ^{27}Al(n,α)^{24}Na monitor reaction. The cross section values of both the reactions were compared with the data reported in literature, theoretical calculations using TALYS-1.96 and evaluated data from JENDL-5 and EAF-2010. The total uncertainty in the measured cross sections for both the reactions are in between 6 and 8%. Multiple data points with scarcity in measured values are seen for both the reactions. The reason is may be due to using different reference monitor cross section by authors. For ^{85}Rb(n,p)^{85m}Kr reaction, the measured values has a slightly increasing trend with the increase in neutron energy indicating that the high-spin isomer formation is more favored at higher excitation

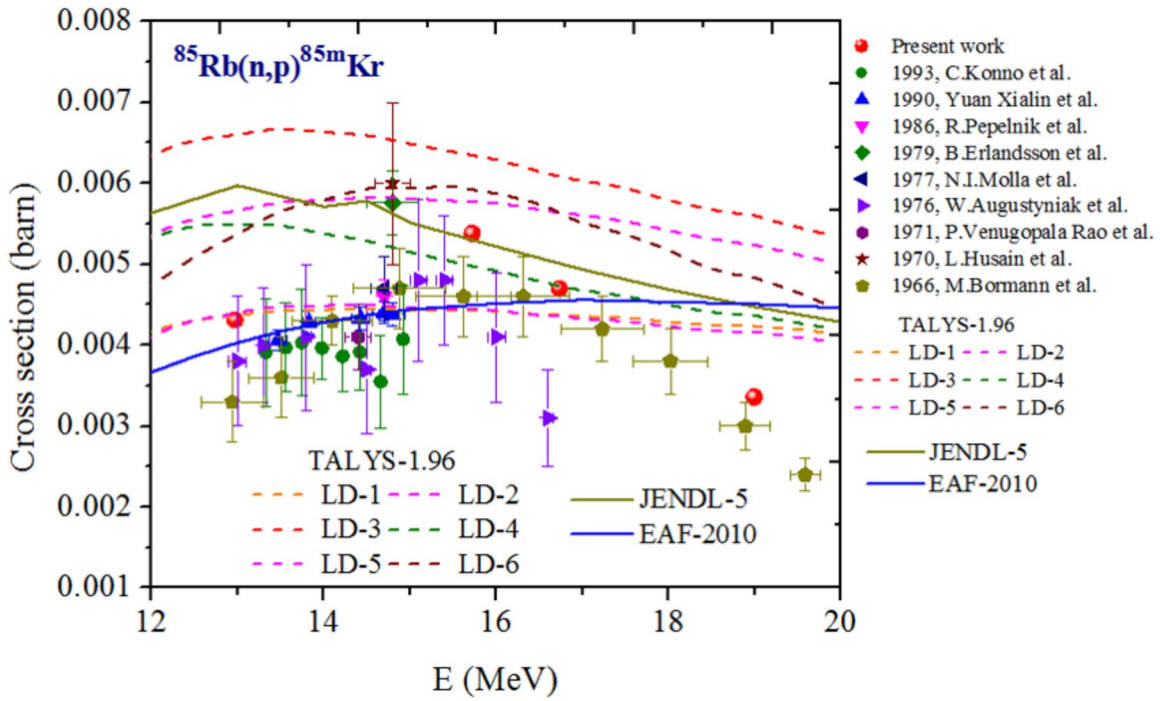

Fig. 5 Comparison of ^{85}Rb(n,p)^{85m}Kr reaction cross section with reported data, theoretically calculated data by TALYS-1.96 and evaluated data

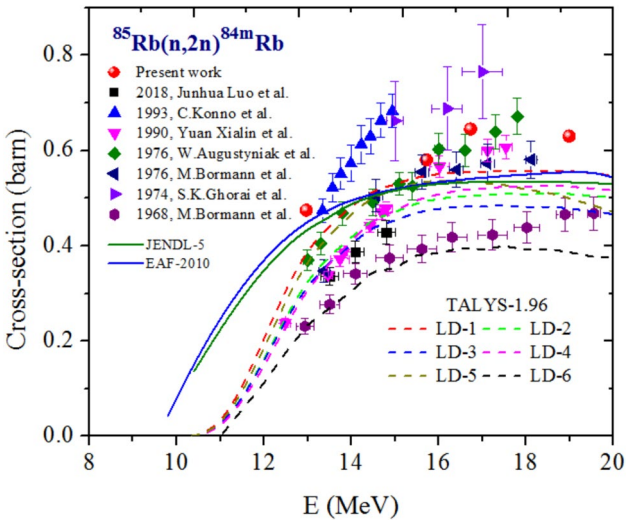

Fig. 6 Comparison of ^{85}Rb(n,2n)^{84m}Rb reaction cross section with reported data, theoretically calculated data by TALYS-1.96 and evaluated data

energies. For ^{85}Rb(n,2n)^{84m}Rb reaction, the measured values at 15.72 and 16.73 MeV energies were in good agreement with the reported values while at 12.97 and 18.99 MeV, the measured values were overestimated with the reported values. The cross section values in the present work were reported with the detailed uncertainties, covariance and correlation matrix. The measurements will fill the gap at the neutron energies where there is a deficiencies in the cross section values.

Acknowledgements The authors would like to thanks the staff members of TIFR-BARC Pelletron facility to conduct the irradiation experiment smoothly and their constant support for experimental arrangements and offline γ-ray counting measurements after the completion of the irradiation experiments.

Funding Open access funding provided by Department of Atomic Energy.

Data availability The authors confirm that the data supporting the findings of this study are available within the article and its supplementary material.

Declarations

Conflict of interests This research did not receive any specific grant from funding agencies in the public, commercial or non-profit sectors.

References

1. McLsne V., Dunford C.L., Rose P.F., (1988) Neutron cross sections (Academic, New York, Vol. 2.
2. Kris H, Wood JL (2011) Shape coexistence in atomic nuclei. Rev Mod Phys 83:1467
3. Otuka N, Lalremruata B, Khandaker MU, Usman AR, Punte LRM (2017) Uncertainty propagation in activation cross section measurements. Radiat Phys Chem 140:502–510
4. EXFOR database, https://www-nds.iaea.org/exfor/
5. Koning A., Hilaire Stephane, Goriely Stephane, (2021) TALYS User manual, TALYS 1.96/2.0, December 2021.
6. Osamu I, Nobuyuki I, Satoshi K, Futoshi M (2023) Japanese evaluated nuclear data library Version 5: JENDL-5. J Nuclear Sci Technol 60(1):1–60
7. Packer L.W. and Sublet J-Ch., (2010) The European activation file: EAF 2010 decay data library. CCFE-R
8. BARC-TIFR Pelletron LINAC Facility at TIFR, Mumbai, http://www.tifr.res.in
9. Ziegler JF (2004) SRIM-2003. Nucl Instrum Methods Phys Res, Sect B 219–220:1027–1036
10. Parashari S, Mukherjee S, Naik H et al (2019) Measurement of the 58Ni(n, p)58Co and 58Ni(n, 2n)57Ni reaction cross-sections for fast neutron energies up to 18 MeV. European Phy J A 55:51
11. Poppe CH, Anderson JD, Davis JC, Grimes SM, Wong C (1976) Cross sections for the 7Li(p,n)7Be reaction between 4.2 and 26 MeV. Phys Rev C 14:438
12. Mashnik S. G., Chadwick M. B., Hughes H. G. et al., (2008) ^{7}Li(p,n) nuclear data library for incident proton energies to 150 MeV. Los Alamos National Laboratory, Los Alamos, NM 87545, USA, arXiv:nucl-th/0011066v1
13. McNaughton MW, King NSP, Brady FP, Romero JL, Subramanian TS (1975) Measurements of 7Li(p, n) and 9Be(p, n) cross sections at 15, 20 and 30 MeV. Nuclear Instrumentation Methods 130:555–557
14. Midhun CV, Musthafa MM, Suryanarayana SV et al (2021) Impact of ^{7}Be breakup on the 7Li(p,n) neutron spectrum. Phys Rev C 104:054606
15. Trkov A, Griffin PJ, Simakov SP et al (2020) IRDFF-II: a new neutron metrology library. Nucl Data Sheets 163:1–108
16. Daniel A, Melih B, Sefa E et al (2009) Nuclear Data Sheets for A=84. Nucl Data Sheets 110:2815–2944
17. Balraj S, Jun C (2014) Nuclear data sheets for A=85. Nucl Data Sheets 116:1–162
18. Firestone RB (2007) Nuclear data sheets for A = 24. Nucl Data Sheets 108(11):2319–2392
19. NuDat 3 (2023) National Nuclear Data Center, Brookhaven National Laboratory. http://www.nndc.bnl.gov/nudat3
20. Martin MJ (2013) Nuclear data sheets for a = 152. Nucl Data Sheets 114:1497–1847
21. Vidmar T (2005) EFFTRAN-A monte carlo efficiency transfer code for gamma-ray spectrometry. Nuclear Instruments Methods A 550:603
22. Vidmar T, Kanisch G, Vidmar G (2011) Calculation of true coincidence summing corrections for extended sources with EFFTRAN. Appl Radiat Isot 69:908–911

23. Singh RK, Singh NL, Chauhan RD et al (2022) Systematic study of the (n,2n) reaction cross section for ^{121}Sb and ^{123}Sb isotopes. Chin Phys C 46(5):054002
24. Mehta M, Singh NL, Singh RK et al (2021) Measurement of ^{90}Zr(n,2n)^{89}Zr and ^{90}Zr(n, p)^{90}mY reaction cross-sections in the neutron energy range of 10.95 to 20.02 MeV. J Radioanal Nucl Chem 328:71–81
25. Siddharth P, Mukherjee S, Suryanarayana SV et al (2019) Systematic analysis of the neutron-induced reaction cross sections for ^{nat}Mo isotopes within 10–20 MeV. Phys Rev C 99:044602
26. Nowotny R., (1998) XMuDat: photo attenuation data on PC, IAEA Report No. IAEA-NDS 195
27. Capote R, Herman M, Oblozinsky P, Young PG et al (2009) RIPL: reference input parameter library for calculation of nuclear reactions and nuclear data evaluations. Nucl Data Sheets 110:3107
28. Konno C., Ikeda Y., Oishi K., Kawade K., Yamamoto H., Maekawa H. (1993) Activation Cross section measurements at neutron energy from 13.3 to 14.9 MeV Report: JAERI Reports No.1329
29. Pepelnik R., Anders B., Bahal B.M., Farooq M., (1986) 14 MeV neutron activation cross sections-, Report: Ges.Kernen.-Verwertung, Schiffbau and Schiffahrt No.86-E-29
30. Erlandsson B, Marcinkowski A, Nilson K (1979) Cross section of Rb at 14 MeV neutron energy and the decay of Rb. Phys Scr 19(3):251
31. Molla NI, Qaim SM (1977) A systematic study of (n, p) reactions at 14.7 MeV. Nuclear Phys A 283:269
32. Husain L, Bari A, Kuroda PK (1970) Neutron activation cross sections at 14.8 MeV for rubidium, zirconium, and niobium. Phys Rev C 1:1233
33. Bormann M, Dreyer F, Neuert H, Riehle I, Zielinski U (1966) Measurements of some fast neutron cross sections with the activation method. Nuclear Data For Reactors Conf., Paris 1:225
34. Yuan X, Zhao W, Weixiang Yu, Hanlin Lu (1990) Cross sections of 85Rb and 87Rb for fast neutrons. Chinese J Nuclear Phys 12(4):289
35. Augustyniak W, Herman M, Marcinkowski A (1976) Cross-sections for the fast neutron induced reactionson rubidium isotopes. Acta Physica Polonica, Part B 7:347
36. Venugopala RP, Wood RE, Palms JM, Fink RW (1971) Neutron activation cross sections for As, Br, Rb and Sr Isotopes at 14.4 MeV. Phys Rev C 3:629
37. Junhua L, Li J, Long He (2018) Measurement of cross sections and isomeric cross-section ratios for the (n,2n) reactions on 85,87Rb in energies between 13 and 15 MeV. Radiochim Acta 106(9):709–717
38. Konno C., Ikeda Y., Oishi K., Kawade K., Yamamoto H., Maekawa H., (1993) Activation Cross section measurements at neutron energy from 13.3 to 14.9 MeV. Report: JAERI Reports No.1329
39. Bormann M, Feddersen H-K, Holscher H-H, Scobel W, Wagner H (1976) (N,2N) excitation functions for Fe-54, Ge-70, Se-74, Rb-85, Sr-86,88, Y-89, Mo-92, and Hg-204 in the neutron energy region 13–18 MeV. Zeitschrift fuer Physik A Hadrons and Nuclei 277:203
40. Ghorai SK, Vos R, Cooper JR, Alford WL (1974) The (n,2n) cross sections of ^{85}Rb, ^{87}Rb and ^{144}Sm. Nuclear Phys A 223:118
41. Bormann M, Behrend A, Riehle I, Vogel O (1968) Measurement of (n,2n) excitation functions. Nuclear Phys A 115:309
42. Minetti B, Pasquarelli A (1968) Isomeric cross-section ratio for (n, 2n) reactions induced by 14.7 MeV neutrons. Nuclear Phys A 118:449